Republic of Iraq

Ministry of Higher Education & Scientific Research

University of Kerbala

College of Engineering

Civil Engineering Department

Experimental Investigation for the Effect of Abutment Geometry on the Local Scour at Bridge Piers

A Thesis Submitted to the Council of the Faculty of the College of Engineering/University Of Kerbala in Partial Fulfillment of the Requirements for the Master Degree in Civil Engineering

By:

Athraa Abdulwahid Khalaf

Supervisors

Assistant Prof. Dr.Aysar Tuama Al-Awadi

Assistant Prof. Dr.Riyadh Jasim Mohammed Al-Saadi

June 2025 Muharram 1447

بسم الله الرحمن الرحيم

يَرْفَعِ اللَّهُ الَّذِينَ آمَنُوا مِنكُمْ وَالَّذِينَ أُوتُوا الْعِلْمَ دَرَجَاتٍ

صدق الله العلي العظيم

(المجادلة: من الآية 11)

Examination committee certification

We certify that we have read the thesis entitled "**Experimental Investigation for the Effect of Abutment Geometry on the Local Scour at Bridge Piers**" and as an examining committee, we examined the student "**Athraa Abdulwahid Khalaf** " in its content and in what is connected with it and that, in our opinion, it is adequate as a thesis for the degree of Master of Science in Civil Engineering.

Supervisor

gnature:
ame : Asstist.Prof. Dr.Aysar Tuama Al-Awadi
)ate: / / 2025

Supervisor

Signature:
Name: Asstist.Prof. Dr.Riyadh Jasim Mohammed Al-Saadi
Date: / / 2025

Member

Signature:
Name: Prof. Dr. Layla A.M.Saleh
Date: / 9/ 2025

Member

Signature:
Name: Asstist.Prof. Dr.Sumayah Amal al-din Majeed
Date: / 9/ 2025

Chairman

Signature:
Name: Prof. Dr. Mahmoud Saleh Al-Khafaji
Date: / / 2025

Signature:
Name: Asstist.Prof. Dr.Aysar Tuama Al-Awadi
Head of the Department of Civil Engineering
Date: / / 2025

Signature:
Name: Prof. Dr.Haider Nazem Aziz
Dean of the Engineering College
Date: / / 2025

Supervisor certificate

We certify that the thesis entitled **"Experimental Investigation for the Effect of Abutment Geometry on the Local Scour at Bridge Piers"** was prepared by **Athraa Abdulwahid Khalaf** under our supervision at the Department of Civil Engineering, Faculty of Engineering, University of Kerbala as a partial of fulfilment of the requirements for the Degree of Master of Science in Civil Engineering.

Signature:

Assist. Prof. Dr.Aysar Thama Al-Awadi

Date: / / 2025

Signature:

Assist. Prof. Dr.Riyadh Jasim Mohammed Al-Saadi

Date: / / 2025

Linguistic certificate

I certify that the thesis entitled " **Experimental Investigation for the Effect of Abutment Geometry on the Local Scour at Bridge Piers** " which has been submitted by **Athraa Abdulwahid Khalaf,** has been proofread, and its language has been amended to meet the English style.

Signature:

Prof. Dr. Husscin M. Kadhim Al-Nasrawi

Date: / / 2025

Undertaking

I certify that research work titled "**Experimental Investigation for the Effect of Abutment Geometry on the Local Scour at Bridge Piers**" is my own work. The work has not been presented elsewhere for assessment. Where material has been used from other sources, it has been properly acknowledged / referred.

Signature:

Athraa Abdulwahid Khalaf

Date: / / 2025

Dedication

To the soul that resides in the depths of every free person, to the one who nurtured us and whose blessings we grew under, to the Master of Martyrs, my lord Abi Abdullah Al-Hussain (peace be upon him), I dedicate this humble effort.

To the great heart that embraced our sorrows before our joys… To the one with the radiant presence, whose soul is promised justice and deliverance… My master, the Imam of our time, Al-Mahdi (may Allah hasten his reappearance), I dedicate this thesis, as I draw from the light of his occultation a certainty in his presence and, from his mercy, the patience to endure the hardship of the journey. We have never forgotten you nor been heedless of your remembrance. You are the one who once wrote to us in the language of the unseen and divine kindness: "We are not neglectful of your care, nor forgetful of your remembrance." May this humble work be a drop in the ocean of anticipation, a token of loyalty from a heart longing for nearness in the time of absence and dreaming of reunion in the time of appearance.

To the soul of my kind and patient mother, who departed in body but remained as a lasting presence, who paved my path with her prayers, I dedicate this effort with all my love.

Acknowledgments

First and foremost, all praise and thanks are due to Allah, Lord of the worlds, whose endless mercy and guidance have brought this journey to its completion. I extend my deepest gratitude to the Prophet Muhammad and his pure household (peace be upon him and his family), whose light continues to guide hearts in times of hardship and hope. Without the grace of the Almighty, this work would not have been completed nor reached its final form.

I would like to express my sincere appreciation to my academic supervisors for their invaluable guidance, constructive feedback, and unwavering support throughout every stage of this research.

My heartfelt thanks go to my family, my beloved father and dear sisters and brothers, especially Ezaldeen and Ali, for their continuous encouragement, emotional support, and patience. Their words, their listening, and their faith in me sustained me during the most challenging moments of this journey.

I am also deeply thankful to my close friends and to everyone who believed in my abilities and inspired me to persevere. Each word of encouragement, each moment of understanding, was a stepping stone toward this achievement.

Abstract

Local scour at bridge abutments and piers is a major factor contributing to hydraulic bridge failures. Even though a lot of research has been done on this subject, there is a deficiency in research addressing the influence of the interaction between the abutment and pier in terms of their combined effect on scour depth, especially considering the abutment geometry and the space concerning the abutment and the pier. This thesis investigates the impact of various abutment shapes on the volume and shape of local scour development around a single cylindrical bridge pier. Experimental work was conducted under clear-water conditions and steady subcritical flow, using five abutments of different shapes. Three vertical wall abutment models varying in width are (5 cm, 7.5 cm, and 10 cm), the inclined wing-wall abutment, and the trapezoidal abutment. According to the results, the presence of abutment in the vicinity of the bridge pier influences the scour depth of the pier; this influence differs according to abutment shape, abutment width, the distance between them, and hydraulic parameters. Abutment scour decreased, and pier scour increased due to scour hole interference between the two structures when the distance is reduced. Where decreased spacing is from 27 cm to 22.5 cm, 25 cm to 20 cm, and 22.5 cm to 17.5 cm under the same conditions, pier scour increased by about 21%, 29%,3%, and 2% for vertical-wall 1, vertical-wall 2, wing-wall, and trapezoidal abutments model, respectively. In the case of vertical-wall 3, reducing the distance from 22.5 cm to 17.5cm was accomplished by decreasing the percentage of pier scour by 4%. The results show that the pier's scour depth increases with increasing Froude number and flow intensity, but decreases with increasing flow depth under constant distance. When the abutment is closer to the pier, the scour holes tend to merge

and form a larger hole. The comparison between abutment models, according to the value of percentage increase in scour depth, showed that the trapezoidal abutment at x=17.5 cm produced the greatest increase in scour depth, while the vertical-wall 1 abutment at x=27 cm produced the smallest. Furthermore, using the dimensional analysis technique and IBM SPSS 30 new empirical formulas were derived to estimate maximum scour depth around pier affected by abutment shape with a high determination coefficient (R^2= 0.948, 0.931, 0.913, 0.916, 0.936) for vertical-wall (V1), vertical-wall (V2), vertical-wall (V3), wing-wall, and trapezoidal models, respectively, displaying a strong relationship between the observed and predicted values. Finally, artificial neural networks (ANNs) were used to simulate the equilibrium scour depth around bridge piers impacted by abutments and have proven to be an excellent tool. The Multi-Layer Perceptron (MLP) model achieved the highest accuracy (R^2 = 0.983), confirming the reliability of ANN for complicated scour prediction tasks by outperforming nonlinear regression overall. Also, the abutment in both width and length has the greatest influence on the projected amount of scour depth around the pier, per sensitivity analysis. These findings provide a valuable contribution to the understanding of abutment–pier interaction in local scour processes, offering guidance for safer bridge design and more accurate prediction of scour depth. The outcomes are particularly useful for improving hydraulic design criteria, optimizing abutment geometry in relation to pier placement, and enhancing predictive models for bridge foundation stability under varying flow conditions.

Table of Contents

List of Tables

List of Figures

List of Abbreviations

ADV	Acoustic Doppler velocimetry
ANN	Artificial Neural Networks
CFD	Computational Fluid Dynamics
FDOT	Florida department of transportation
FHWA	Federal Highway Administration
MAE	Mean Absolute Error
MSE	Mean square error
MLP	Multi-Layer Perceptron
NTSB	National Transportation Safety Board
PI	Percentage increase in pier scour depth
RMSE	Root mean square error
SPSS	Statistical Package for the Social Sciences
SSIIM	Sediment Simulation in Intakes with Multiblock option
TA	Trapezoidal abutment at x=22.5cm.
TB	Trapezoidal abutment at x=17.5cm.
V1A	Vertical-wall abutment with w=5cm at x=27cm.
V1B	Vertical-wall abutment with w=5cm at x=22.5cm.
V2A	Vertical-wall abutment with w=7.5cm at x=25cm.
V2B	Vertical-wall abutment with w=7.5cm at x=20cm.
V3A	Vertical-wall abutment with w=10cm at x=22.5cm.
V3B	Vertical-wall abutment with w=10cm at x=17.5cm.
WA	Wing-wall abutment at x=22.5cm.
WB	Wing-wall abutment at x=17.5cm.

List of Symbols

Symbol	Description	Dimension
a*	Effective pier width	L
B	Flume width	L
b	Pier length	L
C	Soil cohesion factor	$M\ L^{-1}\ T^{-2}$
D	Pier dimeter	L
d_{16}	Sediment size for which 16% of the particles are finer	L
d_{50}	Median particle size	L
d_{84}	Sediment size for which 84% of the particles are finer	L
ds	Equilibrium depth of scour below the mean bed level	L
ds_{max}	Maximum equilibrium depth of scour below the mean bed	L
Fr	Froude number	Dimensionless
g	Gravitational acceleration	LT^{-2}
H	Height of the abutment model	L
K_{dis}	Distance coefficient.	Dimensionless
K_s	Shape factor	Dimensionless
Ksa	Abutment shape factor	Dimensionless

Ksp	Pier shape factor	Dimensionless
L	Length of abutment model	L
Ls	Length of scour hole	L
Q	Total discharge	L^3T^{-1}
R	Radius of curvature	L
R^2	Determination coefficient	Dimensionless
Re_p	Pier Reynolds number	Dimensionless
S	Flume bed slope	Dimensionless
T	Time	T
u*	shear velocity	LT^{-1}
u*c	Critical shear velocity	LT^{-1}
v	Mean flow velocity	LT^{-1}
vc	Critical flow velocity for sediment motion	LT^{-1}
W	Width of abutment model	L
Ws	Width of scour hole	L
x	Distance between pier and abutment	L
xs	Distance between scour holes before intersection	L
y	Flow depth	L
$\propto$	Wall angle	Degree

θ	Pier and abutment angle of attack	Degree
α	Skewness-angle	Degree
φ	Angle of repose	Degree
ρ	Water density	ML^{-3}
ρ_s	Sediment density	ML^{-3}
μ	Dynamic viscosity of water	$ML^{-1}T^{-1}$
ν	Kinematic viscosity	L^2T^{-1}
σ_g	Geometric standard deviation	Dimensionless

Chapter One : Introduction

1.1 General

Bridges are among the most crucial infrastructures in global transportation networks, as they significantly enhance traffic flow, connect different geographical areas, and facilitate economic and social movement. However, these structures encounter challenges related to sustainability and reliability, the most notable of which is local scour, a primary cause of bridge failures worldwide.

Local scour can be defined as the removal of bed sediment by water flow due to an obstruction in the flow field. This process changes the bed elevation and reduces the stability of bridge foundations. The flow interaction with a pier generates highly complex patterns of varying velocities and pressures, leading to sediment entrainment and the development of scour holes. Excessive scour can undermine bridge foundations, potentially leading to catastrophic failure. Therefore, understanding the mechanisms of local scour is essential for engineers in order to implement effective countermeasures and enhance the safety of bridges under different flow conditions. Preventing scour is also critical to sustaining infrastructure resilience and preserving the hydraulic and ecological balance of river systems.

As stated by Lin et al. (2014), local scour accounted for 64% of bridge failures worldwide. For example, in New York and New England, 17 bridges were destroyed by scour during the spring floods of 1987 Melville and Coleman (2000). Similarly, Wardhana and Hadipriono (2003), in their assessment of more than 500 bridge failures in the United States between 1989

and 2000, reported that 266 failures were hydraulically related, with scour alone representing 15.6% of the total cases (78 occurrences).

Figure 1-1 (A, B) presents two well-known cases of bridge collapse due to scour. The first is the 1987 Schoharie Creek Thruway Bridge failure in New York, which caused 10 fatalities and was attributed to severe scour at a pier and adjacent abutment during flooding. Investigations revealed that inadequate maintenance and insufficient scour protection were major contributing factors Arneson et al. (2012). The second case is the Daquq Bridge in Kirkuk, Iraq (2023), where pier scour during rainy seasons and floods led to significant structural damage and partial failure.

Figure 1-1: Bridge failure cases (A) Schoharie Creek Bridge (National Transportation Safety Board (NTSB), 1987), (B) Daquq Bridge (www.nrttv.com).

In addition to these events, a recent field study conducted in Baghdad (Nama et al., 2025) highlighted the growing risk of scour at several bridges along the Tigris River. The investigation revealed that local scour depths in some locations approached critical limits that could compromise foundation stability. The study emphasized that inadequate monitoring and insufficient protective measures increase the likelihood of future structural failures if no remedial actions are taken. This case underscores the urgent need for improved inspection, maintenance strategies, and the incorporation of effective scour countermeasures to safeguard bridge infrastructure in Iraq.

Despite extensive research, much remains unknown about local scour in complex natural environments. Many experimental studies have been conducted under controlled laboratory conditions, utilizing uniform sediments and steady flows, whereas real rivers exhibit irregular sediment mixtures, debris accumulation, and unsteady hydraulic conditions. Additionally, factors such as foundation layout, pier-abutment interaction, and variable approach flow conditions are often oversimplified, reducing the accuracy of current predictive models.

Bridge failures caused by scour have been investigated using different methods, including visual field inspections, diver or sonar surveys to measure scour depth, sediment sampling, hydraulic and numerical modeling, and historical flood analysis. These investigations often highlight that bridge piers and abutments are the most vulnerable structural elements. Piers generate strong downflow and horseshoe vortices that initiate local scour, while abutments alter the approach flow and induce sidewall vortices that intensify erosion near the banks. When a pier and abutment are located in proximity, their scour holes may interact, resulting in either an amplification or

mitigation of the maximum scour depth, depending on their geometry and spacing.

The shape and configuration of piers and abutments have a significant influence on scour development. Cylindrical piers typically produce symmetric and deeper scour holes, whereas sharp-edged or rectangular piers may induce more severe scour due to flow separation. Similarly, vertical-wall abutments create larger and deeper scour holes near the wall, while wing-wall or trapezoidal abutments can redistribute the flow, sometimes reducing scour intensity. However, when these abutments are positioned close to piers, the resulting interference between their scour holes may exacerbate local scour.

Given these challenges, there is a clear need for further research to better understand the interaction between abutments and piers under different configurations and hydraulic conditions. This thesis focuses on the effect of abutment geometry and spacing relative to a single cylindrical pier on local scour processes, with the aim of improving predictive capability and contributing to safer bridge design.

1.2 Problem statement

Increased water levels due to climate change have resulted in bigger floods, which have eroded banks under bridges and reduced their strength, while resulting in higher maintenance expenses. Although numerous studies exist, limited attention has been given to the interaction between piers and abutments when they coexist in the flow. Concerning the role of abutment geometry in scour reduction , it is still not well understood, which makes it necessary to study this further. Hence, the importance of conducting the current study to determine the extent of the abutment form's influence on local scour.

1.3 Aim of the Thesis

The current thesis aims to determine the influence of abutment geometry on local scour around a bridge pier. This aim is achieved by executing the following objectives:

1. Experimentally investigating the interface between pier and abutment scour under different hydraulic parameters, including flow intensity, Froude number, flow depth, and spacing between these structures.
2. To assess the effectiveness of different shapes of abutment in reducing scour depth and identifying the most efficient design.
3. To develop new empirical formulas for predicting scour depth around a pier affected by abutment under diverse hydraulic conditions, utilizing dimensional analysis and SPSS software.
4. To evaluate the effects of abutment geometry on scour depth around the bridge pier using Artificial Neural Networks (ANNs).

1.4 Methodology of the Thesis

The methodology of the present thesis can be summarized by the diagram shown in Figure 1-2.

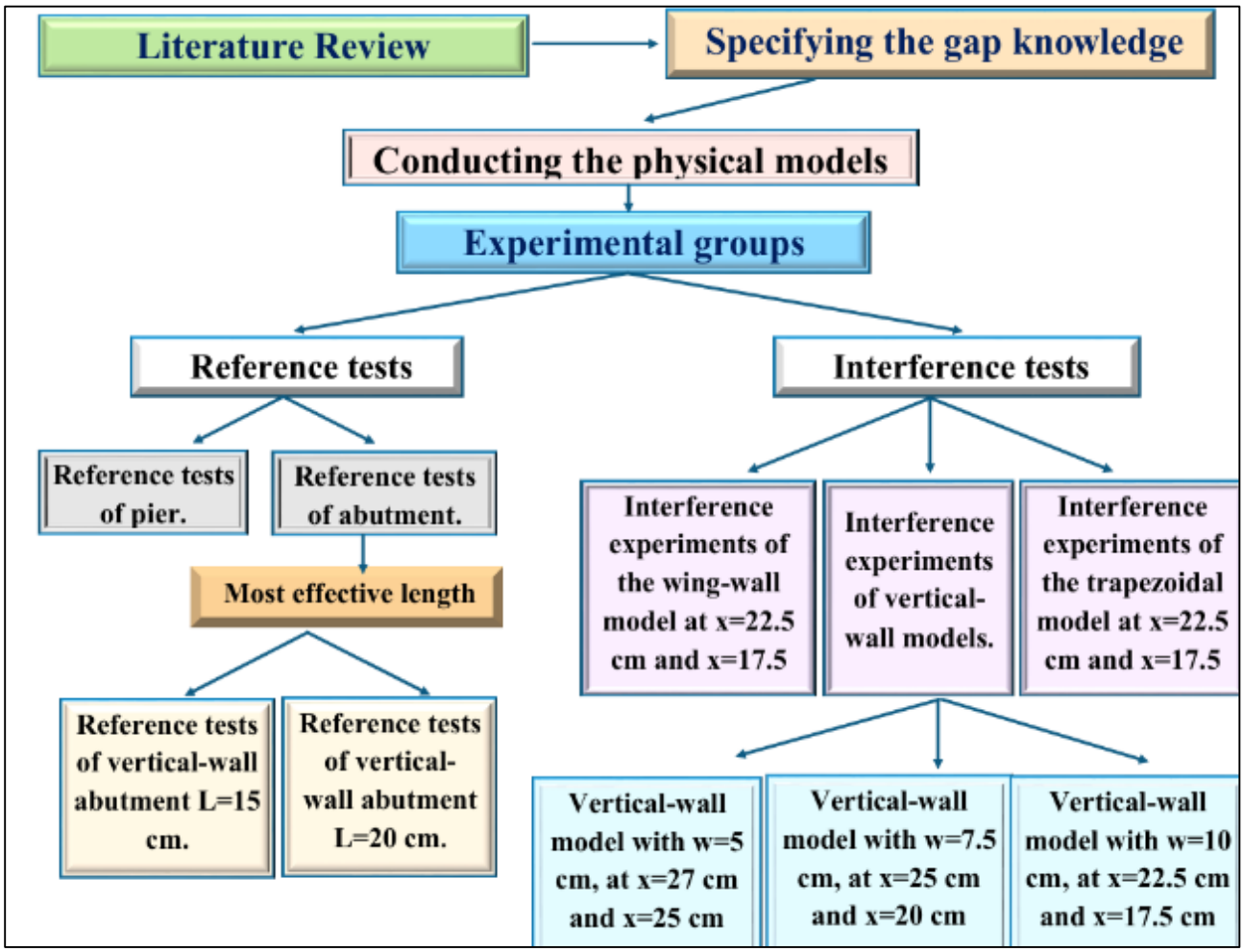

Figure 1-2: Diagram of the methodology of this study.

1.5 Limitations of the Thesis

The results of this thesis were obtained under the following limitations:

1. All experiments were conducted in a closed recirculation system, including a rectangular channel that has dimensions of 9.1 m length, 0.7 m width, and 0.50 m height, with head and basin tanks for experimental tests.

2. The experiments were conducted under clear-water conditions with steady, subcritical flow and a fixed time duration of 3 hours.
3. Several parameters were investigated within specific ranges: discharge (8.33-22.22 l/sec), flow depth (7-11 cm), flow intensity (0.5-0.9), Froude number (0.16-0.33), and spacing (17.5-27 cm).
4. The median particle size (d_{50}) was 0.716 mm as bed material in the flume.
5. The physical models for the experiments had the following dimensions: pier (D = 3.1 cm), the first vertical-wall abutment (W= 10 cm, L= 15 cm, H= 37 cm), the second vertical-wall abutment (W= 5 cm, L= 20 cm, H= 37 cm), third vertical-wall abutment (W= 7.5 cm, L= 20 cm, H= 37 cm), fourth vertical-wall abutment (W= 10 cm, L= 20 cm, H= 37 cm), wing-wall abutment (W= 10 cm, L1= 20 cm, L2=10cm H= 37cm), trapezoidal abutment (W= 10 cm, L1= 20 cm, L2=14cm H= 37 cm).

Chapter Two : Literature Review

2.1 Basic Concepts

Researchers worldwide have extensively studied the scour problem from various perspectives and under different conditions. It is well-documented that one of the primary concerns regarding the stability of bridge foundations is the occurrence of scour near piers and abutments. Understanding the mechanisms and influencing factors of scour is crucial for designing more resilient bridge structures.

2.2 Definitions of scour

Several studies and hydraulic engineers have proposed classifications of scour. Breusers et al. (1977) defined scour as a natural phenomenon caused by the flow of water in rivers and streams. Ettema (1980) defined scour as a natural phenomenon that arises from the erosive impacts of rushing water on the alluvial channel walls and bottom layer. The scour typically occurs during floods, which involve unsteady flows and can deviate in direction from normal currents. These floodwaters interact with various sediment types, including alluvial sands, gravels, stiff clays, weathered rock, or a combination of these materials. Arneson et al. (2012) stated that the erosion of the soil surrounding a bridge foundation (piers and abutments) due to water is known in engineering as scour. Barbhuiya and Dey (2004) described scour as a natural phenomenon that happens due to the erosive action of a running stream on alluvial beds. Scour is typically used to describe significant localized bed material erosion that occurs when the water's erosive power exceeds the bed material's capacity to withstand it. As illustrated by previous studies, scour can be produced by usual flow or flood actions. The amount of scouring is significantly increased with bigger flow events, although it can happen under

any flow situation that causes the bed to become movable near the obstacle Alabi (2006). The range of the scour that results depends on whether the bed material is made of rock, cohesive material, or non-cohesive material Mohamed et al. (2005). The removal of sediment by flowing water causes a localized depression or cavity known as a scour hole to form in the bed of a river, stream, or channel, while the vertical distance between a river or channel's initial bed level and the lowest point where the bed is action by flowing water is known as the scour depth.

2.3 Types of scour

Scour has long been recognized as a serious risk to the performance of bridge piers and abutments. Cheremisinoff et al. (1987) separated scour into two major types, specifically general scour and localized scour. Additional subdivisions of scour are shown in Figure 2-1. Richardson and Davis (2001) claimed that the three components that make up the overall scour at a river crossing may generally be combined. These consist of contraction scour, local scour, and general scour. Some other subdivisions of scour are, as stated by Melville and Coleman (2000), bridge scour may be conveniently classified into four types:

1-General scour (long-term aggradation/degradation).

2-Contraction scour.

3-Local structure-induced pier and abutment scour.

4-Lateral migration.

Figure 2-2 illustrates the scour categories around the bridge foundations.

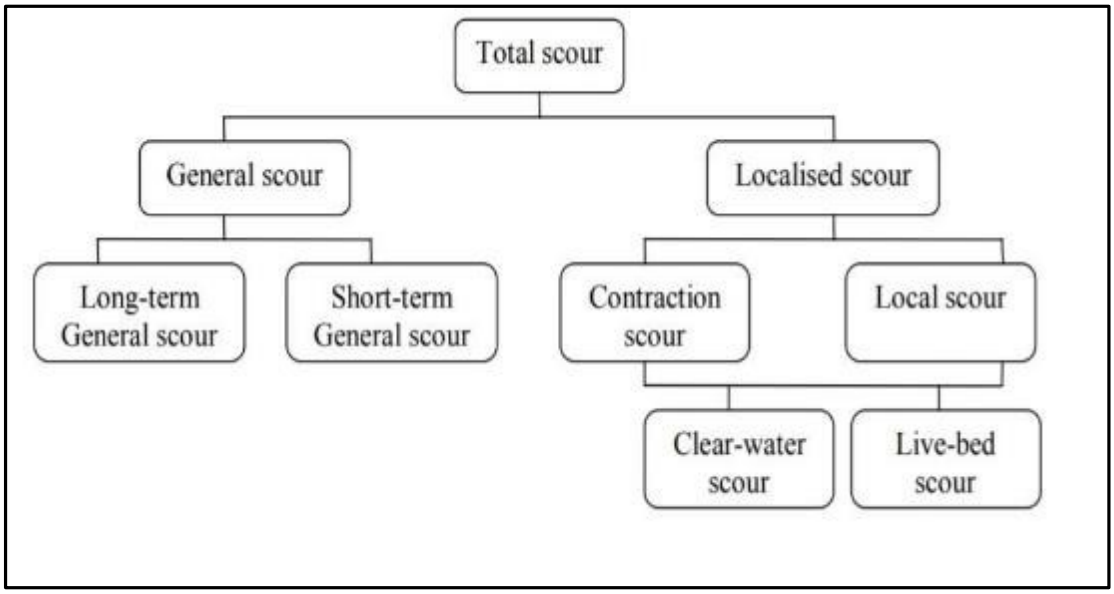

Figure 2-1: Types of scour (Cheremisinoff et al., 1987).

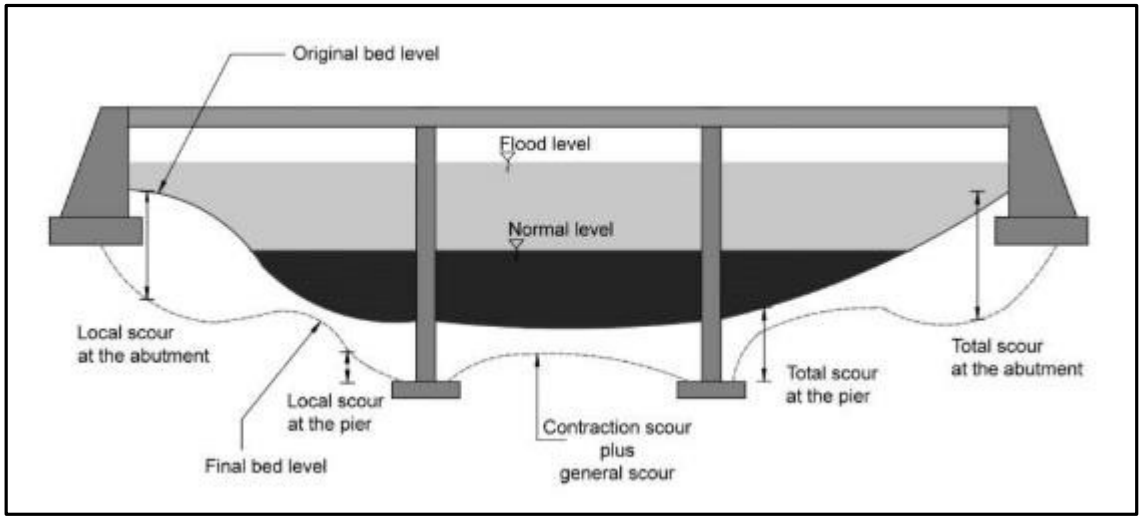

Figure 2-2: Types of scour around bridge piers and abutments (Melville and Coleman, 2000).

2.3.1 General Scour (Degradation/Aggradation)

General scour refers to the change in riverbed elevation over a long reach, independent of any local obstructions such as bridge foundations. It is driven by large-scale watershed or channel processes, including sediment supply imbalance (deficit or surplus), alterations in flood regimes, or anthropogenic activities such as dam construction or removal, sand removal, and land-use changes. For bridges, general scour is significant as it alters the reference bed level used for design and analysis. While typically a slow process occurring over seasons or years, it can become rapid when certain thresholds are exceeded, for example, during a major flood that mobilizes a large volume of sediment. According to the Federal Highway Administration (FHWA), general scour is defined as "the combination of short-term and long-term scour" and should be assessed by comparing pre- and post-flood bed profiles outside the contracted flow, are Mueller and Wagner (2005). Short-term general scour results from a single flood event or a series of closely spaced floods. In contrast, long-term general scour develops gradually over many years and encompasses advanced bed deprivation and cross-bank erosion. The "long-term scour" is the total design scour for structures subject to clear-water scour. For structures subject to live-bed scour, the "long-term scour" is the normal scour at the piers combined with the degradation scour anticipated during the life of the structure Arneson et al. (2012).

2.3.2 Localized Scour

Localized scour, unlike general scour, is directly caused by the presence of a bridge obstruction. Contraction and local scour are two other categories for localized scour.

2.3.2.1 Contraction Scour

Contraction scour occurs when the effective flow area of a river channel is reduced due to the presence of a bridge or its approaches, such as piers, abutments, or embankments that extend into the channel. According to Richardson and Davis (2001), contraction scour is defined as the exclusion of sediment from the bed and banks through all or most of the channel width, caused by a reduction in flow area. Unlike the localized scour around piers, contraction scour typically forms a longer and shallower depression in the riverbed. Field observations indicate that contraction scour often interacts with local scour, as the narrowing of the channel tends to intensify the flow around piers and abutments, exacerbating erosion. In practice, contraction scour is usually estimated by measuring the change in bed elevation before and after a flood event, with the bridge section treated as the constricted area Mueller and Wagner (2005).

2.3.2.2 Local Scour

Local scour refers to the erosion of bed material that occurs directly around bridge foundations (piers and abutments). This type of scour is caused by the disruption of the flow pattern due to the presence of these structural elements, which leads to an acceleration of the flow and the development of vortices that remove sediment from the immediate vicinity of the foundation. Flow acceleration and flow separation create vortices that form scour holes at the base of these structures. Typically, the depth of local scour increases until reaching an equilibrium state. Figure 2-3 illustrates the typical configuration of local scour around a bridge pier. Subsequent sections will discuss local scour in greater detail, given its relevance to this study's primary focus.

Figure 2-3: Photo of local scour around rectangular piers (www.pepevasquez.com).

2.4 Mechanism of Local Scour

The main mechanisms of local scour around bridge piers and abutments are:

1- The pressure gradients and mean flow velocities near the structure.

2- The formation of vortices as secondary flows.

3- The increased turbulence in the local flow field

2.4.1 Mechanism of Local Scour around the Pier.

It has long been known that downflow at the bridge pier's upstream face and the creation of vortices at the pier base are the primary mechanisms responsible for local scour Muzzammil et al.(2004).

Melville and Raudkivi (1977) stated that when the flow gets closer to the pier, it slows down and rests on the pier's face. As a result, the pressure at the pier face increases, as at the stagnation point on the pier's upstream side, the approach flow velocity is reduced to zero. The stagnation pressure is

greatest near the water surface and gradually decreases with depth, creating a downward pressure gradient along the pier face.The ensuing downflow creates a hole around the pier base and impacts the streambed. Just below the bed's level, the downflow's power reaches its maximum.

2.4.1.1 Formation of Vortices around Bridge Pier

According to Melville and Raudkivi (1977) the primary scouring agent is the downflow that impinges on the bed. The scour pattern around a circular pier is shown in Figure 2-4. The figure demonstrates how the presence of the pier generates a strong vortex motion that entrains bed sediments around the pier base Lauchlan and Melville (2001). As the scour hole develops, the down-flow rolls up and forms a complicated vortex system by interacting with the approaching flow. After that, the vortex continues downstream along the pier's sides. Due to its obvious similarity to a horseshoe, this vortex is frequently called a horseshoe vortex Breusers et al. (1977). Consequently, the horseshoe vortex developed due to the separation of flow at the upstream face of the scour hole that the down-flow had constructed. The horseshoe vortex is a lee eddy that resembles the ground roller or eddy that forms downstream of a dune crest Breusers and Raudkivi (1991). Beyond the pier, the dislodged particles are effectively transported by the horseshoe vortex. Although it represents a component of the scour process. The horseshoe vortex strength decreases with increasing scour depth, which reduces the sediment transport rate from the pier's base Lagasse and Richardson (2001). In addition to the horseshoe-shaped vortex around the pier base, Figure 2-5 illustrates the wake vortices, which are vertical downstream of the pier.

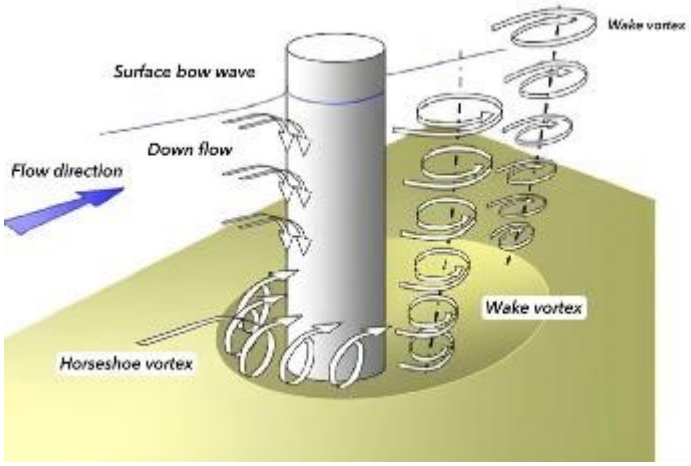

Figure 2-4: Sketch of the flow scour patterns at a circular pier (Melville and Coleman , 2000).

Wake vortices are created when the flow along the pier's sides separates. These wake vortices alternately shed from each side of the pier, and they are not stable. Riverbed sediments are removed by wake vortices, which are transported by approach flow, down flow, and horseshoe vortex Melville (1975). However, it should be mentioned that both the wake and horseshoe vortices erode material from the pier's base. The intensity of the wake vortices is significantly decreased with distance downstream, leading to sediment deposition that is common immediately downstream of the pier Richardson and Davis (2001).

The complex 3D flow, as shown schematically in Figure 2-6, means scour can occur on all sides of the pier. When an upward flow creates a circulation close to the free surface, bow waves are produced Melville and Raudkivi (1977). A bow wave does not dominate the scour mechanism of piers. It is observed that unless the flow depth is very shallow, it is approximately equal to the sum of the diameters of a bow wave and a horseshoe vortex. The horseshoe vortex and the bow wave conflict with each

other when the flow depth decreases Lee (2006); the bow wave weakens the horseshoe vortex and reduces the scour depth Hirshfield (2015).

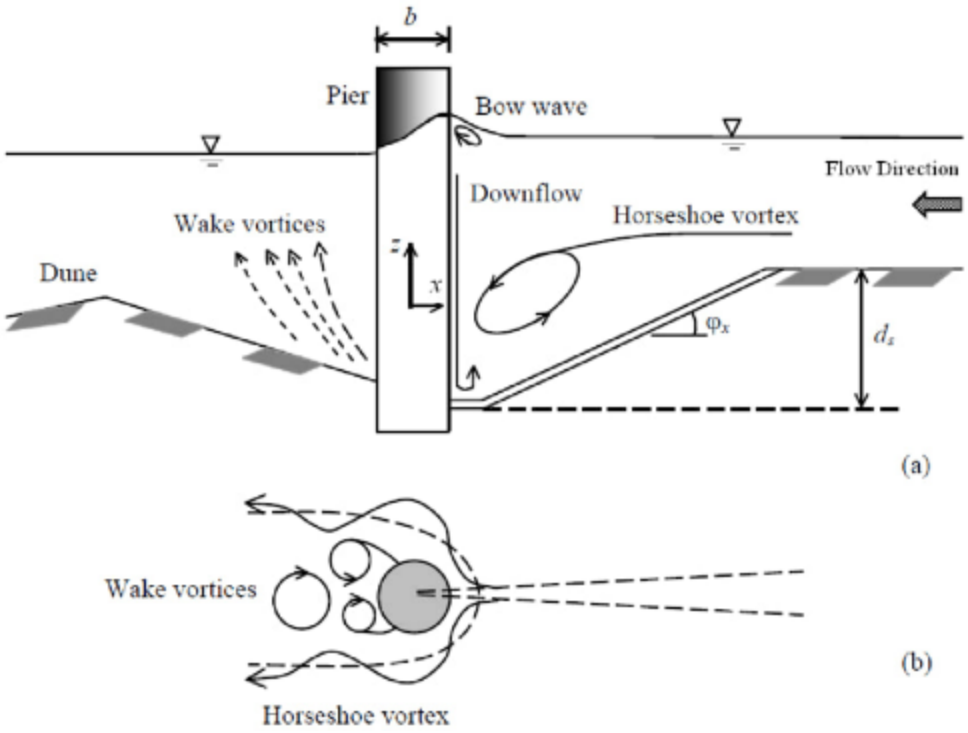

Figure 2-5: Flow structure at cylindrical pier: (a) vertical cross-section, (b) horizontal cross-section (Das et al., 2013).

2.4.2 Mechanism of Local Scour Around the Abutment

The way that abutments and their wing walls impede flow differs at the upstream corner; the flow approaching an abutment wall splits, creating a primary (horseshoe-shaped) vortex at the abutment's face. Kwan (1988) Kwan and Melville (1994) determined that the main source of abutment scour is downflow combined with a primary vortex that resembles the horseshoe vortex at piers. Due to the incoming flow's stalling, a vertical pressure differential forms at the abutment's upstream face. The pressure gradient drives the fluid downward, and it rolls up to become the primary vortex, which enlarges in size with the development of the scour hole.

The principal vortex and downflow are primarily restricted to the scour hole beneath the initial bed level, according to Kwan and Melville (1994). As the approaching flow depth changes, the downflow and vortex flow are mostly unaffected. Up to 78% of the flow's total circulation occurs in the inner core of the major vortex, taking up 17% of the scour hole's size. With an outside core region as a free vortex and an inner core region as a forced vortex, the main vortex has an oval form. They discovered a secondary vortex that was located adjacent to the original vortex and had a direction opposite to the primary vortex's spin. It is thought that the secondary vortex has the effect of limiting the first vortex's scouring ability.

The separation of flow upstream and downstream of the abutment corners results in wake vortices downstream of the abutment. When the flow separation rolls up to generate eddy structures known as wake vortices, unstable shear layers are produced. The mean flow causes wake vortices to move downstream, which operate as miniature tornadoes and pull up materials from the bed. In comparison to the main vortex, these wake vortices are quite feeble. Major flow components at a wing-wall abutment, identified by Kwan(1988), are shown schematically in Figure 2-6.

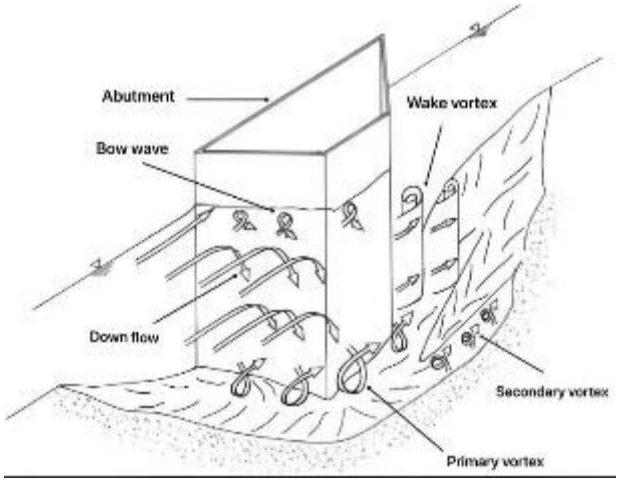

Figure 2-6: Schematic diagram of flow field at an abutment (Kwan, 1988).

2.5 Classification of Local Scour

Local scour at bridge piers can occur under two distinct regimes, depending on the upstream flow and sediment transport conditions. Chabert and Engeldinger(1956) initially categorized these regimes as clear-water scour and live-bed scour, based on the sediment transport characteristics of the approaching flow. The classification hinges on whether the incoming flow has sufficient capacity to mobilize bed sediments Chiew and Melville (1987). Clear-water scour refers to the condition in which sediment is not being transported upstream of the structure, typically occurring over a flat, non-erodible bed Raudkivi and Ettema (1983). In contrast, live-bed scour arises when sediment is actively supplied to the scour region by the upstream flow Dey (1999). Under clear-water conditions, the maximum scour depth is achieved when the flow loses the capacity to entrain further particles from the scour hole Breusers et al.(1977). In live-bed conditions, equilibrium is reached when the rate of sediment inflow to the scour hole equals the rate of sediment removal by the flow Melville (1984). Figure 2-7 illustrates how the maximum scour depth evolves over time under both scour regimes.

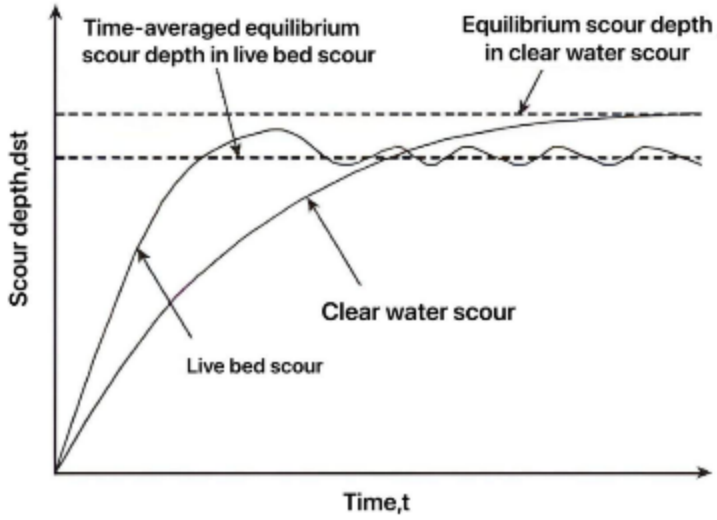

Figure 2-7: Clear-water and live-bed scour conditions (Raudkivi and Ettema, 1983).

Clear-water scour takes place when the average flow velocity does not exceed the critical velocity required to initiate sediment motion on the bed, that is, when v ≤ vc (or v/vc ≤ 1), Melville (1997). Conversely, live-bed scour develops when the flow velocity surpasses this critical threshold, i.e., v> vc (or v/vc > 1). The ratio v/vc, commonly referred to as flow intensity, serves as an indicator of whether bed sediment is mobilized.

According to Melville (1997), critical mean velocity (vc) and critical shear velocity (u*c) can be determined using the following equations:

$$\frac{\mathbf{Vc}}{\mathbf{u_{*c}}} = \mathbf{5.75 \log\left(5.53\ \frac{y}{d_{50}}\right)} \qquad \textbf{(2.1)}$$

Where u_{*c} = critical shear velocity based on the d_{50} size. The shields diagram for the appropriate size is used to calculate the shear velocity. For quartz sediments in water at 20°C, a useful approximation of the Shields diagram is:

$$\boldsymbol{u_{*c} = 0.0115 + 0.0125 d_{50}^{1.4}} \quad , \quad \mathbf{0.1\ mm < d_{50} < 1mm} \qquad \textbf{(2.2)}$$

$$\boldsymbol{u_{*c} = 0.0305 d_{50}^{0.5} - 0.0065 d_{50}^{-1}} \ , \quad \mathbf{1mm < d_{50} < 100mm} \qquad \textbf{(2.3)}$$

Where ($\mathbf{u_{*c)}}$ is in m/s and ($\mathbf{d_{50}}$), (**y**) are in mm.

Compared to a live-bed situation, the clear-water scour depth achieves its maximum over a longer period. Additionally, it can take many floods for local clear-water scour to reach its maximum depth Richardson and Davis (2001). According to Richardson and Davies, the maximum scour depth around piers under clear-water conditions is roughly 10% greater than the equilibrium depth observed under live-bed conditions. Furthermore, Melville and Chiew (1999) noted that in clear-water scenarios, the time required to reach equilibrium scour depth increases rapidly with increasing flow velocity.

In contrast, for live-bed scour, the time to equilibrium decreases significantly as flow velocity increases.. The formation of the equilibrium scour hole can take a very long period, as the equilibrium clear-water scour depth is attained asymptotically over time.

2.6 Factors Affecting Local Scour

According to (Raudkivi and Ettema (1983); Arneson et al. (2012); Richardson and Davis (2001); Lagasse and Richardson (2001); and Ettema and Melville (2011)), the following factors influence the local scour depth at piers and abutments:

(1) Velocity of the approaching flow (v)
(2) Upstream flow depth (y)
(3) Width of the pier (b)
(4) Acceleration gravity (g)
(5) Effective length of the pier in skewed flow and projected length of the abutment
(6) Size and gradation of the bed material (σ_g, ρ_s).
(7) Angle of attack of approach flow to the pier and abutment skew
(8) Pier shape and abutment shape configuration.
(9) Bed configuration.
(10) Ice or debris jams.
(11) Channel/Floodplain Geometry.
(12) Time and flow Duration.

The processes contributing to pier scour at a cylindrical pier in a single stratum of non-cohesive foundation material involve the basic variables shown in Figure 2-8.

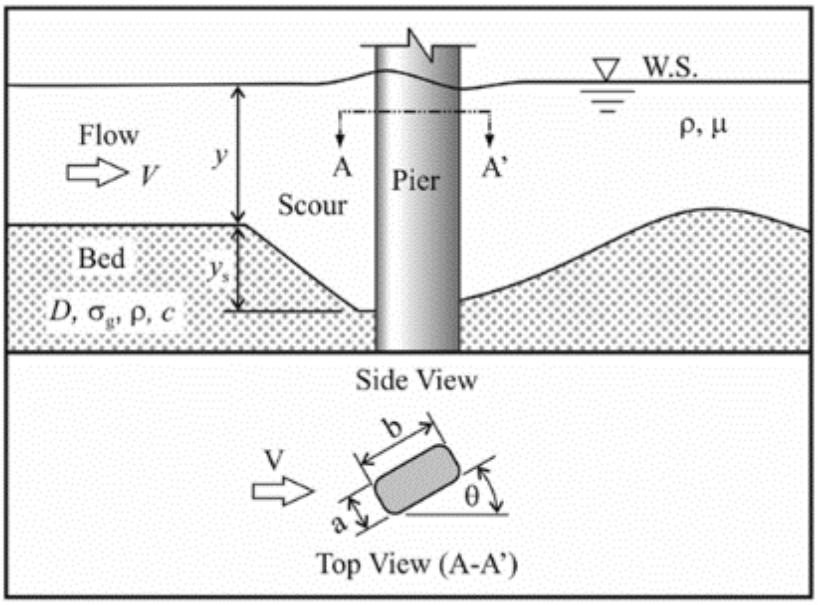

Figure 2-8: Variables influencing pier scour at a cylindrical pier (Ettema and Melville, 2011).

The metrics listed above may be categorized under four main headings, according to Breusers et al.(1977) and Ansari et al. (2002).

• **Approaching stream flow parameters:** flow intensity, flow depth, shear velocity, mean velocity, velocity distribution, flow duration, and bed roughness.

• **Pier and abutment parameters:** pier dimensions, abutment dimensions, geometry, number, spacing, and orientation concerning the direction of the highest flow (i.e., angle of attack).

• **Bed sediment factors:** include cohesiveness, angle of repose, particle shape, mass density, and grain size distribution.

• **Fluid parameters:** Kinematic viscosity, mass density, and acceleration gravity.

2.6.1 Flow Intensity (v/vc)

According to Melville and Chiew (1999) flow intensity is defined as the ratio of the approach mean velocity (v) to the critical mean velocity (vc),

or the ratio of the shear velocity (u*) to the critical shear velocity (u*c). As noted by Melville and Coleman (2000), under clear-water conditions and with uniformly graded sediment, the local scour depth increases approximately linearly with flow velocity, reaching a maximum value at the threshold velocity. The relationship between local scour depth at bridge piers and flow intensity (or approach velocity) is illustrated by laboratory results, as shown in Figure 2-9. The maximum scour depth occurs when v/vc = 1, a point referred to as the threshold peak.

For uniform sediments, scour depth initially decreases and then increases to form a second peak when flow velocity exceeds the threshold; however, the threshold peak is not reached again as long as the sediment remains uniform. Breusers et al.(1977) reported that no local scour develops when flow intensity is $v/vc \leq 0.5$, while clear-water scour conditions exist for both uniform and non-uniform sediment when the flow intensity ranges between 0.5 and 1.0.

These patterns have been documented in multiple earlier studies, including those by (Laursen and Toch (1956); Chabert and Engeldinger (1956);Shen et al.(1969); Gill (1972); Breusers et al.(1977); Ettema (1980), and Raudkivi and Ettema (1983);Garde et al.(1985)).At the threshold for clear-water conditions, the maximum scour depth in uniform sediments is observed. As summarized by Richardson and Davis (2001), "the greater the velocity, the deeper the scour depth."

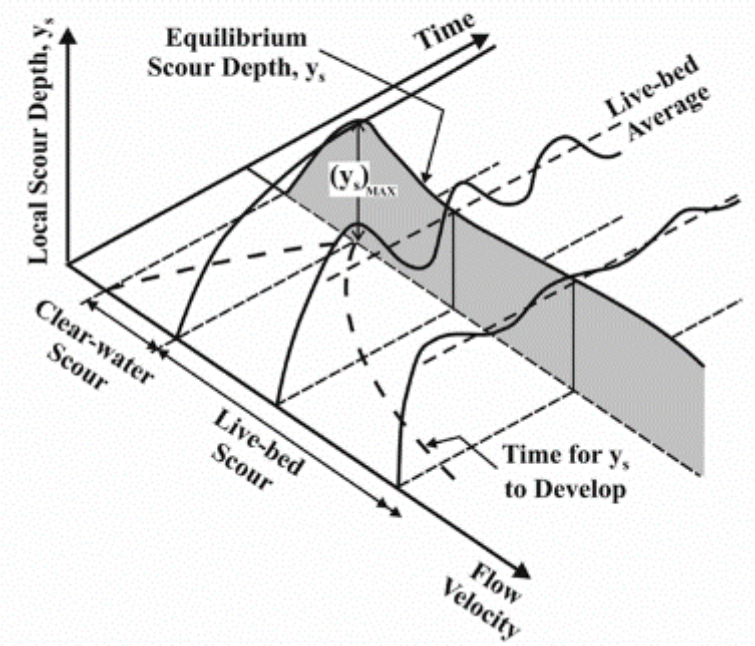

Figure 2-9: Local scour depth variation with flow intensity, v/vc (Melville and Coleman 2000).

2.6.2 Flow Depth (y)

The role of flow depth in influencing local scour has been extensively investigated by several researchers (e.g., Chabert and Engeldinger(1956); Laursen and Toch (1956); Breusers et al. (1977); Ettema (1980); Breusers and Raudkivi (1991); Hoffmans and Verheij (1997), and Melville and Coleman (2000)). Flow depth is recognized as a critical parameter that significantly influences the magnitude of local scour. For bridge piers, an increase in flow depth can result in a twofold or greater increase in scour depth. In contrast, for abutments, the influence of flow depth is generally less pronounced and depends largely on the specific geometry of the abutment. Arneson et al.(2012). Because the pier is located within the channel, a surface roller develops around it, and a horseshoe vortex forms at its base. Flow depth affects the local scour depth when the horseshoe vortex interacts with the surface roller

(bow wave) that happens at the pier's leading edge.As long as there is no interference between the two rollers, the local scour depth is independent of the flow depth and only depends on the pier diameter.

Local scour is believed to occur at narrow piers in such situations, sometimes called deep flow. The surface roller becomes comparatively more prominent as the flow depth decreases, which reduces the horseshoe vortex's ability to entrain sediment. Consequently, local scour depth decreases for shallower flows. It is then said that local scour occurs at a broad pier in very shallow flow, depending on flow depth Alabi (2006). According to Richardson and Davis (2001), scour depth is directly influenced by flow depth. An increase in flow depth can cause pier scour to increase by a factor of two or more.

Ashtiani and Kordkandi (2013) stated that when the ratio of flow depth to pier width surpasses 4, scour depth becomes independent of flow depth. Melville (2008) clarified that the influence of the flow depth concerning the pier width is represented by the flow shallowness y/b. The scour depth is independent of y and increases proportionally with pier width for narrow piers or deep flows relative to pier width. On the other hand, the scour depth increases proportionally with y and is independent of b for shallow flows relative to the pier width, but depends on both y and b for intermediate depth flows. Figure 2-10 provides a graphic representation of these tendencies.

In conclusion, observation showed that local scour at piers increases with flow depth at shallow flow depths, but that the scour depth becomes independent of flow depth and instead depends on pier diameter at deeper water depths (i.e., deep flow).

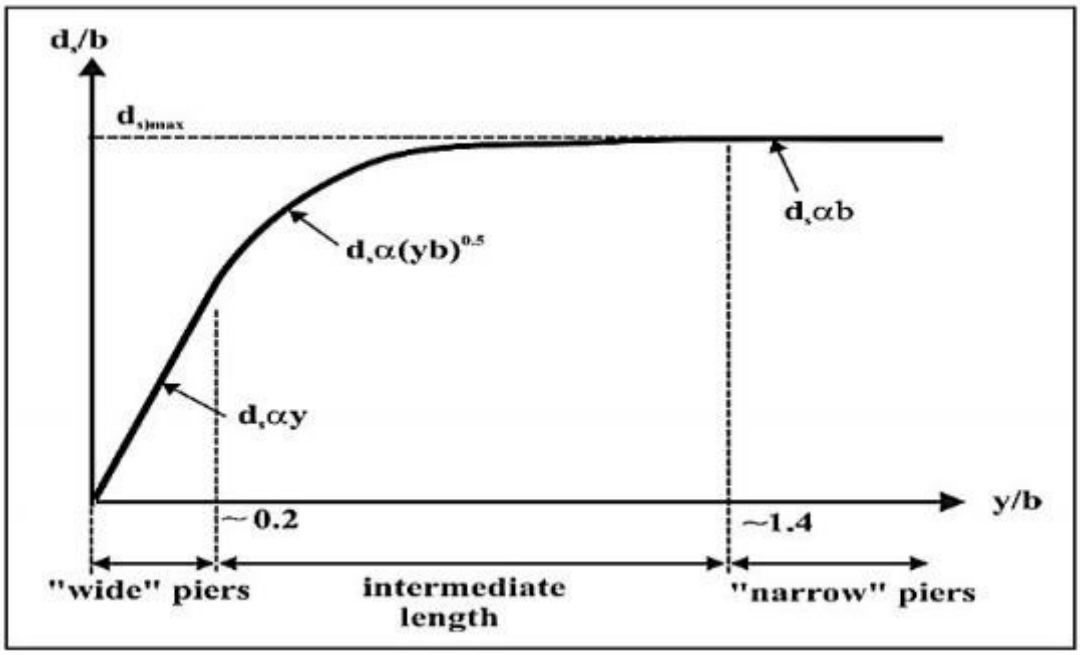

Figure 2-10: Local scour depth variation with flow shallowness (Melville, 2008).

2.6.3 Sediment Size and Gradation

Laboratory experiments of Ettema (1980) show that the greatest local scour depths occur for uniform diameter sediments. For this reason, most researchers conduct their experiments with near-uniform sediments (i.e., sediments with low values of sigma (geometric standard deviation of particles), $\sigma_g = \sqrt{\frac{D_{84}}{D_{16}}}$. The critical flow velocity for the beginning of sediment motion is frequently used to describe the impacts of the sediment material's density and particle size. The study of Raudkivi and Ettema (1977) which examined the impact of sediment size on the local depth of scour at a bridge pier, this observation was reported by Breusers and Raudkivi (1991). The experiments were conducted under clear-water conditions using a pier with a diameter of 102 mm in a flume measuring 1.5 meters in width. It was found that ripples tend to form when the median sediment size (d_{50}) is less than 0.7

mm, while no ripple formation occurs when d_{50} is equal to or greater than 0.7 mm. Furthermore, the study indicated that the scour behavior differs notably between sediments that produce ripples ($d_{50} < 0.7$ mm) and those with larger grains that do not ($d_{50} \geq 0.7$ mm).

According to Raudkivi and Ettema (1977) stable experimental conditions can be maintained with a shear flow velocity of approximately $u=0.95u*_c$ for coarser sediments ($d_{50} \geq 0.7$ mm) that do not form ripples, without causing disturbance to the upstream bed. However, this is not feasible for finer sediments ($d_{50} < 0.7$ mm), as ripples develop and slight general sediment transport occurs, replenishing the scoured area around the pier. Consequently, a flat bed cannot be preserved near the threshold shear stress for uniform fine sands, meaning that true clear-water conditions cannot be achieved under these circumstances.

Breusers and Raudkivi (1991) further concluded that for silts with $d_{50} <$ 0.7 mm, ripple formation typically begins when the shear velocity exceeds $u >0.6u*_c$. Since live-bed scour commences shortly after the experiment begins, clear-water conditions are not maintained long enough for finer sands to reach the same maximum scour depths as coarser, non-ripple-forming sediments. An exception exists when the geometric standard deviation (σ_g) of the sand is between 1.3 and 1.5, indicating non-uniform sediment. In such cases, coarser particles may armor the bed surface but are not sufficient to protect the scour hole under stronger flow conditions. Thus, it becomes possible to observe clear-water scour depths comparable to those seen in coarser, ripple-free sediment beds.

2.6.4 Sediment Coarseness

Melville and Coleman (2000) defined sediment coarseness as the ratio of the sediment material's mean grain size (d_{50}) to its pier width (D), or D/d_{50}.The authors claim that as long as the sediment coarseness ratio D/d_{50} is less than 50, the size of the sediment has an impact on local scour. The coarseness of the sediment has little effect on local scour when D/d_{50} >50. Figure 2-11 shows the local scour depth against the sediment coarseness ratio, where D is pier diameter, Z is scour depth, and Z_{max} is maximum scour depth.

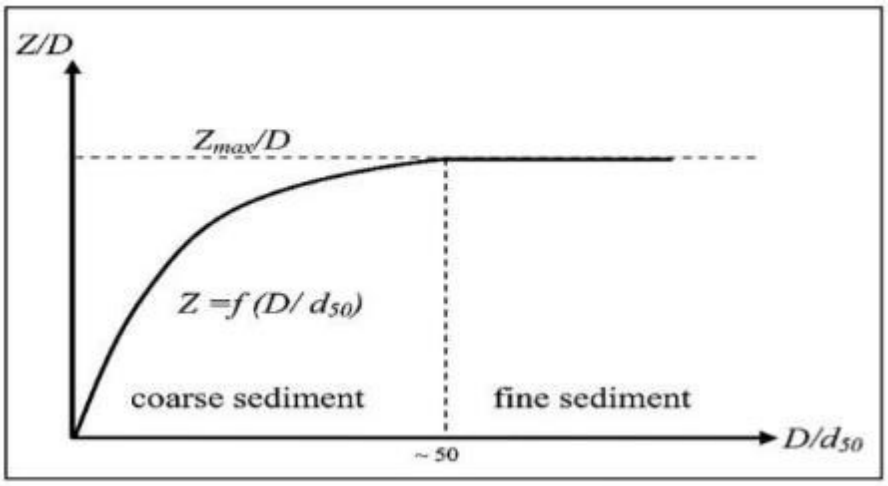

Figure 2-11: Local pier scour depth against sediment coarseness (Melville and Coleman, 2000).

According to Ettema (1980), erosion is hampered by pier scour because the porous bed absorbs some of the downflow energy. For small values of the sediment coarseness ratio, individual grains are large relative to the scour groove that the downflow excavates. When D/d_{50} is less than 8, the individual grains are so big that the pier entrainment at the pier's sides is the primary cause of scour Melville and Coleman (2000). Typically, the geometric standard deviation of the sand size, $\sigma_g = \sqrt{\frac{D_{84}}{D_{16}}}$, is used to quantify sediment gradation. According to (Hoffmans and Verheij , 1997), σ_g is around 1.8 for

natural river sand and 1.3 for uniform sand. Under clear-water scour conditions, Ettema (1980) investigated how sediment gradation affected the local scour depth at a circular pier. The median size of the sediment material was utilized, and the study was carried out at the threshold of motion condition. It was determined that as the standard deviation of the particle size distribution increases, the rate of scour hole development and the equilibrium scour depth reduce. Around the threshold condition, u/u*c=1, armored takes place at the base of the scour hole and on the approach flow bed for a non-uniform sediment material (i.e., at a larger value of σ_g). A significant decrease in the local scour depth is caused by the armoring at the scour hole's base. The scour depth is only marginally impacted by sediment with non-uniformity at high u/u*c values, when the flow may entrain the majority of particle sizes in the non-uniform sediment.

2.6.5 Pier Shape

Bridge piers can be built in a variety of shapes. The most often utilized shapes include oblong, lenticular, square, rectangle with chamfered ends, round, rectangular, and Joukowski. An instance of several pier forms is shown schematically in Figure 2-12.

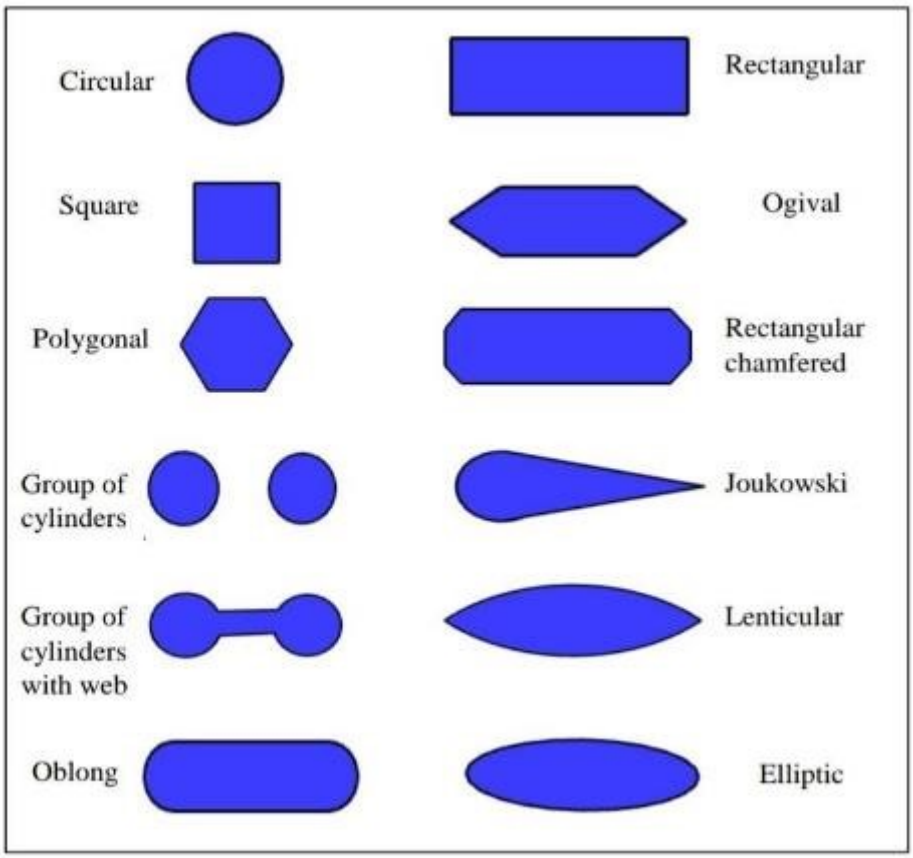

Figure 2-12: Diagram sketch of some common pier shapes (Alabi, 2006).

Numerous researchers, including (Laursen and Toch (1956); Breusers et al.(1977); Breusers and Raudkivi (1991), and Melville and Coleman (2000), have documented the impact of pier shape. The general conclusion was that the local scour has often been found to be deeper on blunter piers. Shen et al. (1969) divided pier forms into two groups: blunt-nosed and sharp-nosed piers. Due to the powerful horseshoe-vortex system created by blunt-nosed piers, the pier nose experiences the greatest scour depth. The shape of the upstream pier plays a dominant role in influencing the scour depth, whereas the shape and length of the downstream pier have minimal impact, particularly when a blunt-nosed pier is aligned with the flow direction. In such cases, the horseshoe vortex system is notably weak, and the greatest scour depth tends

to form near the downstream extremity.Melville (1975) classified pier geometry based on form, width, length, and alignment with flow as simple piers and complex piers. Piers with a consistent section throughout their depth are known as simple piers.

According to Melville (2008), complex piers have tapering piers, caissons, slab footings, and piled foundations. The amount of scour was significantly impacted by the piers' form. Simplifying the front end of a pier lowers the scour depth and horseshoe vortex strength. The wake vortices' intensity is decreased by simplifying the piers' downstream ends. Richardson and Davis (2001) claimed that the equilibrium scour depth may be influenced by the pier nose shape by up to 20%. The transition-pier category is in the middle of the narrow-pier and wide-pier categories of pier scour, with the flow field being significantly different for each Ettema and Melville (2011). According to their report, these groups are roughly defined as:

- Narrow piers ($y/a^* > 1.4$). The pier face usually has the deepest scour.
- Transition piers ($0.2 < y/a^* < 1.4$). The pier face has the deepest scour depth, which is governed by y/a^*.
- Wide piers ($y/a^* < 0.2$), where the pier flank usually has the deepest scour. Bridge piers are somewhat uncommon in this group. Where y = undisturbed approach flow depth, and a^* = effective pier width.

2.6.6 Abutment Shape

The abutment shape has a significant impact on the equilibrium scour depth. Streamlined obstacles, such as semicircular, spill-through, and wing-wall abutments, create weak turbulent vortices, but blunt obstructions, like vertical-wall abutments, can create powerful turbulent vortices. This results

in a comparatively significant scour depth at a blunt obstruction. According to laboratory experimental data, vertical wall abutments generate a deeper scour than spill-through and wing-wall abutments (Laursen and Toch (1956)**;** Garde et al. (1985) , and Wong (1982)). Shape factor Ks was employed by Melville (1992, 1995, 1997) to take into consideration how abutment form affects equilibrium scour depth. Table 2-1 lists frequently used abutment forms along with the corresponding shape factor values. Since the vertical plate is the most basic abutment form, it serves as a reference. The length of the abutment at mid-depth in the flow is used for spill-through abutments. Table 2-1 shape variables are based on laboratory experimental data from (Dongol (1994); Gill (1972); Wong (1982); Tey (1984); Kwan (1984), and Kandasamy (1989). However, according to Melville (1992), the significance of abutment shapes becomes less in longer abutments.

Table 2-1: Abutment shape factors.(Barbhuiya and Dey, 2004).

Abutment model	Abutment shape	Shape factor, K_s
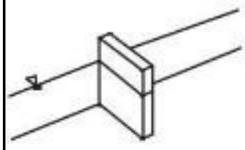	Vertical-wall	1·00
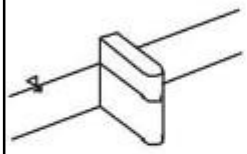	Semicircular ended	0·75
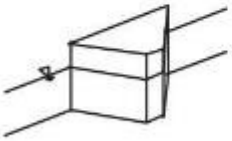	45° wing-wall	0·75
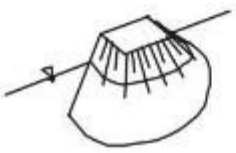	Spill-through with slope horizontal : vertical 0·5 : 1 1 : 1 1·5 : 1	 0·60 0·50 0·45

2.6.7 Pier and Abutment Size

It is evident from experiments that there is a relationship between the scour depth and pier size Breusers et al.(1977). This phenomenon was physically explained by the formation of a horseshoe vortex system, whose size depended on the diameter of the pier. Shen et al.(1969) noted that the horseshoe vortex, one of the primary scouring agents, is proportional to the pier Reynolds number (Re_p) ($Re_p = VD/\nu$), which is ultimately determined by the pier diameter. The scour depth is consequently proportional to the pier width for a given value of mean approach flow velocity.

The scour hole volume increases with pier size, and the scour hole formation period for a given shear stress ratio similarly increases with pier size Alabi (2006). Arneson et al. (2012) stated that the length of a pier does not significantly affect the depth of local scour when it is aligned with the flow direction. However, if the pier is positioned at an angle to the flow, its length becomes an important factor influencing the scour depth. The impacts of the wall channel at the abutment will lower the flow velocity, resulting in less scour than at the pier for the same size Kwan and Melville (1994).

In laboratory flume experiments, increasing the length of an abutment or embankment that extends into the flow tends to increase the scour depth. However, this relationship does not hold consistently in field conditions. Due to the limited size of laboratory flumes, the flow from the floodplain that is blocked by the embankment and redirected to the main channel is closely tied to the length of the obstruction. In contrast, in natural settings, embankment length does not accurately reflect the amount of floodplain flow returning to the main channel. This leads to the presence of "ineffective flow" on the floodplain, especially on wide, densely vegetated floodplains. To correctly apply abutment, scour equations developed from laboratory studies to real-

world scenarios, it is essential to identify the boundary separating "live flow" from "ineffective flow." This boundary should then be used to define the effective length of the abutment or embankment when calculating scour Arneson et al. (2012).

2.6.8 Angle of Attack (Alignment)

The angle formed between the direction of the flow and the orientation of a pier or abutment is referred to as the angle of attack Hoffmans and Verheij (1997). The alignment of the pier relative to the flow direction plays a crucial role in determining the extent of local scour across various pier shapes, though circular piers are a notable exception. As the angle of attack increases, so does the effective frontal width of the pier, which in turn leads to greater scour depth Melville and Coleman (2000). When a pier is aligned parallel to the flow, its length has minimal influence on scour. However, if the pier is skewed, the length becomes a significant factor in scour development. For instance, Melville and Coleman (2000) showed that a rectangular pier with an aspect ratio of eight, skewed at 30°, experiences nearly four times the scour depth compared to the same pier aligned with the flow.

In the case of abutments, tilting the structure downstream tends to reduce scour, while upstream tilting increases it. Ahmad (1953) found that orienting an abutment at a 45° angle downstream can reduce the maximum scour depth by approximately 20%, whereas orienting it 45° upstream can increase it by about 10%. As the skew angle grows, the point of maximum scour around a pier shifts toward the downstream side, with the rear face experiencing greater scour than the front. To minimize scour risk, Breusers and Raudkivi (1991) recommended maintaining angle of attack values below

5°–10°. Figure 2-13 presents a visual representation of a pier and abutment skewed relative to the flow direction.

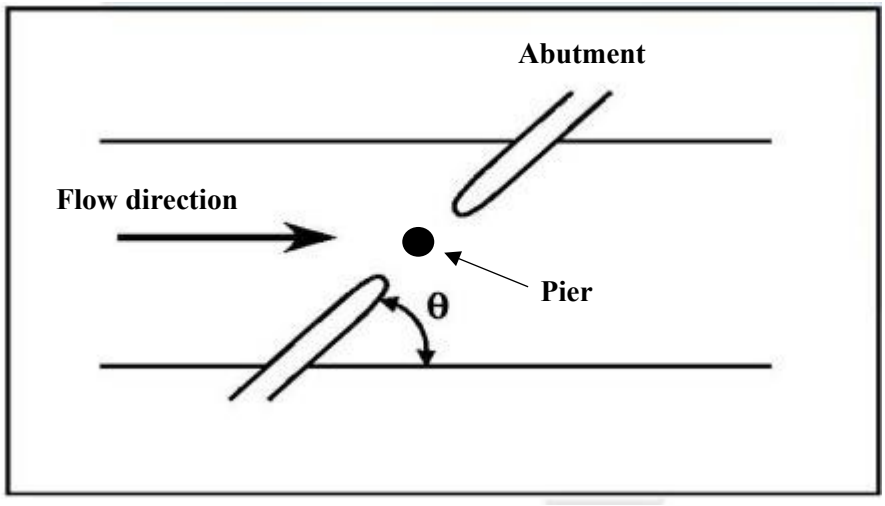

Figure 2-13: The skewed pier and abutment to the stream in the upstream direction (Ahmad, 1953).

2.6.9 Contraction Ratio

The contraction ratio, defined as the ratio of pier width to channel width, plays a significant role in determining the equilibrium scour depth at piers. To minimize flow blockage effects in experimental settings, it is recommended that the flume width be at least eight times the pier diameter under clear-water scour conditions Shen et al.(1969). For live-bed scour experiments, where sediment transport can be influenced by flow constriction, a wider flume at least ten times the pier diameter, is advised to avoid alterations in bed conditions. However, Raudkivi and Ettema (1983) suggested that the ratio of flume width to pier diameter should not be less than 6.25 to ensure representative flow behavior.

Moreover, when the pier diameter exceeds approximately 10% to 12% of the flume width, flow constriction effects become more pronounced. Under such conditions, interactions occur between the reverse eddies generated near the flume walls and the primary horseshoe vortex forming at the base of the

pier, similar to the interference observed between surface rollers and primary vortices in shallow flow scenarios. These interactions can significantly alter the flow field and scour patterns near the pier Mia and Nago (2003).

2.7 Time Effect on Local Scour Depth

The temporal development of scour around a cylindrical pier was initially characterized by Chabert and Engeldinger (1956), who described how scour depth evolves. It is essential to recognize that variations in flow patterns around the pier and differences in the properties of the foundation material significantly influence the rate at which scour progresses Ettema and Melville (2011). Notably, the development of local scour differs markedly under clear-water and live-bed conditions due to the distinct sediment transport mechanisms governing each regime. In clear-water conditions, scour progresses gradually, approaching the equilibrium depth asymptotically, whereas in live-bed conditions, scour develops more rapidly and fluctuates due to the movement of bedforms Ettema and Melville (2011). The equilibrium scour depth under live-bed conditions is typically about 10% less than that observed in clear-water conditions Shen et al. (1969), as illustrated in Figure 2-9.

The definition of "time to equilibrium scour" plays a critical role in the interpretation of experimental results. Fanzetti et al. (1982) emphasized that inconsistent or ambiguous definitions of this timeframe can significantly influence the conclusions drawn from experiments, even when conducted under identical conditions. Because reaching true equilibrium may require extended durations, various researchers have proposed different criteria for defining the time to equilibrium scour depth (e.g., Heidarpour et al., (2003);

Zarrati et al., (2004); Mia and Nago, (2003), and Sheppard et al. (2004)). Ettema(1980), for example, defined equilibrium as the point at which the increase in scour depth does not exceed 1 mm over a four-hour period. Alternatively, Melville and Chiew (1999), along with Sheppard et al.(2004), considered equilibrium to be achieved when the scour depth remained stable, with no more than a 5% change relative to the pier diameter over 24 hours.

2.8 Equilibrium Scour Depth

The vertical distance between the stable bed level and the deepest point in the scour hole is known as the equilibrium scour depth, according to Gazi and Afzal (2020). Conversely, the equilibrium scour depth was described by Laursen and Toch (1956) as the condition of balance when the amount of material provided by the approach flow's normal transport equals the amount of sediment removed from the scour hole. Erosion of the flow border gradually achieves a balance between the flow's erosive capacity and the bed sediment's resistance to motion. It can take an endless amount of time for the equilibrium scour hole to form, according to Melville and Chiew (1999), since an equilibrium clear-water scour state is approached asymptotically with time. Under live-bed conditions, the scour depth can quickly approach equilibrium, and the bed forms cause the scour depth to oscillate over time.

2.9 Previous Works

Reviewing previous studies is a fundamental part of any scientific research, as it provides a theoretical and practical background that helps clarify the context of the current work. It highlights the progress made in the field, identifies existing knowledge gaps, and supports the rationale for the present study. Primary approaches and recent studies related to this topic are reviewed as follows:

Maatooq (2008) described the scour around the bridge pier near the abutment and offered the findings of a limited experimental program that addressed the issue. The experiments were conducted in a closed system, water-recirculating flume that was 2 m long, 0.61 m wide, and 0.2 m deep. The maximum discharge used was 3.3 l/s. A layer of sand with a thickness of 8 cm and a mean particle size of d_{50} = 0.575 mm was used as a bottom layer of the working section. There were seven runs, two of which are referred to as pier alone and abutment only. The remaining five runs are provided to illustrate how the distance between a pier and an abutment affects local scour around a pier and its pattern. The findings typically indicate that the scour is dependent on the pier-abutment interaction distance.This distance is addressed by a modification factor, which is shown as a multiplicative factor and applied to an empirically derived scour depth prediction formula surrounding the bridge pier as follows:

$$\frac{d_s}{b} = \left(0.519 + 2.5\left(\frac{V}{VC} - 0.57\right) y/b \right) k_{dis} \qquad \textbf{(2.4)}$$

It should be noted that the K_{dis} can be taken from Figure 2-14 or the following empirical equation:

$$k_{dis} = 1 - 0.013\left(\frac{X}{b}\right)^2 + 0.130\left(\frac{X}{b}\right) \qquad \textbf{(2.5)}$$

Where: d_s = maximum scour depth, b = width of pier or abutment,

x =spacing between pier and abutment, y = flow depth,

and K_{dis} = distance coefficient.

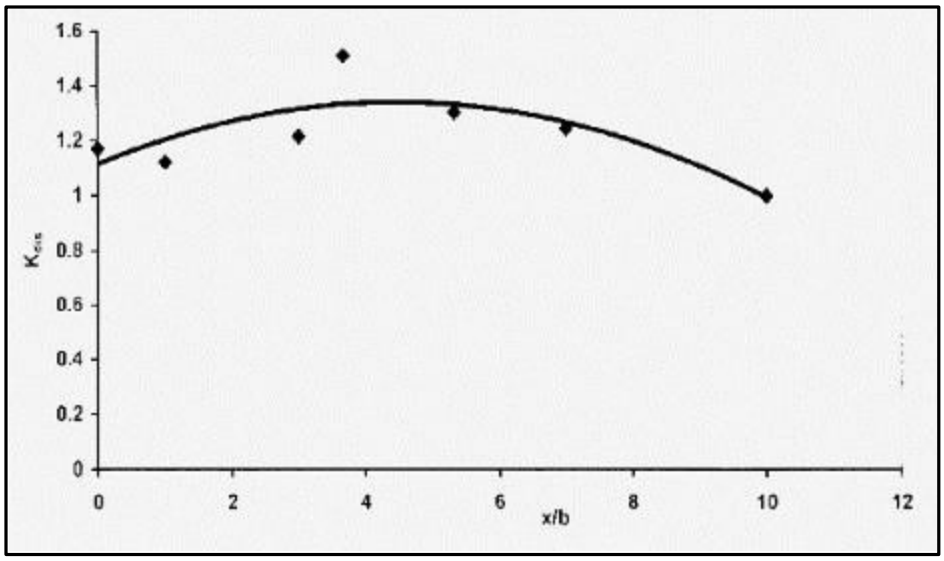

Figure 2-14: The close-fitting curve for the distance coefficient.

Oben-Nyarko and Ettema (2011) a series of flume experiments were conducted to investigate the potential interaction between pier scour and abutment scour in a non-cohesive boundary. Bathymetric data, scour locations, and scour depths were recorded for two common abutment types: wing-wall and spill-through. The results for the tested abutment–pier configurations indicated that the presence of a pier did not significantly increase the abutment scour depth; however, it could reduce the scour depth when the pier was positioned near the spill-slope toe of a spill-through abutment. In such cases, the pier acted as a stabilizing element, retaining spill-slope soil and riprap material within the scour zone. Nevertheless, scour at a pier located adjacent to an abutment was largely governed by the scour at the abutment, and consequently, it could substantially exceed the depth predicted for an isolated pier.

Mohamed et al. (2016) both experimental and numerical investigations to evaluate the maximum scour depth that developed around

bridge abutments in sandy soils. The study examined the effects of varying channel contraction ratios and abutment entrance angles using physical models and a three-dimensional numerical model (SSIIM software). The results indicated that scour depth at the abutment increased with higher contraction ratios. Moreover, abutments with gentler entrance angles (10° and 15°) experienced significantly less scour compared to those with steeper angles. In particular, adopting a 10° entrance angle resulted in a 92% reduction in scour depth relative to a 90° angle. The numerical simulations performed with SSIIM showed strong reliability in predicting scour patterns, achieving an average correlation coefficient of 97% when compared with the experimental data.

Memar et al. (2016) used wing-wall abutments with lengths of 25, 37.5, and 50 cm, along with circular, round-edge, and sharp-edge piers, which were positioned at two distances: 17.5 cm and 35 cm from the bank wall in the floodplain. The study aimed to demonstrate how abutment length and pier form influence scour depth. The findings indicated that the scour depth of the abutment increases as the pier approaches, with the round pier showing the lowest scour depth and the sharp-edge pier indicating the greatest.For instance, a sharp-edge pier positioned near the abutment was found to significantly increase the scour depths of both the abutment and the pier compared to their individual scour depths.

Alkhouly et al. (2019) conducted a series of laboratory experiments to assess the maximum scour depth associated with various abutment shapes. This study compared four abutment configurations: vertical abutment, semicircular-ended abutment, abutment with a vertically sloped face, and wing wall abutment. Additionally, the effect of installing piles on reducing maximum scour depth was examined. For vertical abutments, changes in

width had only a minor effect on scour depth. In the case of semicircular-ended abutments, increasing the radius of curvature (R) resulted in a reduction in scour depth. For abutments with sloped vertical faces, a greater side slope angle (θ) was found to reduce scour depth. Similarly, for wing wall abutments, a decrease in wall angle (∝) led to a reduction in scour depth. Among all configurations, the wing wall abutment with a wall angle of 60° exhibited the least scour depth, achieving a 22.68% reduction compared to the vertical abutment. Furthermore, the inclusion of piles (with $D_p/B = 0.08$ and $X/B = 0.25$) reduced the maximum scour depth by 22% relative to the case without piles. Across all abutment types, an increase in the Froude number was associated with greater scour depth. Empirical equations were also developed to estimate the maximum scour depth for each abutment shape studied.

Al-Awadi and Al-Khafaji (2020) examined how debris accumulation affects the length, width, and submerged depth of the scour depth close to the bridge pier. Experiment with three different woody debris accumulations under clear-water conditions.The findings showed that the scour depth increases by around 140% when the blocked area of debris is increased to 27%. Two empirical exponential formulas were derived to forecast how debris would affect the maximum scour depth, with ($R^2 = 0.96$) and the modification factor needed for a single pier.

Ben Mohammad Khajeh and Vaghefi (2020) explored the influence of abutments in the presence of a pier on scour depth and changes in bed topography through a series of experiments. The tests involved abutments that were twice the length of the pier and included both vertical and inclined piers, with inclinations directed upstream, downstream, as well as toward the inner and outer banks. The findings indicate that in all scenarios, the greatest scour depth consistently occurred on the upstream side of the outer abutment.

Additionally, in most cases, the maximum scour depth was observed at an angle of 89 degrees and within the bend region located 92% to 94% across the channel width from the inner bank. However, in the specific case where a single pier was inclined downstream, the maximum scour occurred at a 90-degree angle and 88% of the channel width from the inner bank.

Abed and Majeed (2020) employed numerical simulation to investigate scour patterns and the influence of spacing between bridge piers under defined hydraulic conditions, including flow velocity, water depth, and effective sediment diameter. The research also examined how different pier cross-sectional shapes affect local scour depth, using Computational Fluid Dynamics (CFD) via ANSYS Fluent software. The numerical results were validated by comparing them with existing laboratory data, demonstrating good overall agreement between the simulation and experimental outcomes. A clear inverse relationship was observed between scour depth and pier spacing; larger spacing resulted in reduced scour depths. For pier spacing ratios of 2, 3.5, 4.6, and 5.5, the corresponding maximum scour depths were 50 mm, 37 mm, 34 mm, and 32 mm, respectively .Among the pier shapes tested, the triangular-nose pier exhibited the least scour depth, followed by the oblong pier, while the circular pier resulted in the highest scour depth.

Al-Shukur and Hussein (2021) conducted laboratory tests to assess how bridge pier design and skewness angle affected local scour. A transparent rectangular flume with a steel frame structure was used for the experiments in the lab. Three sets of piers (4 cm in width and 40 cm in length) arranged in a single row with two distinct shapes (lenticular and oblong) and four different skewness-angles (α) (0°, 15°, 30°, and 45°) were used in the experimental work, which was conducted in clear water. The ratio of the width pier to the spacing between piers was maintained at 2. Furthermore, three velocities were

used to investigate how flow velocity affected local scour: 0.17, 0.23, and 0.27m/s. Sand with a geometric standard deviation of 1.14 and an average grain size (d_{50}) of 0.71 mm was used as the flume bed. The collected data demonstrated that all of the characteristics under study (skewness-angle, flow velocity, and pier form) had a substantial impact on the depth of the local scour. In the lenticular piers, the lowest scour depth (1 cm) was observed when the skewness-angle and flow velocity were 0° and 0.17 m/s, respectively, while the greatest scour depth (13.2 cm) was observed when the skewness-angle and flow velocity were 30° and 0.27 m/s, respectively.

Ali and Güna (2021) conducted a comprehensive study utilizing Artificial Neural Networks (ANN) to estimate equilibrium local scour depth around bridge piers. The authors trained eight ANN models using 400 laboratory datasets collected from various experimental studies, incorporating both dimensional and non-dimensional variables, including pier diameter, flow velocity, flow depth, sediment diameter, and critical velocity. The primary objective was to assess the effectiveness of ANN models compared to traditional regression-based methods in predicting scour depth under steady flow conditions.The most accurate model developed in the study, referred to as DM-1, used the Levenberg–Marquardt backpropagation algorithm with 11 hidden nodes. This model achieved a high regression coefficient (R^2= 0.9585).A key contribution of the study is the sensitivity analysis performed to evaluate the relative influence of each input parameter. Results revealed that the pier diameter is the most critical factor affecting the prediction accuracy. When the pier diameter was excluded from the model input, the regression coefficient decreased drastically to (R^2=0.415).

Muhsen and Khassaf (2022) focused on measuring the maximum scour depth and analyzing the interaction effects between piers and abutments

through controlled laboratory experiments. A vertical-wall abutment was tested alongside two pier shapes (oblong and lenticular) at three different spacings (23.5 cm, 16.0 cm, and 9.0 cm). The findings revealed a significant increase in the scour depth ratio with rising flow intensity, higher Froude numbers, and decreasing flow depths. Additionally, as the spacing between the pier and abutment decreased, pier scour increased for both pier shapes, while abutment scour decreased. The oblong pier produced a maximum scour depth approximately 10.8% greater than that caused by the lenticular shape. Moreover, new empirical equations were developed using IBM SPSS Statistics 21, with (R^2 =0.969, 0.974, and 0.978) for oblong, lenticular, and abutment scour, respectively.

Saeed et al. (2023) conducted laboratory experiments and flow analysis to investigate the interaction between bridge piers and abutments and their influence on clear-water scour. The experiments were carried out in a rectangular flume and comprised 18 primary tests involving different combinations of pier and abutment types, along with five control tests using individual piers or abutments. Three types of piers were tested, a rectangular pier with rounded edges, a group of three cylindrical piers, and a single cylindrical pier, along with two abutment types: a wing wall abutment and a semicircular abutment. A three-dimensional Acoustic Doppler velocimetry (ADV) was employed to measure flow characteristics, including streamlines, velocity magnitudes, vertical velocities, and bed shear stress.

Results revealed that flow velocity near piers and abutments increased by as much as 80%. The maximum scour depth near the abutment increased by up to 19%, while around the pier it increased significantly, up to 171%. When a pier was located near an abutment, the volume of the resulting scour hole increased by up to 87% compared to an isolated abutment. Additionally,

empirical equations were developed to reliably estimate the maximum scour depth at piers positioned adjacent to abutments Eqs. (2.6 and 2.7). Equation (2.6) was derived from the tests to estimate the scour depth around the pier when influenced by the abutment using the principle of superposition:

$$\frac{d_{sp}}{D} = \frac{d_{sp0}}{D} + \left|\frac{d_{sa0}}{D\,tan\,\varphi} - \left(\frac{X}{D} + \frac{1}{2}\right)\right| \tan\varphi \qquad \frac{X}{D} \leq 6 \qquad \textbf{(2.6)}$$

Where φ represents the angle of repose of the bed material, and d_{sp} and d_{sp0} denote the maximum scour depths around the pier in the main and control tests, respectively. Equation (2.6) allows for the estimation of the maximum scour depth at a pier positioned at any distance X from an abutment, using d_{sp0}, d_{sa0}, and the angle of repose of the bed material as inputs. In turn, Equation (2.7) predicts the scour depth around a pier located near an abutment based on the geometry, type, and configuration of both the pier and the abutment.

$$\frac{d_{sp}}{D} = K_{sa}K_{sp}\left[0.19\left(\frac{X}{D}\right)^2 - \frac{1.8X}{D} + 6.2\right] \qquad \textbf{(2.7)}$$

where K_{sa} is an abutment shape factor with K_{sa} =1.14 for wing-wall abutment and K_{sa} = 1.00 for semi-circular abutment; and K_{sp} is a pier shape factor with K_{sp} = 0.94, 0.95, and 0.88 for a single cylindrical pier, a group of three cylindrical piers, and a rectangular pier with a rounded edge, respectively. This equation accurately estimated d_{sp} in the vicinity of the abutment (R^2 = 0.98). The advantage of Eq. (2.7) is that this equation can calculate the scour depth given the distance between the pier and abutment and their shapes.

Rezaie et al. (2023) the influence of roughness elements on clear-water scour around bridge abutments was experimentally examined. The findings revealed that decreasing the spacing between the roughness elements and

increasing their thickness on the abutment surface significantly reduced the scour depth. In contrast, a higher ratio of roughness spacing to protrusion height (s/p) corresponded to a greater scour depth. The introduction of surface roughness also altered the response of the scour hole slope to changes in flow depth. In the absence of roughness, the slope of the scour hole became steeper as the flow depth increased, whereas with roughness, the slope consistently remained lower across all tested flow depths. The steepest slope and the greatest scour depth occurred when the roughness elements were oriented at angles between 50° and 70°. Conversely, the minimum scour depth and slope were observed at specific roughness configurations, particularly when both spacing (s) and protrusion (p) were set to 0.17 times the abutment length (L).

Zolghadr et al. (2023) explored the use of roughness elements to disrupt the downward flow that initiates the primary vortex responsible for such scour. Two vertical-wall abutments of varying widths were tested under four different clear-water flow conditions. Roughness elements with equal thickness and protrusion dimensions (P = t = 0.05 L, 0.1 L, 0.2 L, and 0.3 L, where L is the abutment length) were evaluated at different installation depths (Z). These elements were positioned either within the sediment or between the sediment surface and the water level. To determine the optimal depth, the study began with a single element placed on the sediment surface, increasing the number of elements in each successive test. Results revealed that positioning elements between the water surface and sediment bed had no consistent effect on reducing scour depth. In contrast, the most effective installation depth was found to be 0.6–0.8 L below the initial bed level. Among the tested configurations, elements with P = t = 0.2 L provided the greatest protection, reducing maximum scour depth by up to 30.4% and 32.8% for the narrower and wider abutments, respectively.

2.10 Summary of Previous Works

Table 2-2: Summary of Scour Studies.

Author(s)	Year	Bridge model/type	Studied variables	Key findings
Maatooq	2008	Pier near abutment (rectangular flume)	Pier-abutment spacing, flow depth, velocity	Scour depends on pier-abutment interaction; a modification factor (K_{dis}) was developed.
Oben-Nyarko and Ettema	2011	Wing-wall & spill-through abutments with pier	Abutment type, pier location	Pier reduced scour at the spill-through abutment toe; pier scour is governed by the abutment
Mohamed and Shawky	2016	Bridge abutments (sandy soil, SSIIM model)	Channel contraction ratio, abutment entrance angle	Gentle angles (10°–15°) reduced scour; SSIIM predicted scour with 97% correlation
Memar et al.	2016	Wing-wall abutments with piers (circular, round, sharp)	Abutment length, pier shape, spacing	Closer pier increased abutment scour; sharp-edge piers caused the greatest scour
Alkhouly et al.	2019	Vertical, semicircular, sloped, wing wall abutments	Abutment shape, piles, Froude number	Wing wall (60°) least scour; piles reduced scour by 22%; scour increased with Froude number
Al-Awadi and Al-Khafaji	2020	Pier with debris	Debris accumulation size	Scour depth increased 140% with 27% blocked area; exponential prediction formulas were derived
Khajeh and Vaghefi	2020	Abutments with vertical/inclined piers	Pier inclination, abutment-pier position	Greatest scour at upstream outer abutment; location varied with pier inclination
Abed and Majeed	2020	Piers (CFD simulation)	Pier spacing, pier shape	Larger spacing reduced scour; triangular-nose pier least scour, circular most
Al-Shukur and Hussein	2021	Lenticular & oblong piers	Skewness angle, velocity, pier shape	Higher skewness & velocity increased scour; max scour 13.2 cm at 30° and 0.27 m/s

Ali and Güna	2021	Bridge piers (ANN models)	Pier diameter, velocity, depth, sediment size	Pier diameter most influential; ANN (R^2=0.9585) outperformed regression
Muhsen and Khassaf	2022	Vertical abutment with oblong/lenticular piers	Pier-abutment spacing, flow intensity, Froude number	Closer spacing increased pier scour, decreased abutment scour; new empirical equations developed
Saeed et al.	2023	Wing-wall & semicircular abutments with piers	Pier-abutment combinations, velocity	Pier near abutment increased scour hole volume by 87%; empirical equations developed (R^2=0.98)
Rezaie et al.	2023	Abutments with surface roughness	Roughness spacing & thickness, flow depth	Closer/more pronounced roughness reduced scour; roughness altered the scour slope
Zolghadr et al.	2023	Vertical abutments with roughness elements	Roughness size & depth, flow condition	Optimal depth= 0.6-0.8L; roughness (0.2L) reduced scour by30%

The literature review highlighted recent experimental studies on local scour around bridge piers and abutments, individually or in combination. However, limited research exists on how the proximity of a pier to an abutment influences scour depth. To address this gap, the current thesis examines the influence of abutment geometry on local scour near bridge piers using various abutment models under different hydraulic conditions and develops empirical equations to predict scour depth and identify the optimal abutment configuration with the least scour.

Chapter Three : Materials and Methods

3.1 Experimental Setup

3.1.1 Flume Characteristics and Equipment

All experiments were conducted in a closed recirculation system, including a horizontal rectangular flume with dimensions of 9.00 m in length, 0.70 m in width, and 0.50 m in depth. The system also incorporated head and sump tanks to support the experimental tests, as depicted in Figures 3-1 and 3-2. These dimensions ensure minimal contraction effects related to the pier diameter and flow depth for this thesis. A net channel length of 7 m constructed with a sturdy steel frame. The sidewalls are made of highly transparent polyethylene, while the flume bed is lined with a fixed steel plate.

To facilitate water circulation, the system includes two steel sump tanks, each measuring 1.60 m in length, 1.36 m in width, and 0.70 m in depth. These tanks supply water to a pump with a maximum capacity of 27 liters per second via a 0.10-meter-diameter high-density polyethylene pipe. The head steel tank dimensions are 1.40 m in length, 0.70 m in width, and 0.80 m in depth. It is equipped with an overflow drain pipe, 0.10 m in diameter and 0.70 m in height, to manage excess water. Inside the head tank, there are two steel meshes (0.70 m wide and 0.55 m deep) to minimize turbulence in the incoming water. Additionally, a sluice gate, adjustable vertically using a hand-wheel lever, is installed to regulate the water flow into the flume.

Figure 3-1: Different view of the laboratory flume.

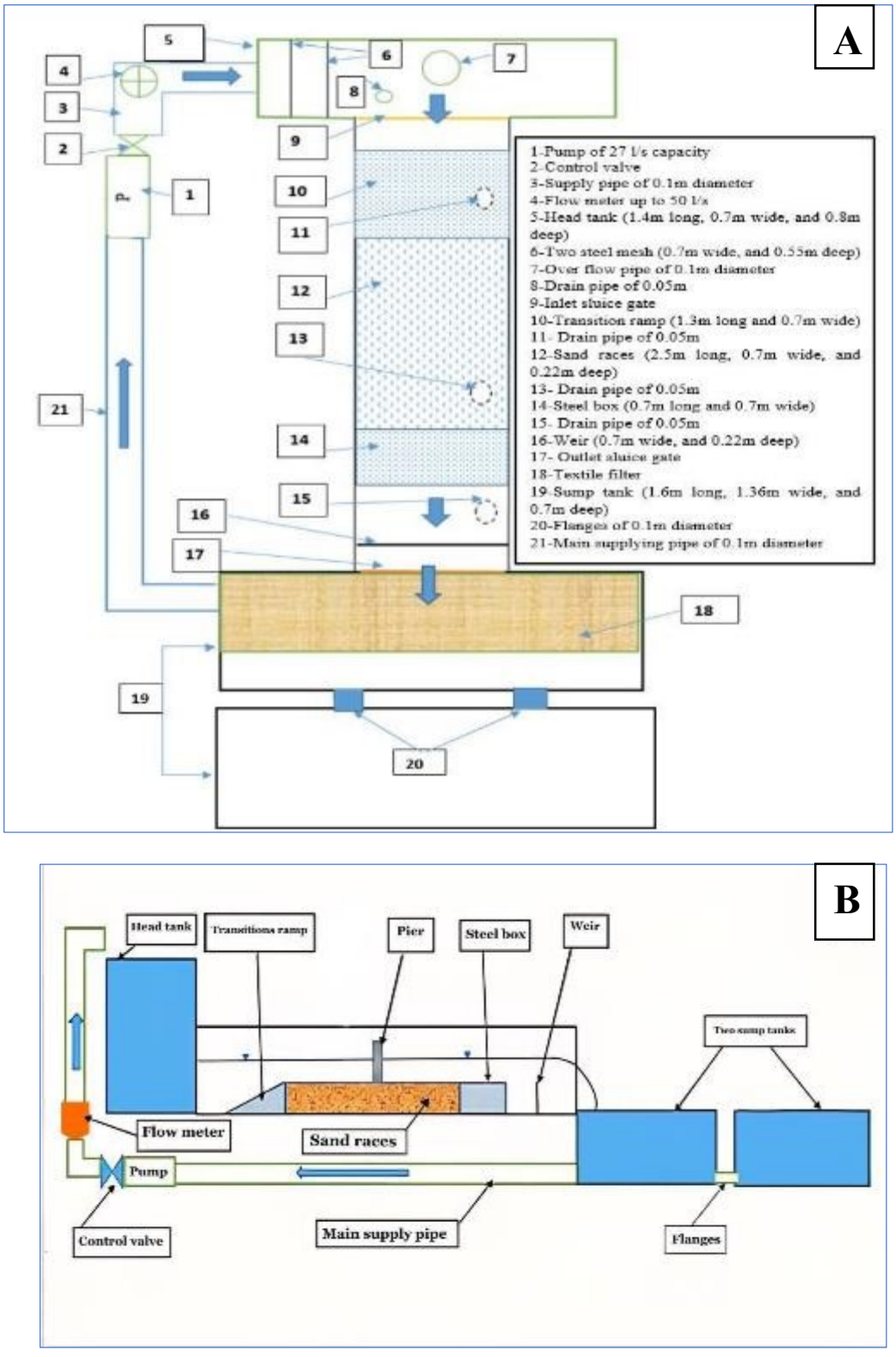

Figure 3-2: Schematic representation of laboratory flume: (A) Plan, and (B) Side view.

The channel system was equipped with a calibrated volumetric flow meter (capacity 50 L/s, precision ±0.2 L/s). This corresponds to a relative error of approximately 0.4% at full capacity. According to the international standard ISO 5167-1:2022, flow meters with a relative error less than 1% are considered high-accuracy instruments suitable for laboratory applications (ISO, 2022). Therefore, the adopted precision of ±0.2 L/s is acceptable and does not significantly affect the reliability of the scour experiments. A false bottom, measuring 2.50 m in length, 0.70 m in width, and 0.22 m in depth, was placed into the channel to simulate the scoured zone. The channel also includes a steel upstream ramp box measuring 1.30 m in length, 0.70 m in width, and 0.22 m in depth, facilitating a smooth transition for water entering the working section.

The top surface of the ramp is coated with a thin concrete layer, 0.05 m thick, to ensure uniform surface characteristics. Similarly, a steel box measuring 0.70 m by 0.70 m exists at the downstream end of the working section, also covered with a thin concrete layer to maintain consistent roughness between the inlet and outlet sections. A manually adjustable sluice gate, operated using a hand-wheel mechanism, is positioned at the downstream end of the flume to regulate the required tailwater depth for testing, as shown in Figures 3-3 and 3-4.

The recirculating system utilized for the experimental work includes four drain pipes, each with a diameter of 0.05 m. These pipes are strategically located at the head tank, inlet zone, and working section to facilitate maintenance and testing procedures. The calibration process involved comparing the flow meter readings with the discharge measured using the standard capacity method, which calculates discharge based on the time

required to fill a tank of known volume, as shown in Figure 3-5. A control valve exists upstream of the flow meter to regulate the pump discharge. A digital point gauge with 0.01 mm precision was utilized to measure the maximum scour depth. Additionally, two types of aluminum rulers were employed for measuring the scour hole: a straight ruler with a right-angle extension equipped with a balance bubble. A fixed reference level along both sides of the transparent flume walls in the working section ensures uniformity in the bed material level. The bed material was leveled using two types of scrapers, one made of wood and the other of metal. To maintain the clarity of the water in the sump tanks and prevent pump fluctuations due to potential sediment inflow, a textile filter was placed over the sump tank. The frame supporting this filter was constructed from steel.

To simulate uniform and steady flow conditions, a comprehensive flow conditioning system was implemented. Two stainless steel meshes were placed inside the head tank to dissipate turbulence and align flow paths. Additionally, a layer of coarse gravel was installed at the upstream of the working section to act as an energy dissipater and flow straightener.

Figure 3-3: Details of the laboratory flume.

Figure 3-4: Transient ramp, flume sections, scour zone, steel box, and outlet sluice gate of the experimental flume.

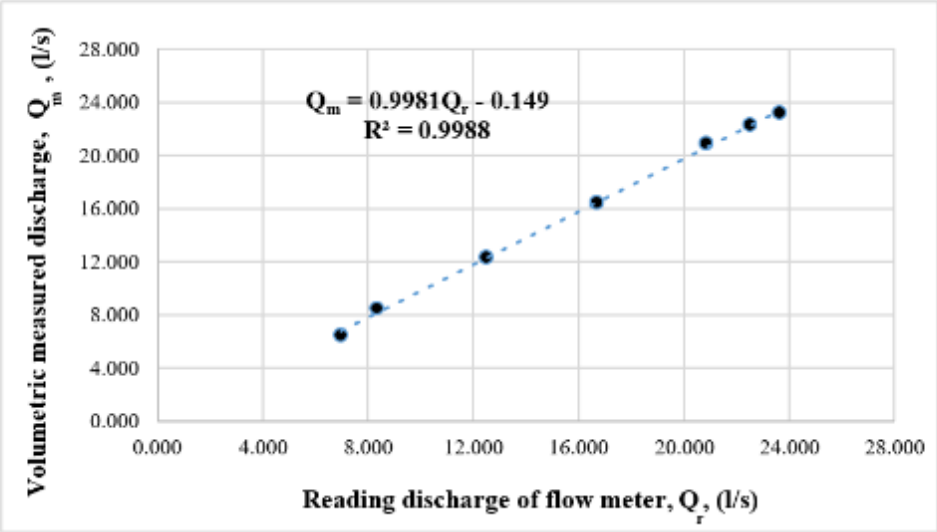

Figure 3-5: Discharge calibration of the flow meter.

3.1.2 Bed Material Characteristics and Hydraulic Conditions

The bed material used in the present thesis was pre-selected as non-cohesive sediment. The material underwent a series of sieve analysis tests, initially conducted by Al-Nawafith Company for Sand and Gravel Filters in Najaf Governorate, to confirm its suitability. Further verification was performed with two additional sieve analysis tests: one at the National Centre for Labs and Construction Research and another at the laboratories of the College of Engineering, Kerbala University Al-Awadi (2020).

The results of the three analyses were closely aligned, and their average values were adopted for the study. The particle size distribution curve and the associated parameters are illustrated in Figure 3-6 and summarized in Table 3-1. The sediment used in the scoured zone was sand with a mean diameter d_{50} of 0.716 mm.

The geometric standard deviation σ_g <1.3, classifying the material as uniform and negating the need to account for armoring effects Raudkivi and

Ettema (1983), and Raudkivi (1986). All experimental tests were conducted under clear water conditions with a flow intensity v/vc ≤1. The critical flow velocity for the initiation of motion (vc=0.321 m/s) was calculated based on a d_{50} value of 0.716 mm using Equation (2.1) Melville (1997). Table 3-2 presents the corresponding discharge for each flow intensity (v/vc).

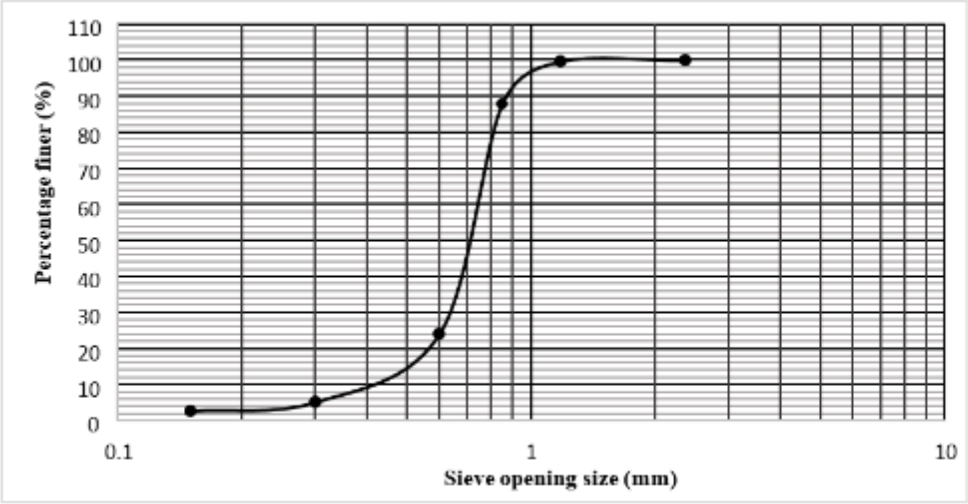

Figure 3-6: Bed material distribution curve (Al-Awadi, 2020).

Table 3-1: Sediment characteristics.

Material	d_{50} (mm)	d_{84} (mm)	d_{16} (mm)	$\sigma_g = \left(\frac{d_{84}}{d_{16}}\right)^{0.5}$	$\frac{\rho_s - \rho}{\rho}$
Sand	0.716	0.85	0.516	1.283	1.596

Table 3-2: Flow intensity, flow depth, and discharge were used in this study.

Flow depth$_{(cm)}$	7				9			11		
v/v_c	0.5	0.65	0.7	0.9	0.5	0.7	0.9	0.5	0.7	0.9
$Q_{(l/s)}$	8.33	9.72	11.11	13.89	9.72	13.89	18.05	12.5	18.05	22.22

3.1.3 Pier and Abutment Models

Various models of abutments were designed and tested to investigate the effects of geometric configurations on local scour around the bridge pier. The models were selected to represent commonly observed shapes in hydraulic engineering, ensuring relevance to practical applications. Abutment models varied in width, while the pier model had a constant diameter, and the relative distance between the two structures differed.

The pier was modeled as a cylindrical structure made of solid aluminum with a diameter of 3.1 cm, enabling a comparative analysis of its hydrodynamic behavior. The reason for choosing this pier diameter is to eliminate the coarseness and side wall effect ($25 \leq D/d_{50}$) and ($D/B \leq 0.1$), where B is the channel width, Raudkivi and Ettema (1983). Similarly, the abutments were designed in various shapes, including vertical, inclined (trapezoidal), and wing-wall configurations.

Six abutment models with different geometric configurations were designed and constructed from durable wood with a smooth surface finish to minimize additional flow resistance, to investigate their effect on local scour around the bridge pier. These models represent common real-world designs from vertical-wall to wing-wall abutments. These models, shown in Figure 3-7 (A, B), were designed with the following geometric features:

1. Model 1: A vertical-wall abutment with dimensions of 0.10 m width, 0.15 m length, and 0.37 m height.

2. **Model 2:** A narrower vertical-wall abutment with dimensions of 0.10 m width, 0.20 m length, and 0.37 m height.

3. **Model 3:** A vertical-wall abutment with decreased width (0.075 m width, 0.20 m length, 0.37 m height).

4. Model 4: A vertical-wall abutment with reduced width (0.05 m width, 0.20 m length, and 0.37 m height) to study the effects of a minimal cross-sectional area on scour.

5. **Model 5:** A trapezoidal abutment designed to reduce flow obstruction and minimize local scour (0.20 m length at the base, tapering to 0.14 m at the top, 0.37 m height) with slanting sides.

6. **Model 6:** A wing wall abutment (0.20 m length at the base, tapering to 0.10 m at the top, 0.37 m height), characterized by a more pronounced tapering angle, to investigate further the impact of steeper side inclinations on flow behavior.

To hold the abutment, a steel strip was used and fixed to the inner sidewall of the flume. The pier was positioned in the center of the working section (Figure 3-7(C)). Their orientation was aligned perpendicular to the flow with a zero-degree angle of attack.

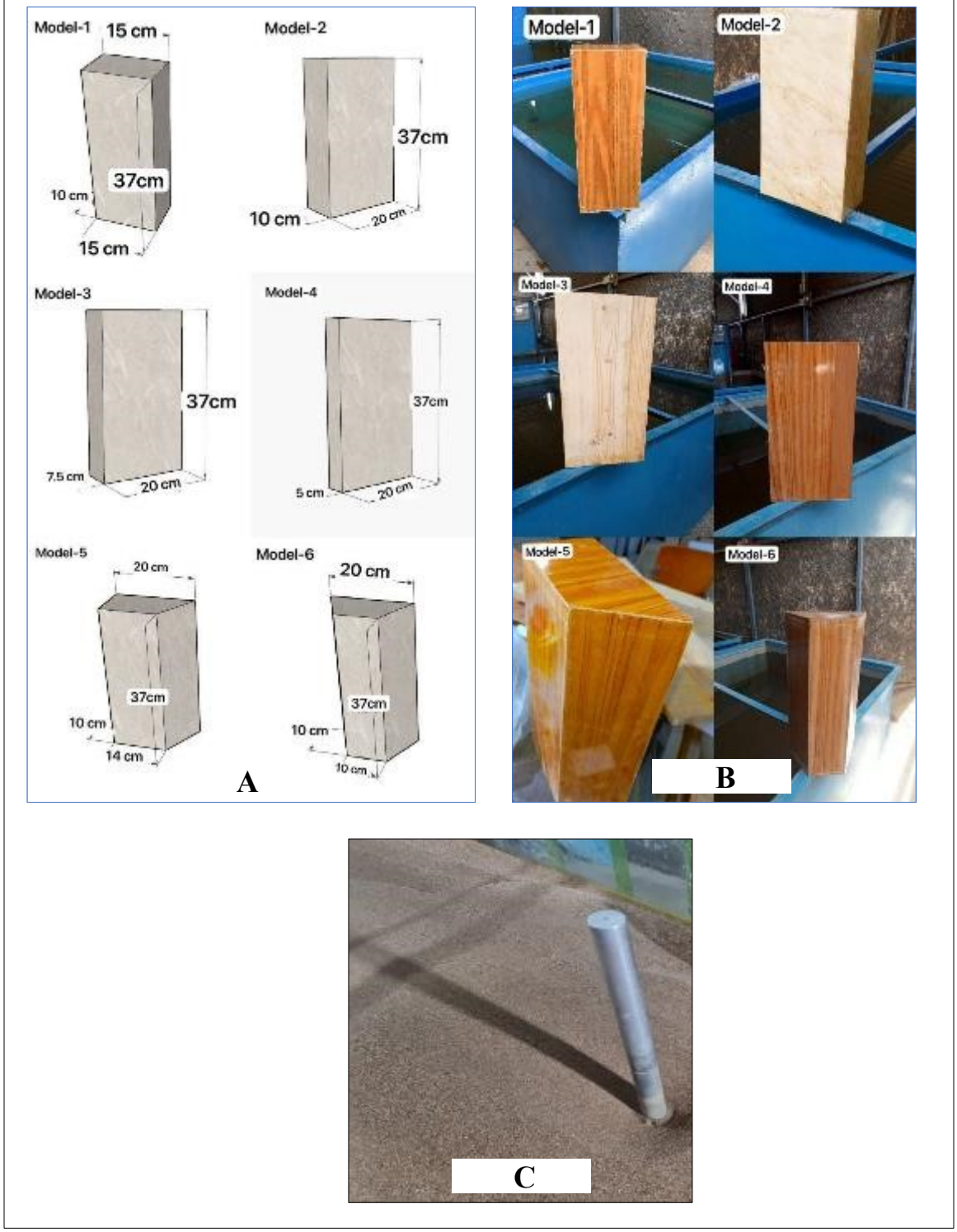

Figure 3-7: (A)Sketches of abutment models (B)Shapes of abutment models (C) Cylindrical aluminum pier model.

3.2 Experimental Procedure

All laboratory experiments were performed under clear-water conditions with steady, subcritical flow and a constant bed slope. The following procedure was repeated for each test,

1- After setting the discharge using a flowmeter and adjusting the water depth with the tailgate, prepare the work section with a scraper to ensure its surface is level, as shown in Figure 3-8A.

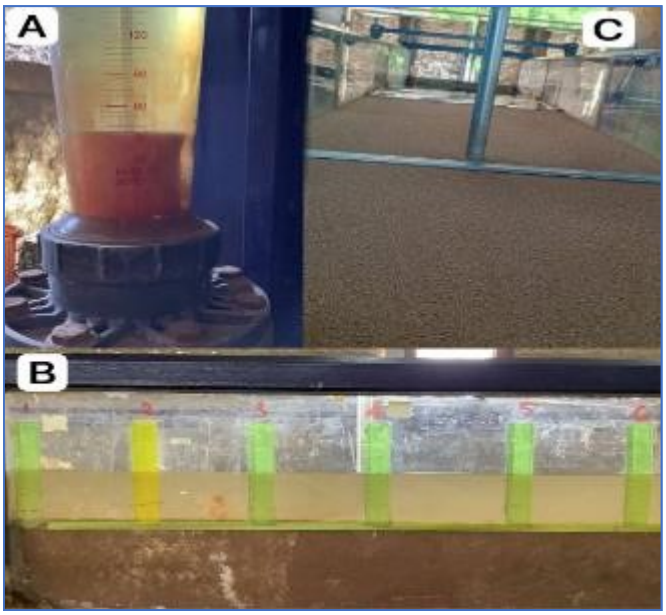

Figure 3-8: Experimental setup (A) discharge setting, (B) flow depth setting, and(C) sand surface level setting.

2- The pump was turned on, allowing the channel to gradually fill to reach the required water depth.

3- After three hours, the pump was turned off, then the water is slowly drained through a drainage located at the bottom of the channel to maintain the shape of the hole formed, as shown in Figure 3-9.

Figure 3-9: Slow drainage of scour holes.

4- The scour hole's measurements were taken. (Ls, Ws, ds), which (Ls) represents the length of the scour hole parallel to the flow direction (the longitudinal dimension), (Ws) the width of the scour hole perpendicular to the flow direction (the transverse dimension), and (ds) the maximum scour depth. The scour depth was measured using a point gauge attached to a moving wheel on both sides of the channel wall (Figures 3-10 - 3-12).

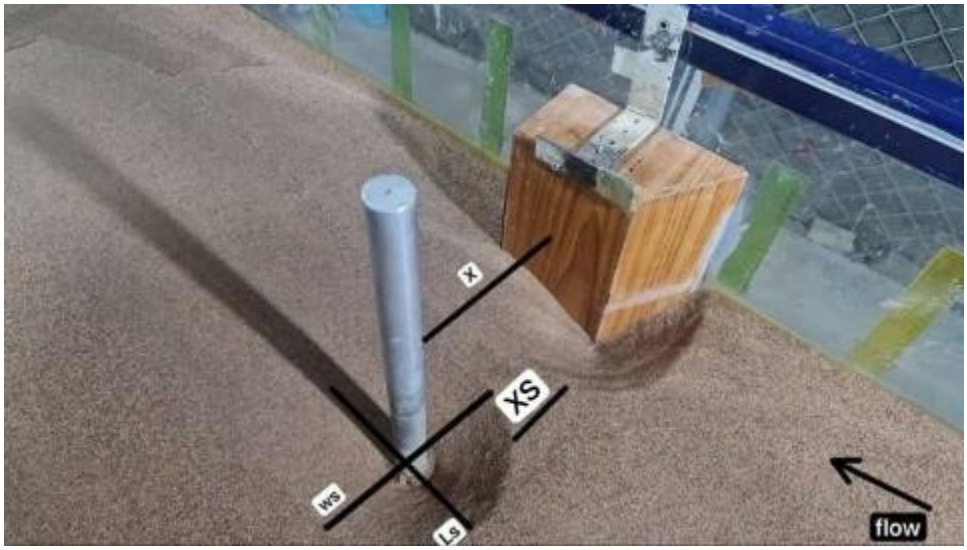

Figure 3-10: Scour hole dimensions of the pier.

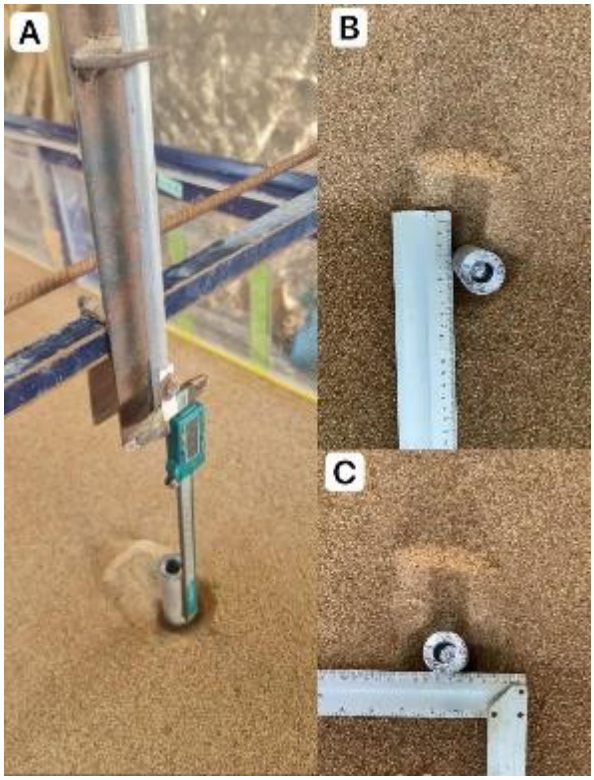

Figure 3-12: Pier scour hole measurements,
(A) scour depth measurement,
(B) scour hole length, and
(C) scour hole width.

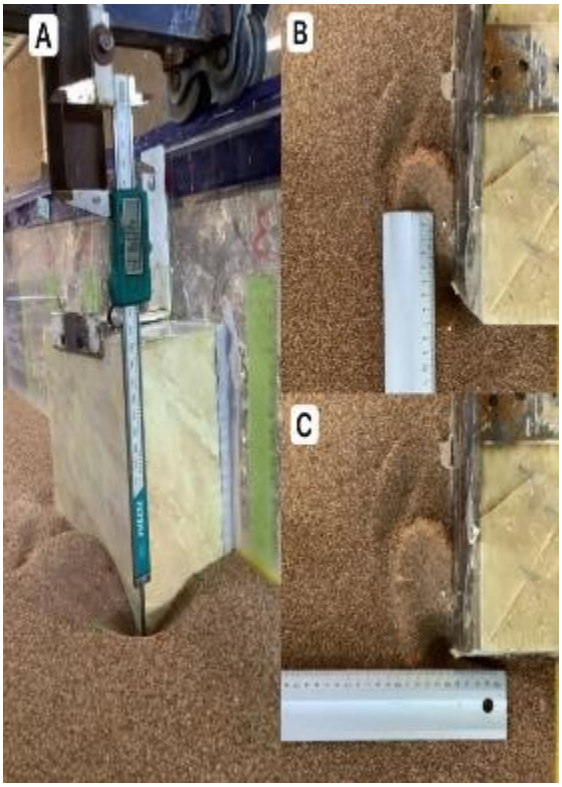

Figure 3-11: Abutment scour hole measurements,
(A) scour depth measurement,
(B) scour hole length, and
(C) scour hole width.

3.3 Experimental Work Summary

The experimental work was divided into thirteen groups, each with a varying number of runs, to meet the study's goals. This grouping was essential for enabling the creation of prediction models and examining how the geometry of the abutment affected the features of scour holes surrounding the bridge pier. An overview of the experimental groups is provided in Table3-3, which also summarizes the hydraulic conditions and objectives of the 130 tests conducted.

Table 3-3: Experimental work purposes.

Runs number	Model	x	Descriptions
1-10	Pier only	-	Exploring the evolution of scour depth at v/vc = 0.5,0.65,0.7,0.9 and flow depths of 7,9, and 11 cm.
10-20	Abutment only (A), L=15 cm	-	Exploring the evolution of scour depth at v/vc = 0.5,0.65,0.7,0.9 and flow depths of 7,9, and 11 cm.
20-30	Abutment only (B), L=20cm	-	Investigating the evolution of scour depth around the abutment only at v/vc = 0.5,0.65,0.7,0.9 and flow depths of 7,9, and 11 cm, and the effect of abutment length on scour depth.
30-40	Vertical-wall abutment (V1A) W=5cm	x=27 cm	Investigating scour hole characteristics between pier and abutment model at a distance x=27cm.
40-50	Vertical-wall abutment (V1B) W=5cm	x=22.5 cm	Investigating scour hole characteristics between pier and abutment model at a distance x=22.5cm.
50-60	Vertical-wall abutment(V2A) W=7.5cm	x=25 cm	Investigating scour hole characteristics between pier and abutment model at distance x=25cm, and the effect of abutment width on local scour near the pier.
60-70	Vertical-wall abutment (V2B) W=7.5cm	x=20 cm	Investigating scour hole characteristics between pier and abutment model at distance x=20cm, and the effect of abutment width on local scour around the pier.

70-80	Vertical-wall abutment (V3A) W=10cm	x=22.5 cm	Investigating scour hole characteristics between pier and abutment model at distance x=22.5cm, and the effect of abutment width on local scour around the pier.
80-90	Vertical-wall abutment (V3B) W=10cm	x=17.5 cm	Investigating scour hole characteristics between pier and abutment model at distance x=17.5cm, and the effect of abutment width on local scour around the pier.
90-100	Trapezoidal abutment (TA)	x=22.5 cm	Investigating scour hole characteristics between pier and abutment model at a distance x=22.5cm.
100-110	Trapezoidal abutment (TB)	x=17.5 cm	Investigating scour hole characteristics between pier and abutment model at a distance x=17.5cm.
110-120	Wing-wall abutment (WA)	x=22.5 cm	Investigating scour hole characteristics between pier and abutment model at a distance x=22.5cm.
120-130	Wing-wall abutment (WB)	x=17.5 cm	Investigating scour hole characteristics between pier and abutment model at a distance x=17.5cm.

Chapter Four : Results and Discussion

4.1 Reference Tests of the Pier

Table 4-1 gives the values of the depth (ds), width (ws), and length (ls) of scour holes produced under one pier in the same hydraulic conditions and without any abutment. At v/vc = 0.91, a second flow structure occurred with a strong downflow, strong horseshoe vortex, and wake vortex, as shown in Figure 4-1. This secondary flow structure corresponding to the maximum scour hole depth of 6.1 cm was adopted as the baseline reference in this study. The effects of secondary flows on scour development are discussed in detail in Chapter 2.

Table 4-1 shows that parameters ds, ws, and Ls directly change with an increase in flow intensity and Froude number without any significant alterations in the depth of flow. It was found experimentally that an increase in flow intensity is accompanied by a strengthening of circulatory features, in particular the horse-shaped vortex, as well as an increase in a kinetic energy value at its base, thus increasing local scour. The differences in the depth of flows have caused insignificant variations in scour depth with constant flow intensity. Observations of runs 4, 7, and 10 supported the conclusion that the effects of flow depth (y) on scour depth are unimportant when the ratio of flow velocity to critical velocity (v/vc) is constant. Despite the slight differences in the flow depth that were 7 cm and 11 cm, the scour never largely exceeded the restricted range of 5.5 cm to 6.1 cm. The gradual increase in the Froude number demonstrated a positive correlation with scour depth, indicating that elevated Fr values corresponded with increased scour hole depths. This observation is consistent with hydraulic theory, which posits that an increase in Fr signifies accelerated and more turbulent flow conditions near

the bed, thereby increasing the potential for sediment mobilization and scour development.According to laboratory findings, the scour depth increases rapidly in the first half hour, then the rate of development declines until it achieves a maximum value after about 90 minutes. Then, the increase in scour depth surrounding the pier and abutment becomes extremely slight.

All hydraulic parameters presented in Table 4-1 will be utilized in all subsequent reference expansions of abutment and intersection experiments.

Table 4-1: The hydraulic parameters for reference tests.

RUN NO.	y (cm)	Fr	Q (l/sec.)	v (m/sec.)	vc (m/sec.)	v/vc	ds (cm)	Ws (cm)	Ls (cm)	T (min)
1	7	0.18	8.33	0.15	0.30	0.5	2.27	9.5	9.5	180
2	7	0.24	9.72	0.19	0.30	0.63	3.3	14	12.5	180
3	7	0.26	11.11	0.21	0.30	0.7	3.62	12.5	14.5	180
4	7	0.33	13.89	0.27	0.30	0.9	5.7	22	26.5	180
5	9	0.17	9.72	0.16	0.31	0.52	2.68	9	8.5	180
6	9	0.23	13.89	0.22	0.31	0.71	4.3	15	15	180
7	9	0.30	18.05	0.28	0.31	0.90	5.5	23	23.5	180
8	11	0.16	12.5	0.16	0.32	0.5	2.5	9.5	9	180
9	11	0.22	18.05	0.23	0.32	0.72	4.8	19	19.5	180
10	11	0.28	22.22	0.29	0.32	0.91	6.1	23	26	180

Figure 4-1: Scour hole at v/vc=0.91 of isolated pier.

4.2.1 Reference Tests of the Abutments

The reference tests of abutment were performed to assess the fundamental scour characteristics surrounding isolated abutments, excluding the effects of nearby structures like bridge piers. Two vertical-wall abutment models were evaluated: Model A, measuring 15 cm in length, and Model B, measuring 20 cm. Both models underwent ten test runs under different hydraulic conditions, as detailed in Appendix A, Tables A-1 and A-2. The only geometric distinction between the two models was the length of the abutment, parallel to the flow direction. The analysis focused on maximum scour depth (ds), scour width (ws), and scour length (Ls). The findings indicated that the longer abutment (Model B), characterized by a 20 cm length, typically produced smaller and shallower scour holes in comparison to Model A, which had a 15 cm abutment length. The longer abutment length distributes the flow disturbance over a wider area, potentially reducing the intensity of local flow contraction and turbulence near the abutment tip. The erosive forces responsible for scouring in Model B may be less concentrated, resulting in a more diffuse and less aggressive scour pattern. The findings indicate that geometric characteristics, including abutment length, can have a slight yet significant impact on local flow behavior and scour development. To enhance the understanding of the interference effect clearly, the longer abutment (Model B) was chosen for the subsequent interference experiments to establish a conservative foundation and maintain consistent geometry throughout the study.

4.2 The Impact of Primary Parameters

To facilitate and clarify the discussion on various abutment designs, a concise notation system is introduced in this chapter. The letter V denotes vertical-wall abutments, W signifies wing-wall abutments, and T indicates

trapezoidal abutments. Each letter is followed by a number as illustrated in Table 4-2.

Table 4-2: Notation System for Abutment Models and Their Geometric Configurations.

NO.	Dimensions (W×L×h)	x (cm)	Notation
1	5×20×37	27	V1A
2	5×20×37	22.5	V1B
3	7.5×20×37	25	V2A
4	7.5×20×37	20	V2B
5	10×20×37	22.5	V3A
6	10×20×37	17.5	V3B
7	20×14×37	22.5	TA
8	20×14×37	17.5	TB
9	20×10×37	22.5	WA
10	20×10×37	17.5	WB

All results of the interface between pier and abutment are illustrated in Appendix A, Tables A-3 to A-12.

4.2.1 The Impact of Flow Depth (y)

Figures (4-2 to 4-4) present the influence of flow depth on the scour depth around the pier when affected by different abutment models under three constant discharges (Q = 9.72, 13.89, and 18.05 l/sec). In these figures, the scour depths are illustrated using bar charts that directly compare the recorded values at two flow depths for each abutment configuration. This representation highlights the relative differences among abutment shapes and spacing conditions without implying a continuous trend.

The results consistently demonstrate an inverse relationship between flow depth (y) and scour depth (ds). At higher flow depths (e.g., y = 9 cm and y = 11 cm), the scour depths are noticeably reduced compared with shallower flows (e.g., y = 7 cm and y = 9 cm). This reduction can be observed from the shorter bar lengths at higher y values across all abutment models. The

reduction trend indicates that as the flow depth increases, the intensity of bed-scouring vortices decreases, leading to smaller scour holes.

Regarding the effect of abutment geometry, the V-shaped abutments (V1A, V1B, V2A, V2B, V3A, and V3B) consistently produced the largest scour depths, reflecting their strong influence on flow contraction and vortex generation. The W-shaped abutments exhibited moderate scour depths, lower than the vertical configurations, while the T-shaped abutments recorded the lowest scour depths among all models. Nonetheless, all tested abutments produced scour values greater than the reference pier, confirming the amplifying effect of abutments on local scour.

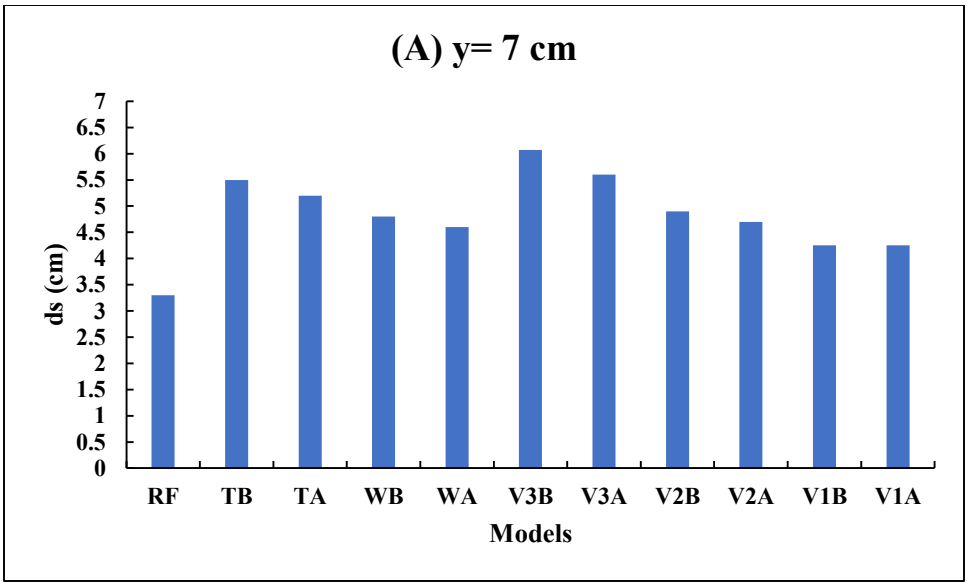

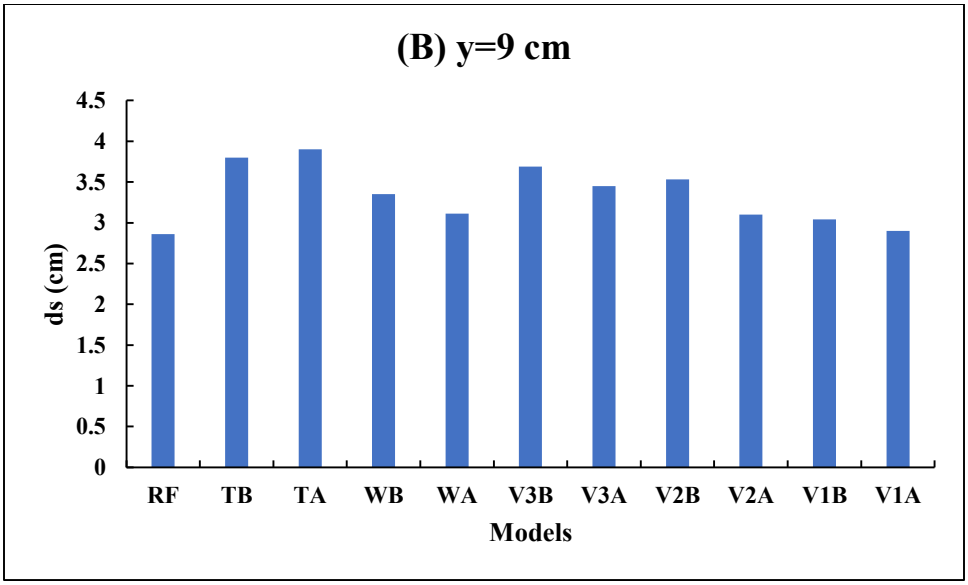

Figure 4-2: Influence of flow depth on scour depth nearby pier affected by abutment models at two different distances for each model with constant discharge Q=9.72 l/secQ

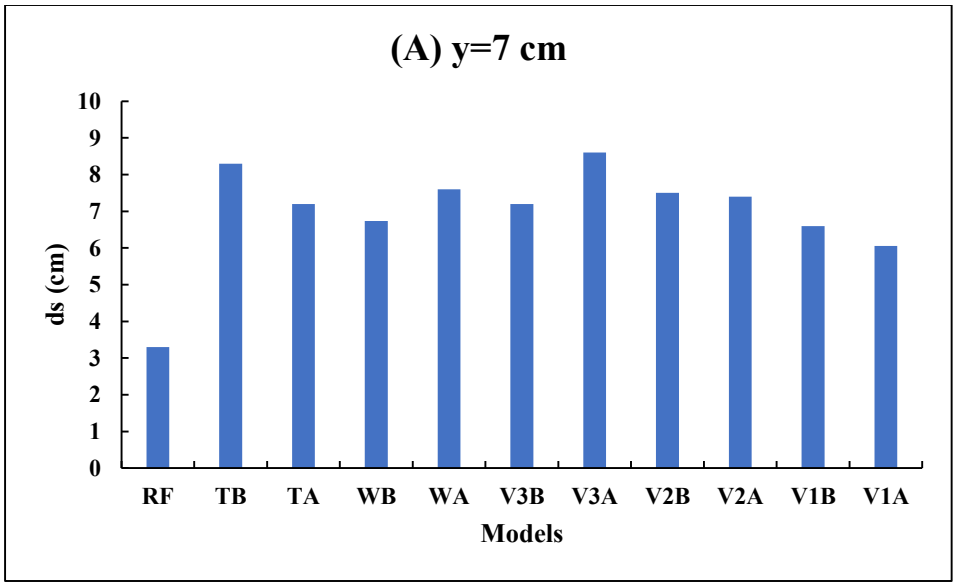

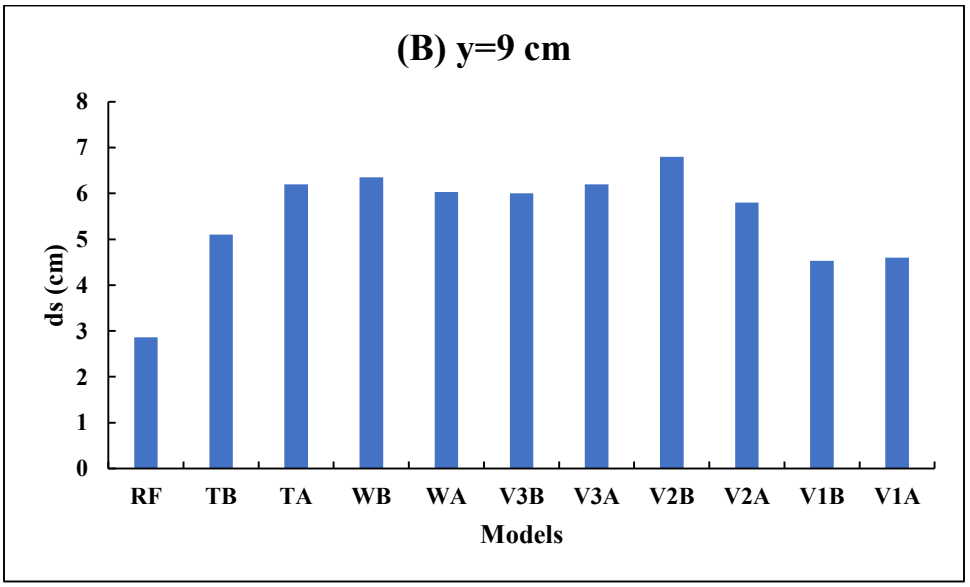

Figure 4-3: Influence of flow depth on scour depth nearby pier affected by abutment models at two different distances for each model with constant discharge Q=13.89 l/sec.

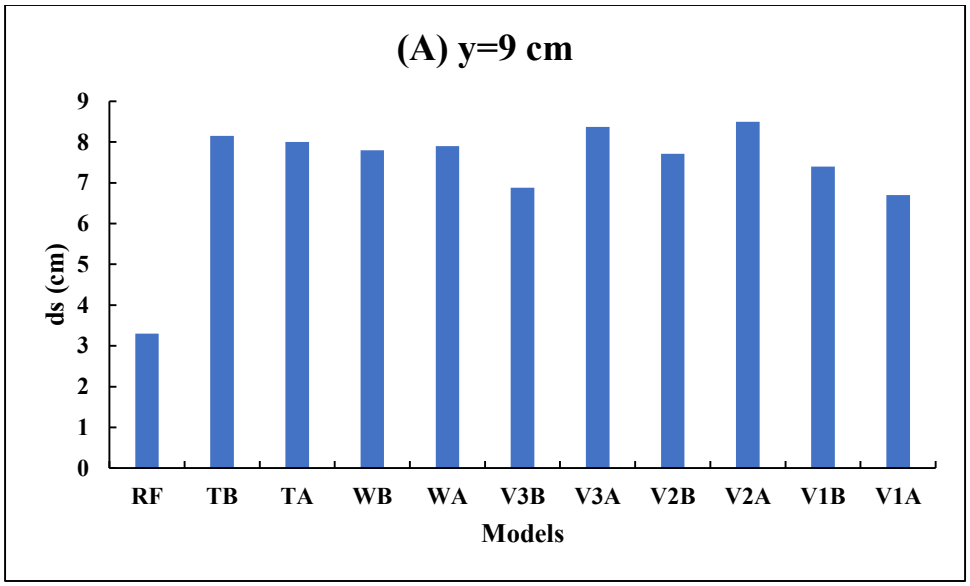

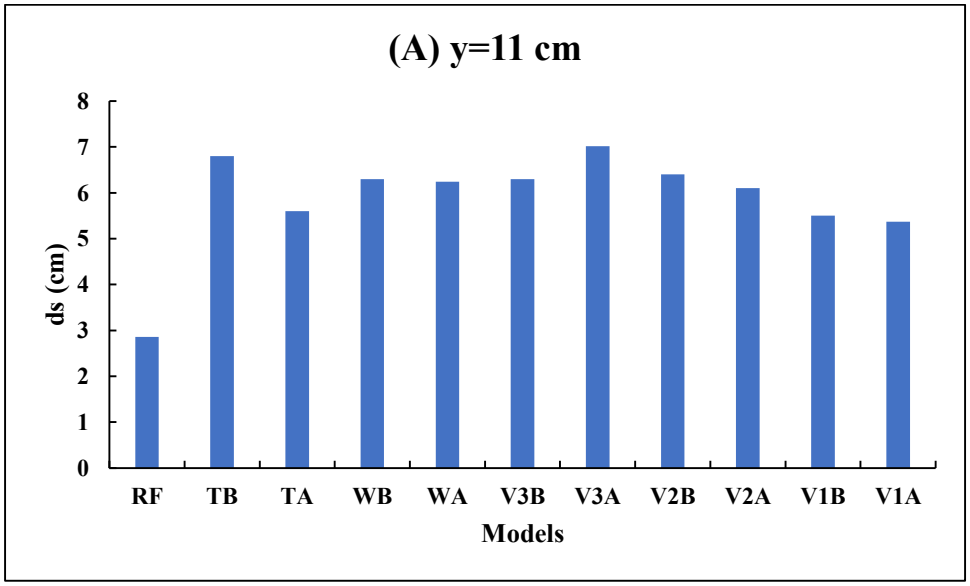

Figure 4-4: Influence of flow depth on scour depth nearby pier affected by abutment models at two different distances for each model with constant discharge Q=18.05 l/sec.

The influence of abutment–pier spacing is also evident. Smaller spacing distances led to greater scour near the pier due to the overlapping of scour holes and intensified turbulence in the contraction zone. In contrast, larger spacing values allowed partial dissipation of vortices and thus reduced the scour depth around the pier.

This pattern is clearly illustrated in Figures (4-5 - 4-7) which show the attenuation of scour formation as flow depth increases.

These findings are consistent with the observations of Chiew (1995), who reported that when the ratio of flow depth to pier diameter (y/D) exceeds approximately 3, the effect of depth on scour becomes insignificant. At higher flow depths (e.g., y = 11 cm in the present study), surface rollers and recirculating motions are weaker, resulting in reduced horseshoe vortex activity and lower scour efficiency. Conversely, at lower depths, intensified turbulence and stronger surface interactions contribute to more severe scouring.

In summary, the bar chart results confirm that both flow depth and abutment geometry/spacing play a critical role in determining scour characteristics near bridge piers. While increasing flow depth generally mitigates scour, the geometry and placement of abutments strongly govern the magnitude of this reduction.

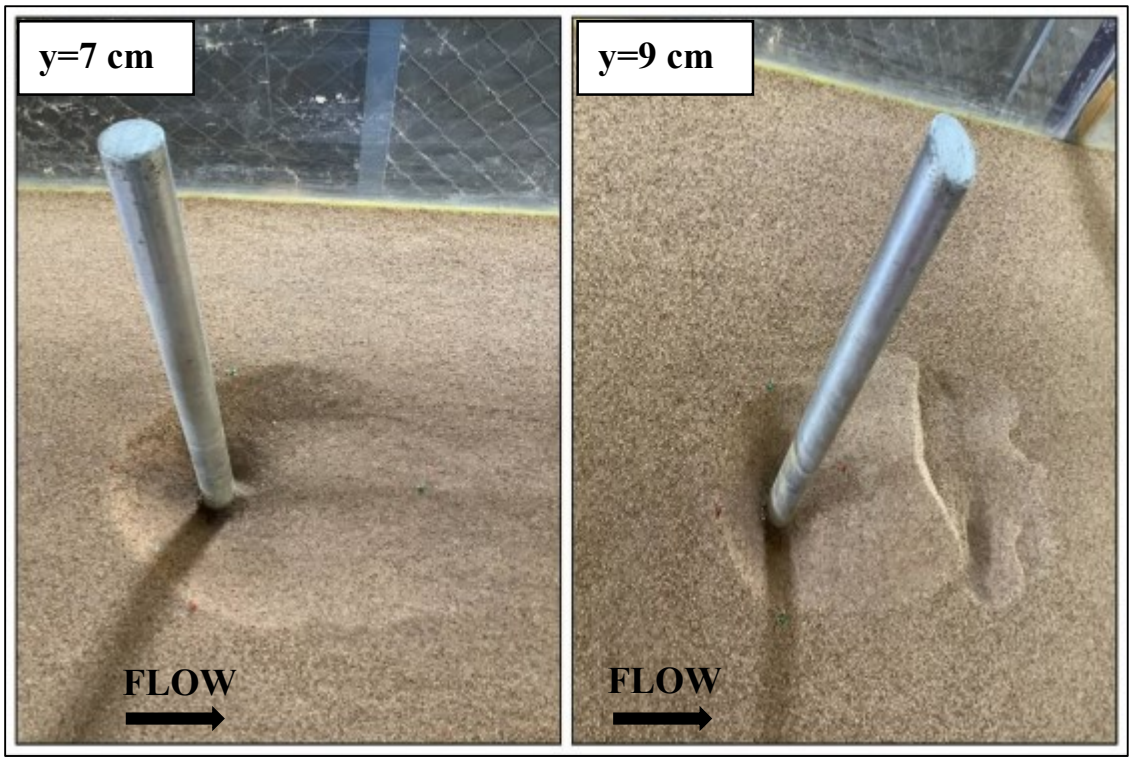

Figure 4-5: The influence of flow depth on scour depth for the reference case at Q=13.89 l/sec.

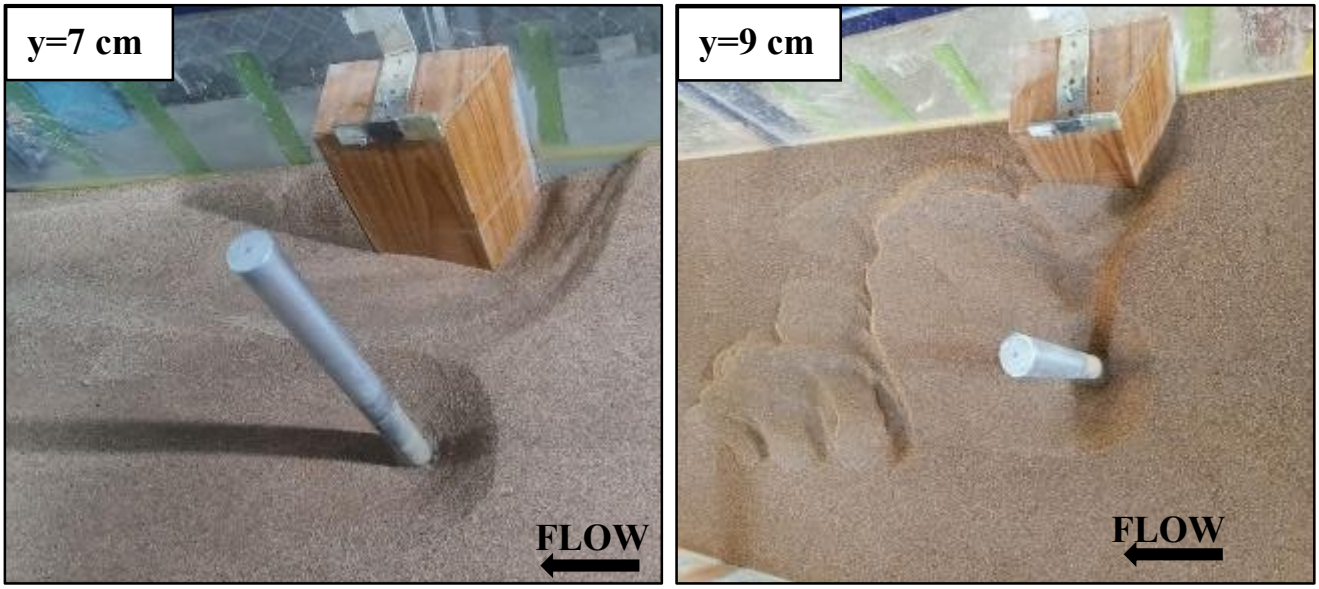

Figure 4-6: The influence of flow depth on scour depth around a pier affected by a trapezoidal abutment at Q=13.89 l/sec and x=22.5 cm.

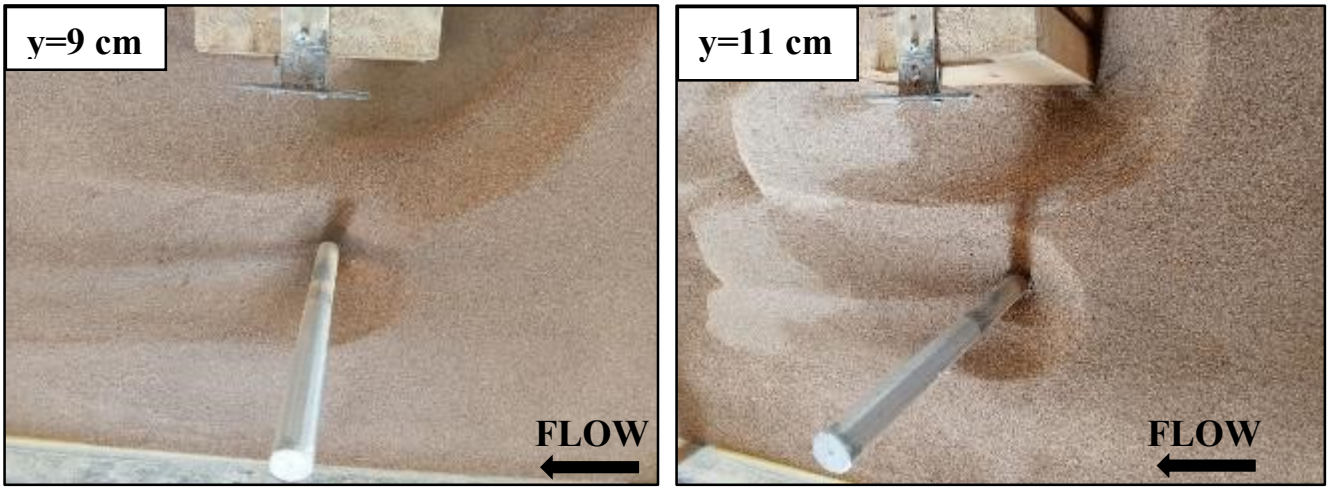

Figure 4-7: The influence of flow depth on scour depth around a pier affected by vertical-wall abutment, w=7.5 cm at Q=18.05 l/sec and x=25cm.

4.2.2 The Impact of Flow Intensity (v/vc) and Froude number (Fr)

The primary hydraulic parameters influencing local scour around submerged structures, such as abutments and piers, are the Froude number and flow intensity . Both variables characterize the flow and energy behavior, as they are directly dependent on flow velocity, which is considered the primary reason for initiating sediment motion and bed destabilization. Therefore, understanding their effect is essential for analyzing scour mechanics, particularly in cases involving pier–abutment interaction. To investigate the influence of these parameters, experimental tests were conducted using three flow depths for each abutment model, at two different pier–abutment distances, while controlling one parameter per group.

The results express that scour depth increases almost linearly with increasing values of both the Froude number and flow intensity, as illustrated in Figures (4-8 to 4-12). This similarity is attributed to their mutual dependence on flow velocity increases with flow velocity, just like flow intensity. Since both parameters exhibit comparable trends concerning scour depth, and to avoid redundancy in graphical analysis, only flow intensity was used in the result illustrations. It was found to sufficiently represent the scour response, as it reflects the same general behavior observed with the Froude number.

Based on Figures (4-8 - 4-10) which illuminate the effect of flow intensity on the relative scour depth (ds/y) at three flow depths (7, 9, and 11 cm) using vertical-wall abutment models with different widths (W = 5 cm, 7.5 cm, and 10 cm) and two pier–abutment distances, a consistent trend is observed. In all cases, increasing flow intensity is central to a corresponding increase in scour depth. Additionally, reducing the spacing (x) between the abutment and the pier results in higher scour values, indicating a negative

interference between the vortices generated by each element. Increasing the abutment width from 5 cm to 7.5 cm and 10 cm, as shown in Figures 4-9 and 4.10, intensifies the scour compared to Figure 4-8. For instance, at y = 7 cm and v/vc = 0.9, ds/y is approximately 1.5 for x = 27 cm, while it drops to around 0.8 at x = 22.5 cm. This supports the notion that reduced spacing between the abutment and the pier enhances vortex interaction, deepening the scour hole. Furthermore, for the larger abutment widths, the same flow conditions (e.g., y = 7 cm, v/vc = 0.9) produce greater scour depths. For example, ds/y reaches about 2.3 at x = 25 cm, compared to around 1.5 at x = 20 cm. This indicates that increasing abutment width magnifies its influence on the flow field, leading to greater vortex concentration and more pronounced pressure gradients behind the abutment, thereby increasing local scour. Figures 4-11 and 4-12 also display a distinct pattern indicating that scour depth (ds/y) increases with flow intensity (v/vc), especially when the abutment is located closer to the pier. The increase is most significant at shallower flow depths (y = 7 cm), where the interaction between abutment-induced and pier-induced vortices is most intense. The wing-wall abutment induced more pronounced scour than the trapezoidal abutment under identical conditions, demonstrating that abutment geometry substantially affects flow dynamics and local scour formation. The wider base and sloped sides of the trapezoidal abutment could reduce flow obstruction and turbulence intensity, hence leading to a marginal reduction in scour.

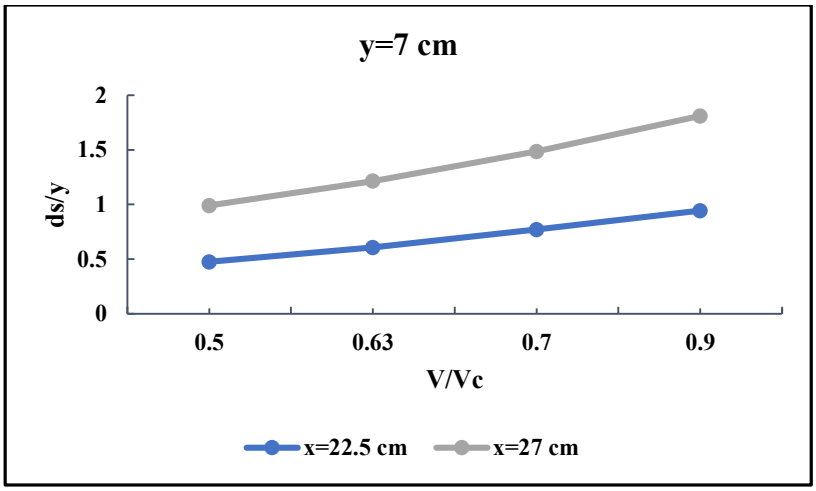

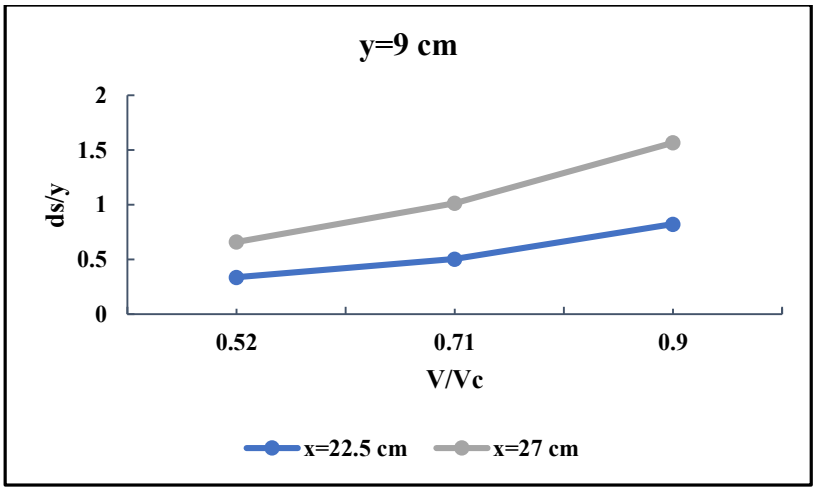

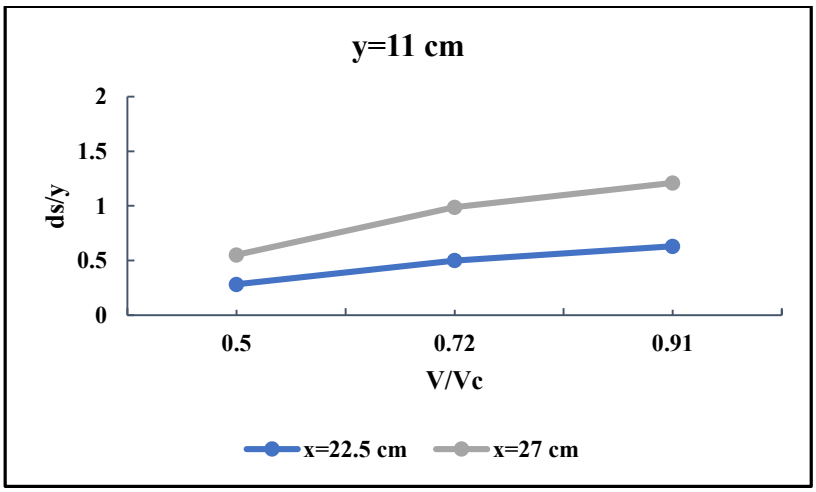

Figure 4-8: Effect of flow intensity on scour depth around pier affected by vertical-wall abutment, W=5 cm at two different distances.

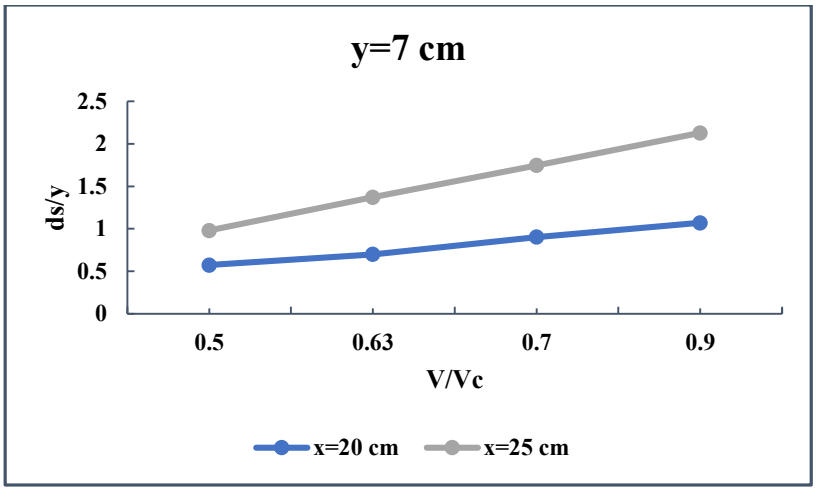

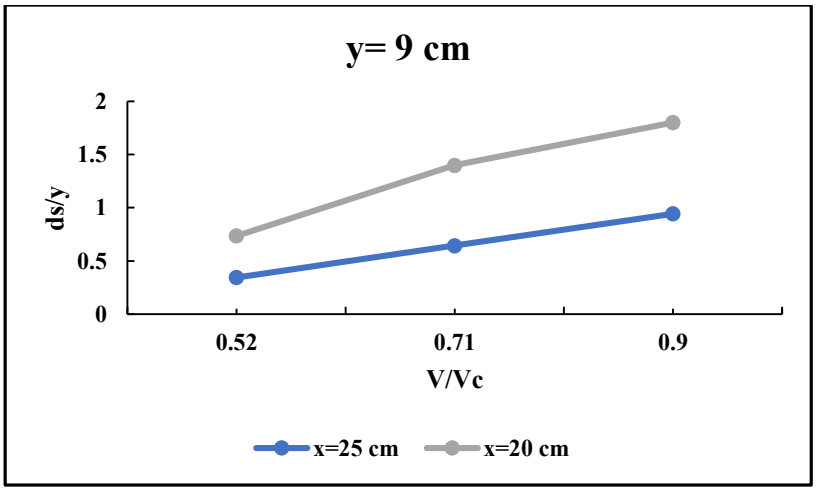

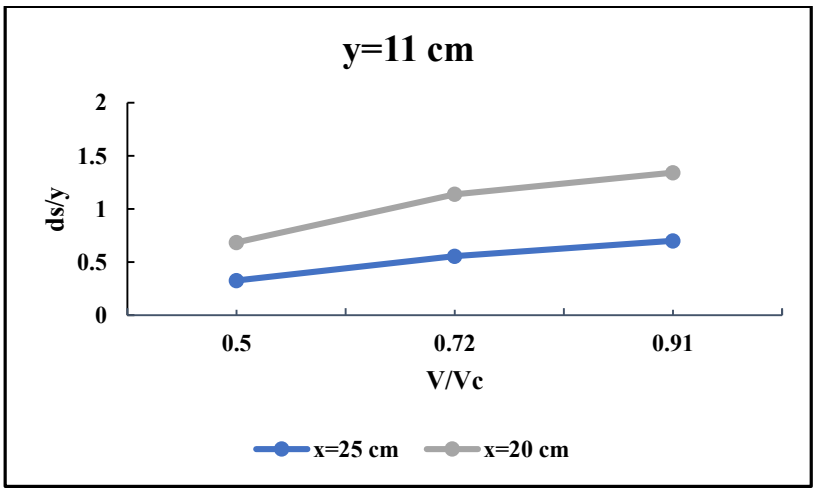

Figure 4-9: Effect of flow intensity on scour depth around pier affected by vertical-wall abutment, W=7.5 cm at two different distances.

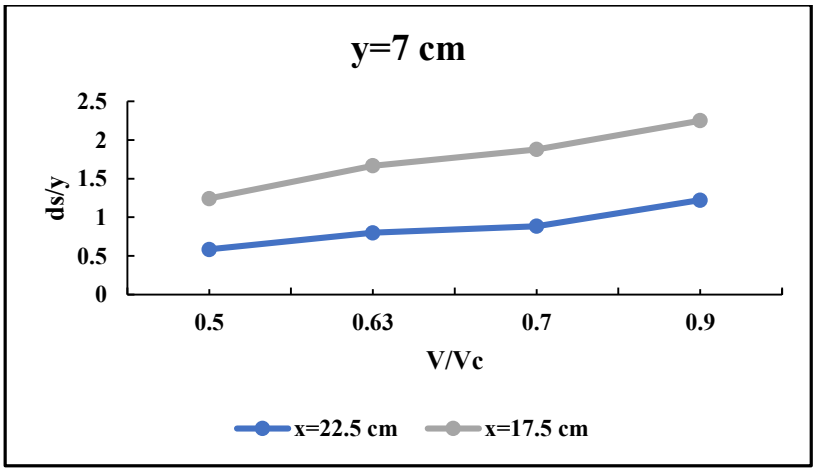

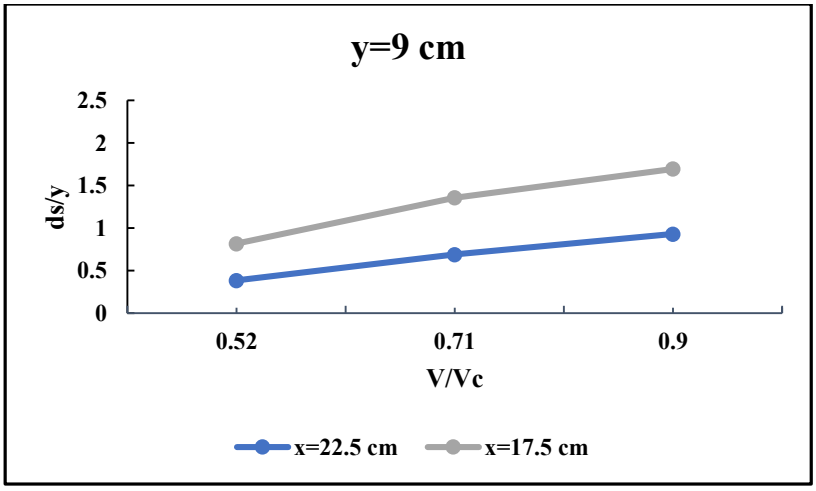

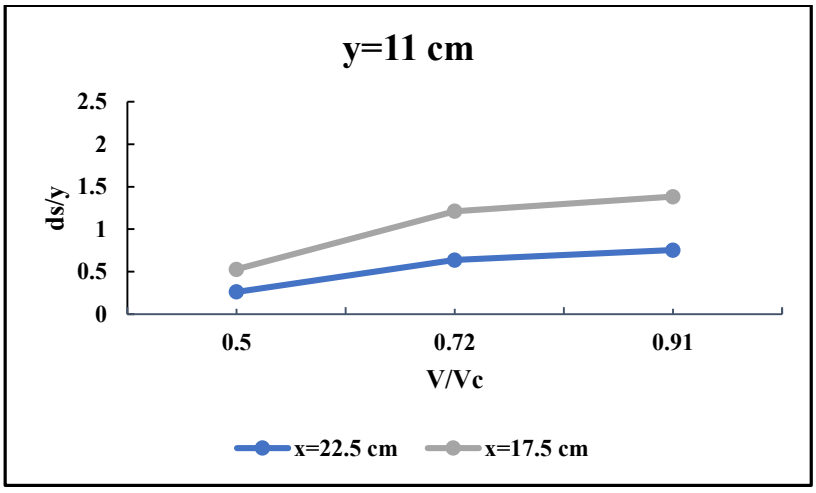

Figure 4-10: Effect of flow intensity on scour depth around pier affected by vertical-wall abutment, W=10 cm, at two different distances.

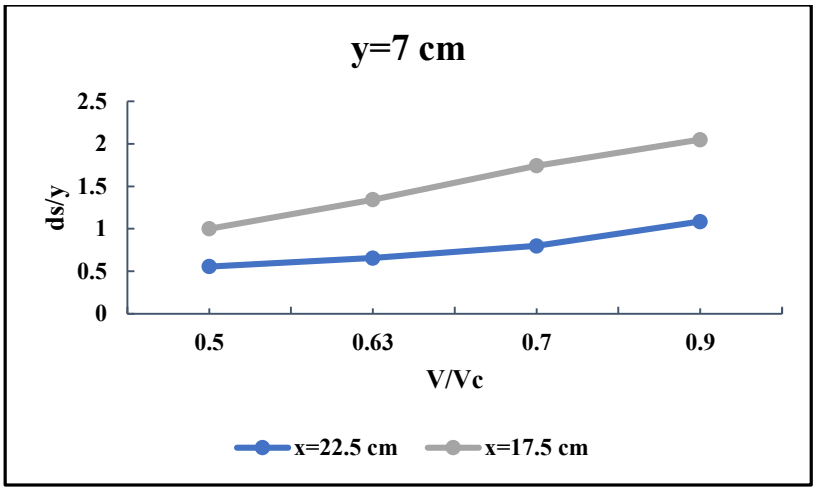

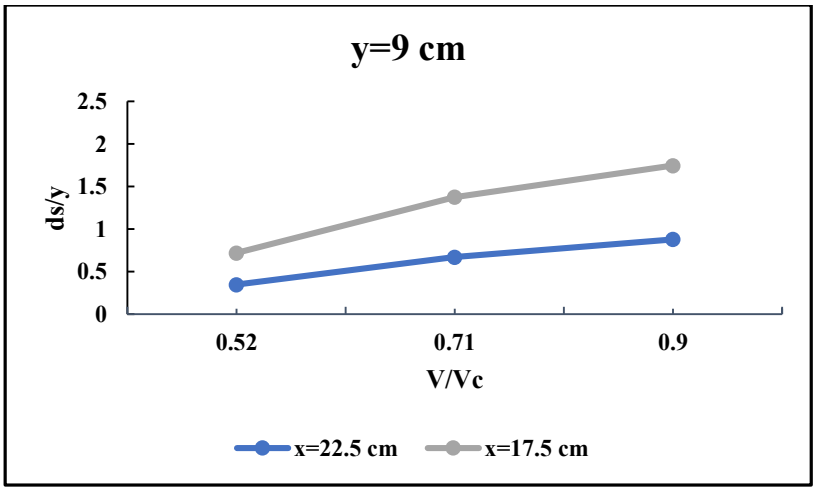

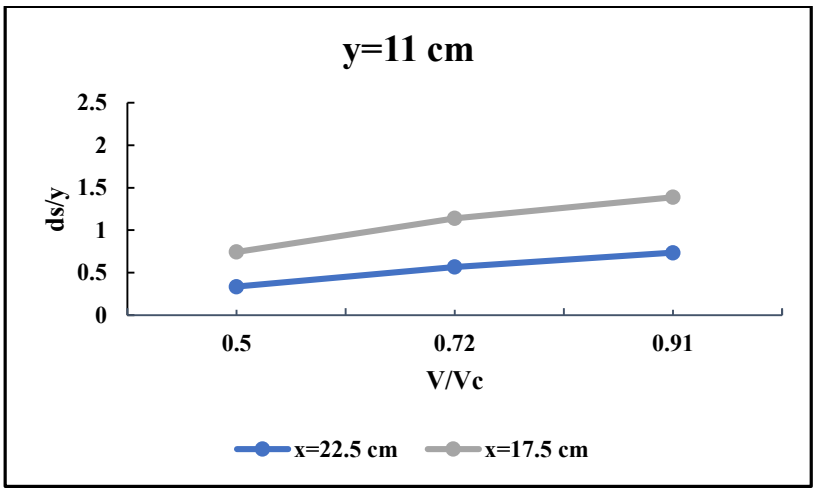

Figure 4-11: Effect of flow intensity on scour depth around pier affected by wing-wall abutment, at two different distances.

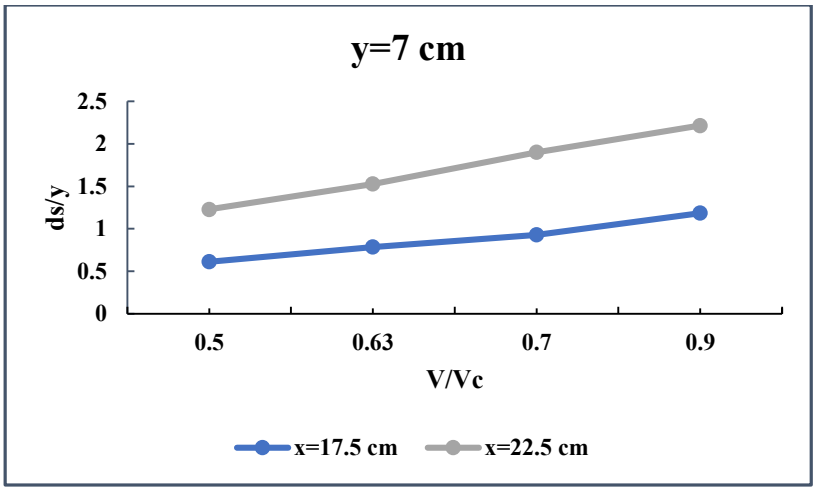

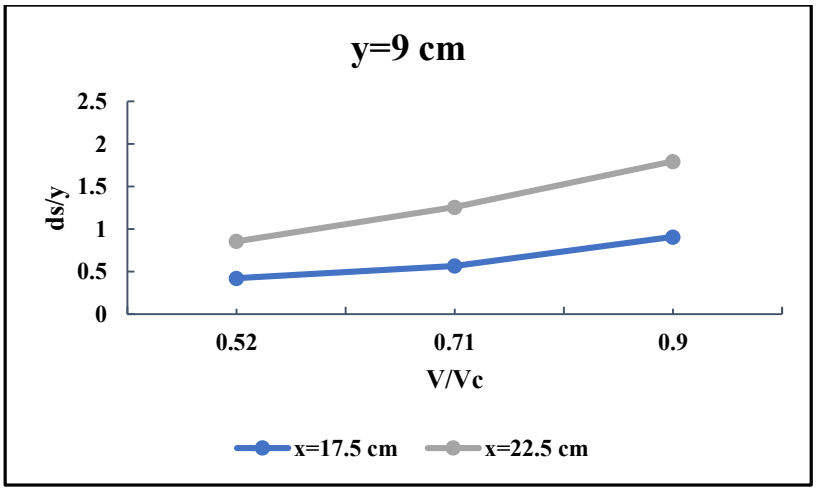

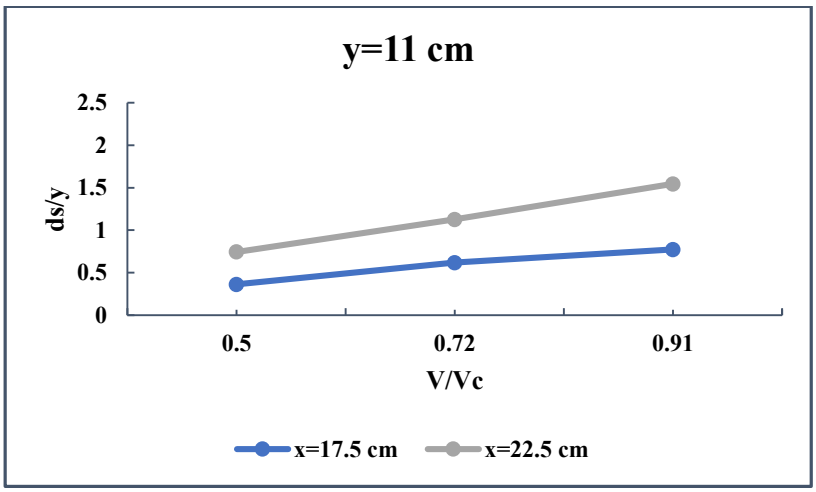

Figure 4-12: Effect of flow intensity on scour depth around pier affected by trapezoidal abutment, at two different distances.

Additionally, select experimental photographs were chosen to validate the laboratory observations about the scour phenomenon surrounding the pier and abutment, as illustrated in Figures 4-13 and 4-14.

The data indicate that the increase in flow intensity resulted in an expansion of both the width and capacity of the scour hole. Consequently, the affected area will extend beyond the sides of the pier and abutment, most probably due to the enlargement of the separation zone downstream of these structures. This phenomenon will generate additional eddies (vortices), leading to increased scour as the strength of the horseshoe vortex and down-flow intensifies. As previously explained, the development of local scour is contingent upon the formation of vortices around the obstruction.

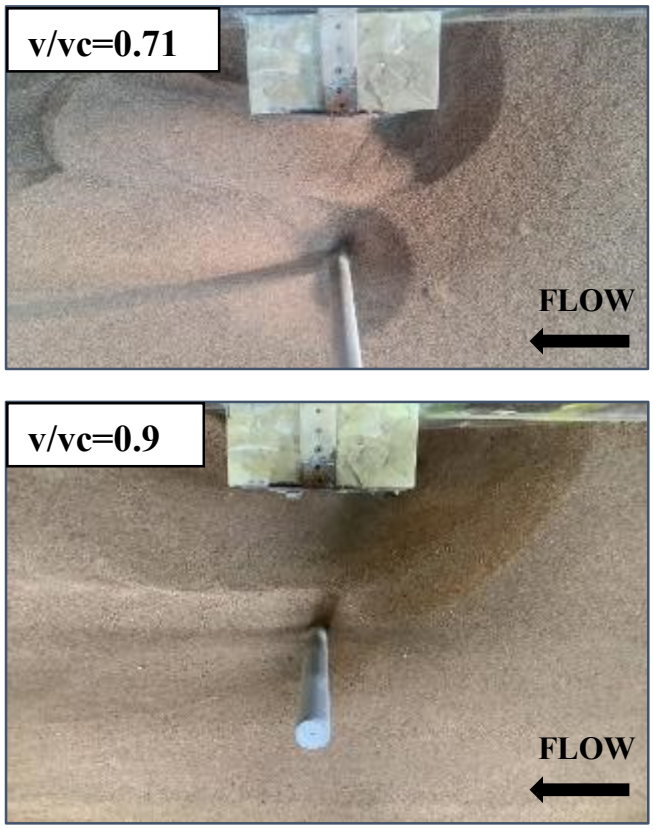

Figure 4-13: Influence of flow intensity on scour expansion around the pier and vertical-wall abutment w=10cm.

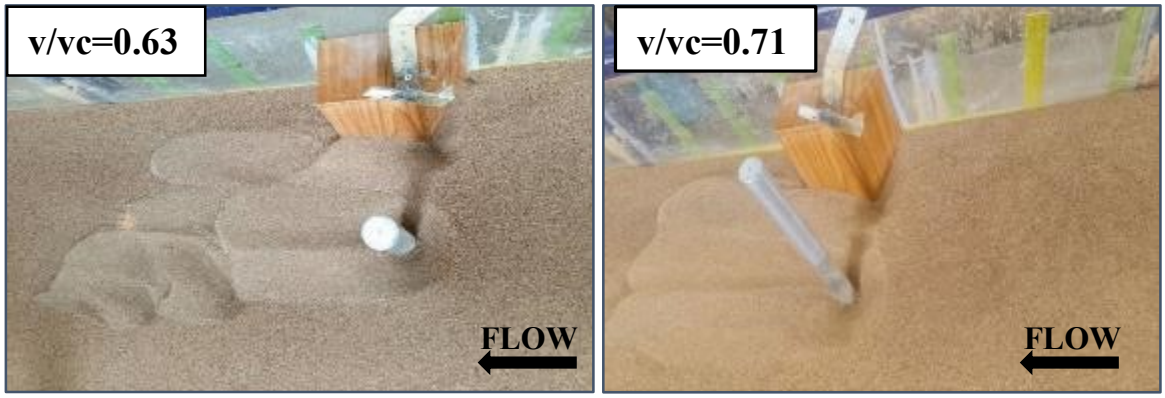

Figure 4-14: Influence of flow intensity on scour expansion around the pier and trapezoidal abutment.

4.2.3 Impact of Distance Between Pier and Abutment

One of the factors influencing the scour geometry surrounding the pier and abutment, which is the focus of this study, is thought to be spacing. For each abutment model, two distinct spacing measured from the pier position (i.e., the spacing defined from pier face to abutment face). These values were used to examine the effect of the spacing ratio (x/y) on the relative scour depth (ds/y) around the pier. For more clarification, the relationship between the two structures is plotted in Figures (4-15 to 4-19). The results illustrated in these figures clearly show that the abutment to pier spacing affects the local scour depth at the pier.

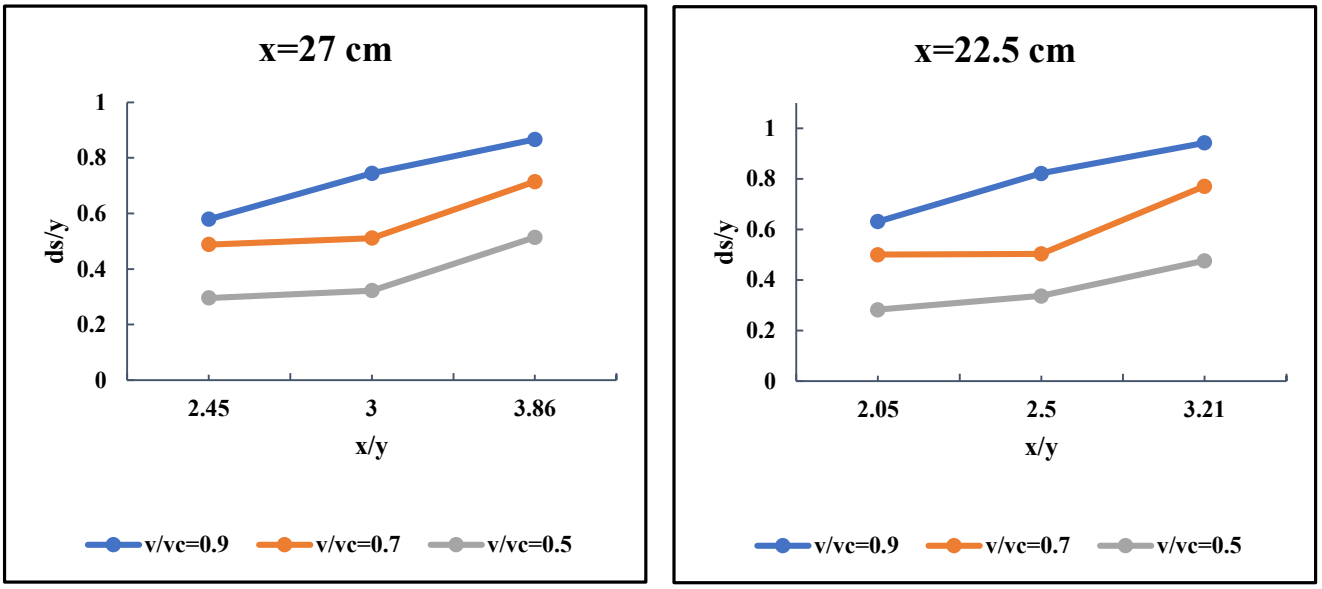

Figure 4-15: Effect of space between pier and vertical-wall abutment, w=5 cm.

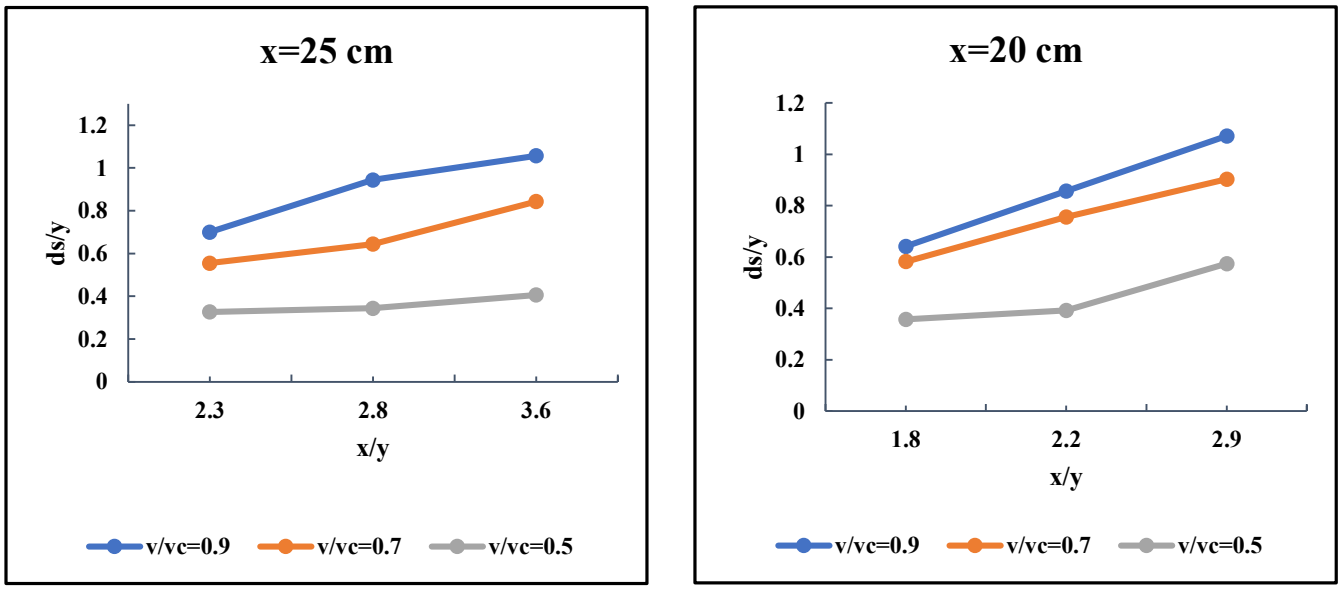

Figure 4-16: Effect of space between pier and vertical-wall abutment, w=7.5 cm.

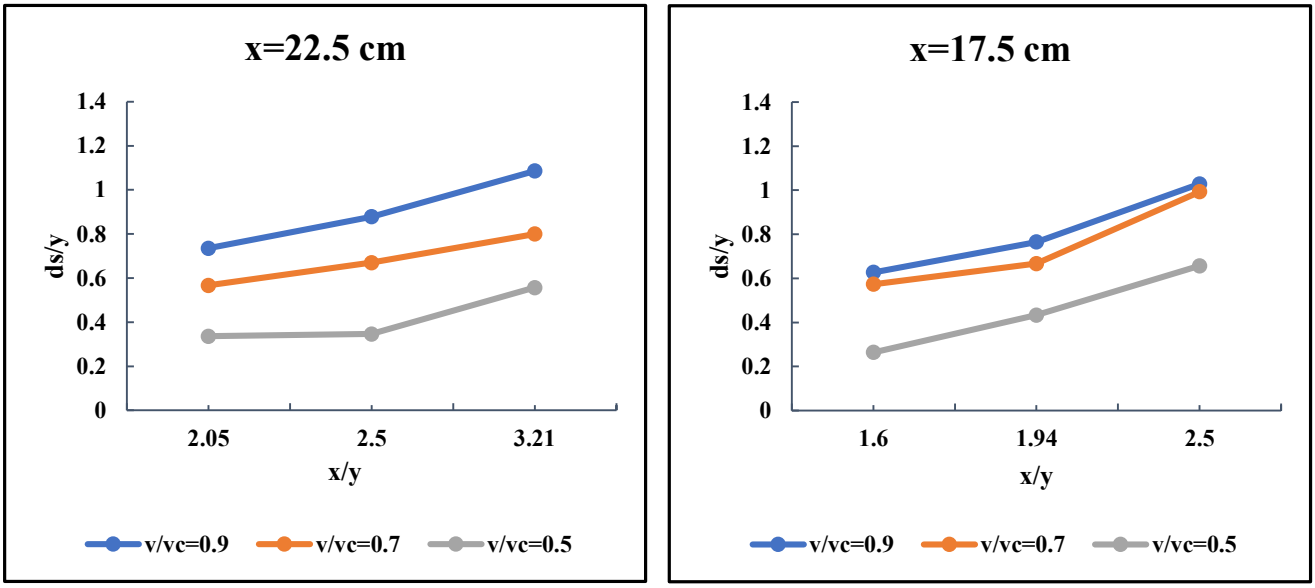

Figure 4-18: Effect of space between pier and vertical-wall abutment, w=10 cm.

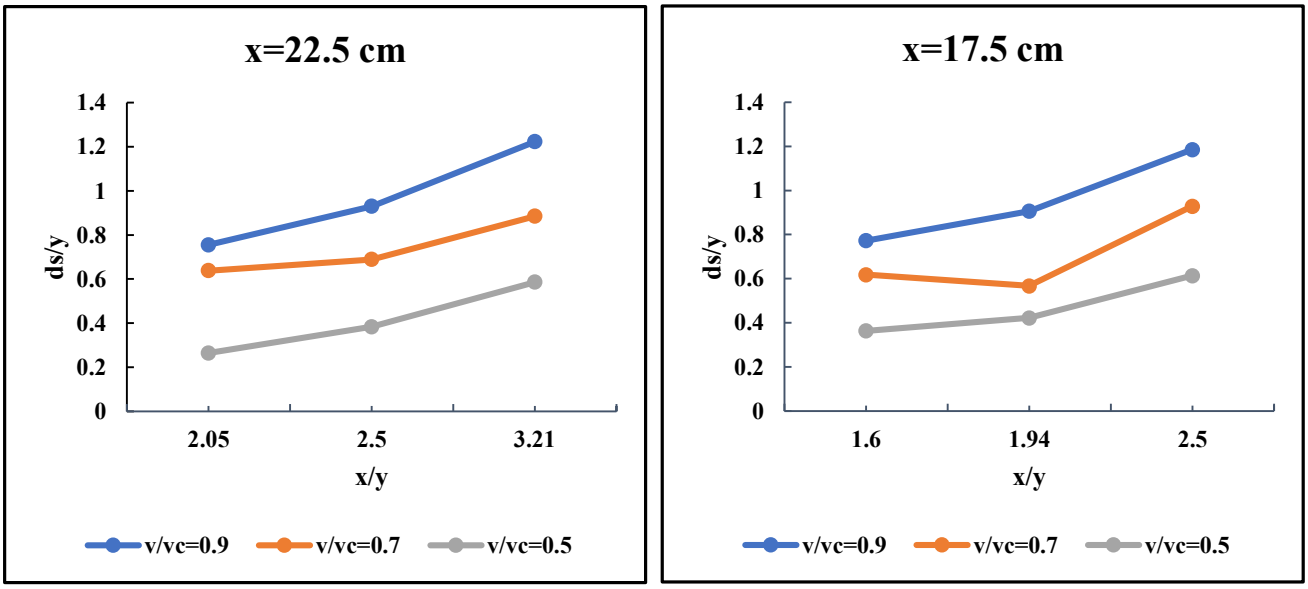

Figure 4-17: Effect of space between pier and wing-wall abutment on scour depth nearby the pier.

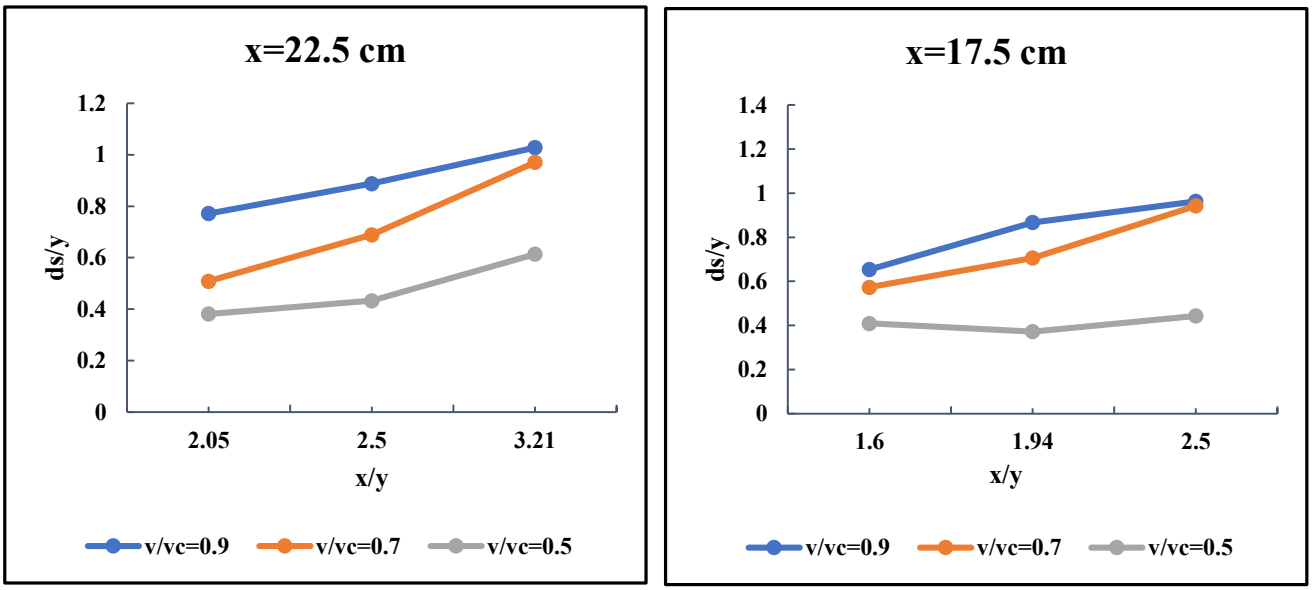

Figure 4-19: Effect of the space between the pier and the trapezoidal on scour depth nearby the pier.

The results indicate that reducing the abutment to pier spacing generally leads to an increase in the total scour intensity. However, this effect is not uniform across both structures. At closer distances, particularly at x = 17.5 cm, the interaction between the horseshoe vortices of the pier and abutment alters the local flow field. This results in increased scour depth at the pier due to intensified turbulence and vortex interactions, while the scour depth at the abutment decreases as a result of sediment backfilling and vortex suppression. This effect can be observed in the cases of the abutment models V3 and wing-wall. Therefore, the reduction in spacing does not uniformly increase scour around both elements but rather shifts the dominant erosion toward the pier while mitigating it at the abutment. At the same time, increasing the abutment width (w) narrows the effective flow passage, thereby increasing the flow velocity and aggravating scour, especially for vertical abutment. Compared to

abutment geometries, the scour depths at wing-wall abutment are shallowest since such abutment has the ability to redirect flow and prevent the formation of corner vortices, whereas trapezoidal abutment produces intermediate behavior.

When spacing becomes small, pier-abutment scour holes will subsequently overlap and unite. This overlapping increases the turbulence and complexity of the flow near the pier, causing additional scour depth, while simultaneously reducing the abutment scour through sediment backfilling.

This results in backfilling off sediment in the abutment scour hole, which eventually lowers the scour depth of the abutment. This means that reducing x does not merely minimize the scour in each of the structures; instead, it redistributes the scour intensit. Some experimental photos are selected to illustrate the influence of reducing the distance between the pier and abutment Figures (4-20 and 4-24).

Experimental observations confirmed this behavior: at wider spacing, two separate holes were observed, whereas at reduced spacing, the scour holes overlapped or merged into one combined hole with similar width and length, but different maximum depths for the pier and abutment.

Generally, as the distance between the abutment and the pier decreases, an asymmetric distribution of scour develops. In some cases, scour increases at the abutment and decreases at the pier, while in other cases, the opposite occurs, depending on the shape of the abutment and the intensity of the flow. Variations in borehole depth and sediment distribution are visible in the images. Figure 4-20 shows that at x = 27 cm, two separated holes appear with a space of 7.5 cm before the margin, while at x = 22.5 cm, the overlap of the holes increases slightly, with an increase in the depth of the pier hole. In Figure 4-21, despite the medium flow intensity, the overlap occurred only in

this model, and despite the overlap, each hole maintained an independent and regular shape. Figure 4-22 shows that the scour hole of the abutment extends longitudinally over wide distances and then begins to join with pier scour, but at x=20 cm, the pier hole remained regular and was not affected by the overlapping. In Figure 4-23, the scour hole of the abutment extends transversely and is concentrated at the edge corner of the abutment. Finally, it can be observed from Figure 4-24 that reducing the distance between them results in a single scour hole with the same width and length but differing in the maximum scour depth of each structure.

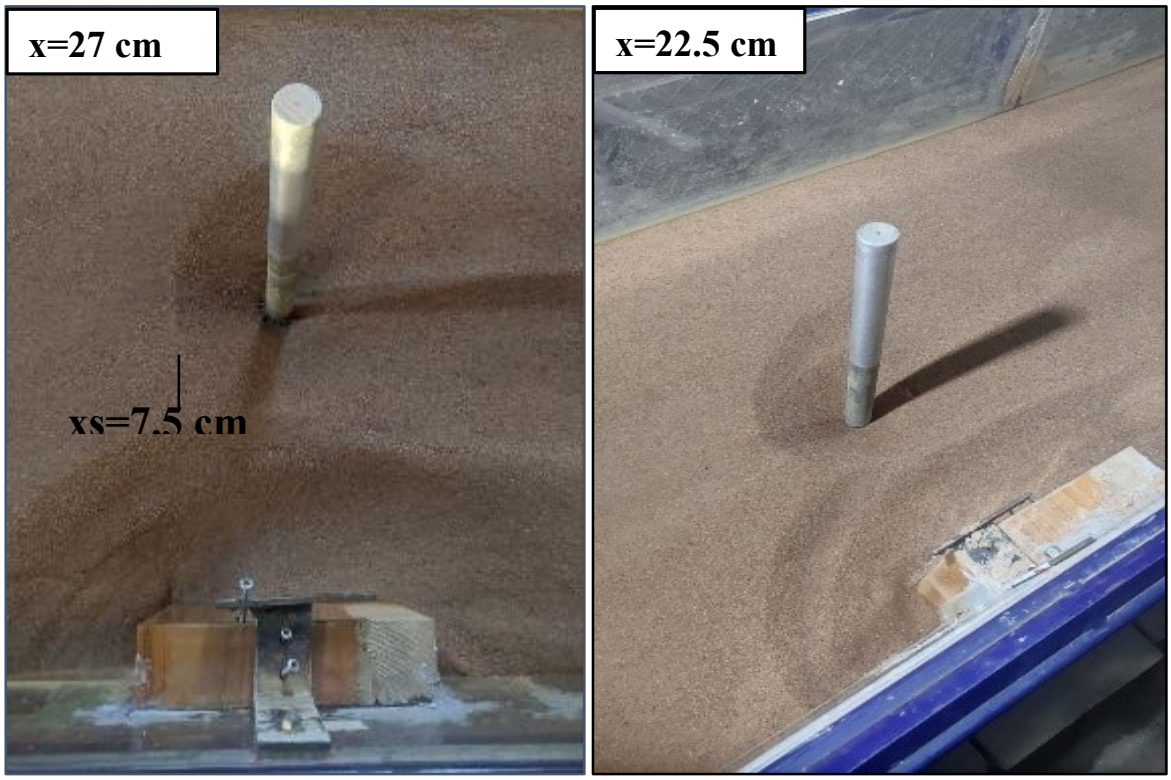

Figure 4-20: The influence of reducing the distance between pier and abutment using the V1 abutment at v/vc=0.9.

Figure 4-21: The influence of reducing the distance between the pier and abutment using the V3 abutment at v/vc=0.63.

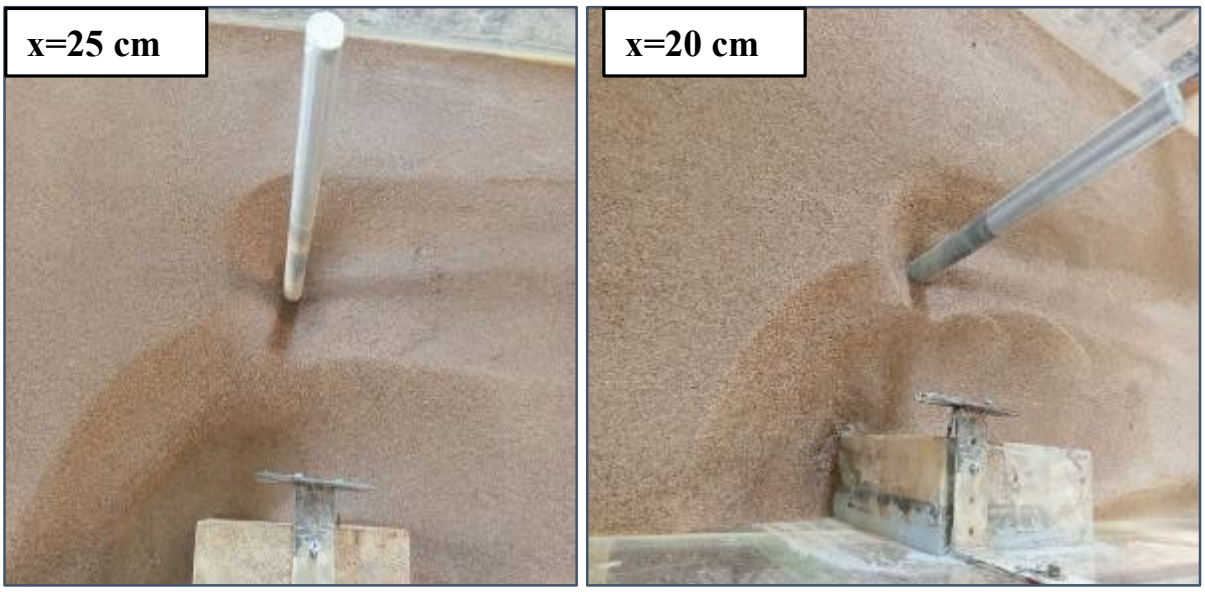

Figure 4-22: The influence of reducing the distance between pier and abutment using the V2 abutment at v/vc=0.7.

Figure 4-23: The influence of reducing the distance between pier and abutment using the trapezoidal abutment at v/vc=0.7.

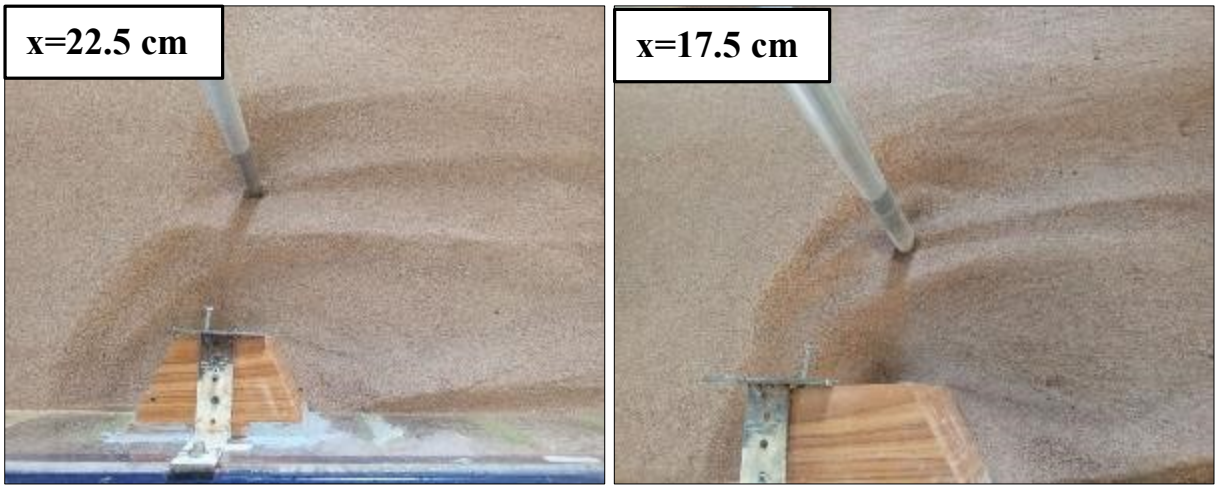

Figure 4-24: The influence of reducing the distance between pier and abutment using the wing-wall abutment at v/vc=0.9.

Furthermore, it can be observed from the figures above and the tables in Appendix A, Tables A-3 to A-12, that at larger spacings between the models, the interaction of scour holes begins to appear at a flow intensity of

v/vc = 0.9 for model V1. For model V2, the interaction starts at v/vc = 0.7, while for model V3, it begins at a lower threshold of v/vc = 0.6. While for cases of the wing-wall and trapezoidal model, their behavior is similar to the V2 case when the interaction begins at v/vc=0.7.

In summary, the experiments have shown that scour patterns vary with abutment geometry. Vertical-wall abutments produced the deepest and most concentrated scour, wing-wall abutments showed the shallowest scour due to flow redirection, while trapezoidal abutments exhibited intermediate behavior with longitudinal spreading. These results indicate that geometry controls not only the scour depth but also the interaction mechanism between pier and abutment scour holes.

4.3 Comparative Analysis Between the Abutment Models Impact

To explain how abutment geometry and relative positioning influence local scour features, a comparative analysis of abutment model tests under the same hydraulic conditions was conducted. Two main variables were considered in the comparison: the width of the abutment wall (w) and the space (x) between the abutment and the neighboring bridge pier. This approach enabled the assessment of flow contraction and vortex interactions between the abutment and the pier. The study tested three vertical wall abutment models (5 cm, 7.5 cm, and 10 cm wide); In addition to a single inclined wing-wall abutment and a trapezoidal abutment, two spacing distances were examined . These setups aimed to simulate various hydraulic scenarios. Figures (4-25 - 4-30) illustrate the maximum scour depths across ten experimental runs for each model, compared to a reference case where the pier was tested alone. According to the hydraulic parameters of Table (4-1).

The data enable detailed comparison of how changes in abutment width, spacing, and the use of angled wing walls influence the severity and development of local scour. Results consistently show that, in all figures, the presence of an abutment near the pier increases the scour depth associated with the reference case. However, the magnitude of increase depended on hydraulic conditions, abutment geometry, and spacing between the pier and abutment. Notably, the greatest scour depths occur with the three vertical-wall and trapezoidal abutment models, while the wing-wall abutment consistently produced the smallest values. This is likely because the inclined angle of the wing-wall abutment helps redirect flow away from the foundation's leading edge, reducing flow concentration and horseshoe vortex intensity around the pier's base. Conversely, vertical-wall abutments directly confront the flow, causing stronger vortex activity and greater local scour.

Previous studies on vertical-wall abutment models have shown that increasing abutment width (w) generally reduces scour depth. (Abdelaziz et al., 2019) reported that a higher ratio of abutment width to flow depth (w/y) decreases scour depth and width due to greater flow resistance and lower velocity near the abutment toe. However, in this study, increasing abutment width led to greater scour depth, particularly once the pier was near the abutment. This apparent contradiction is due to the reduced effective spacing (x) as the abutment widens. The smaller spacing intensified hydraulic interaction between the pier and abutment, especially their horseshoe vortices, resulting in more aggressive scouring. Therefore, although wider abutments can offer hydraulic benefits when isolated, their effects become more complex when placed near a pier. In such cases, the negative impact of reduced spacing can outweigh the stabilizing effects of increased width, leading to deeper scour.

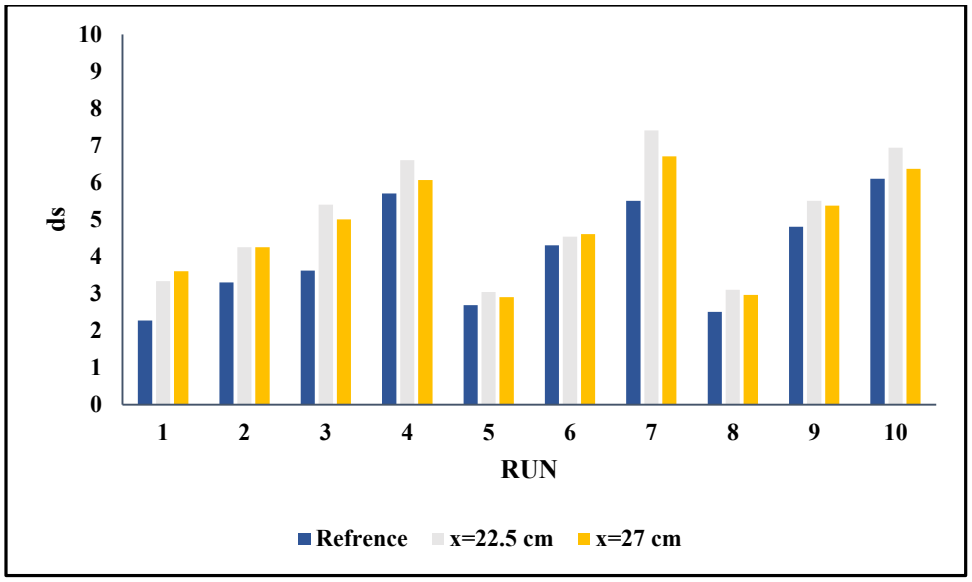

Figure 4-25: Variation of maximum scour depth around pier for vertical-wall abutment (w = 5 cm) at two spacing values (x = 22.5 cm and x = 27 cm) compared to the reference case.

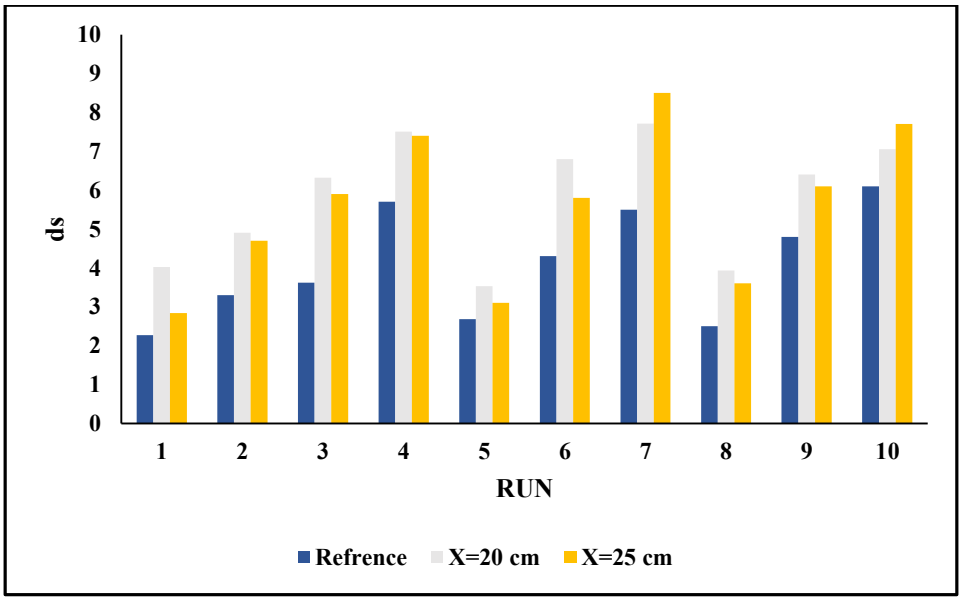

Figure 4-26: Variation of maximum scour depth around pier for vertical-wall abutment (w = 7.5 cm) at two spacing values (x = 20 cm and x = 25 cm) compared to the reference case.

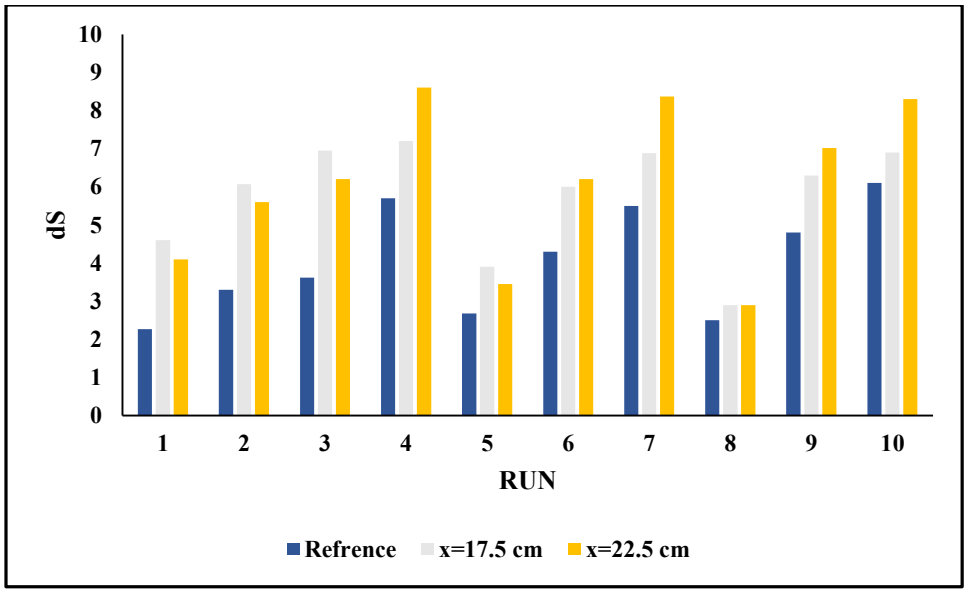

Figure 4-27: Variation of maximum scour depth around pier for vertical-wall Abutment (w = 10 cm) at two spacing values (x = 17.5 cm and x = 22.5cm) compared to the reference case.

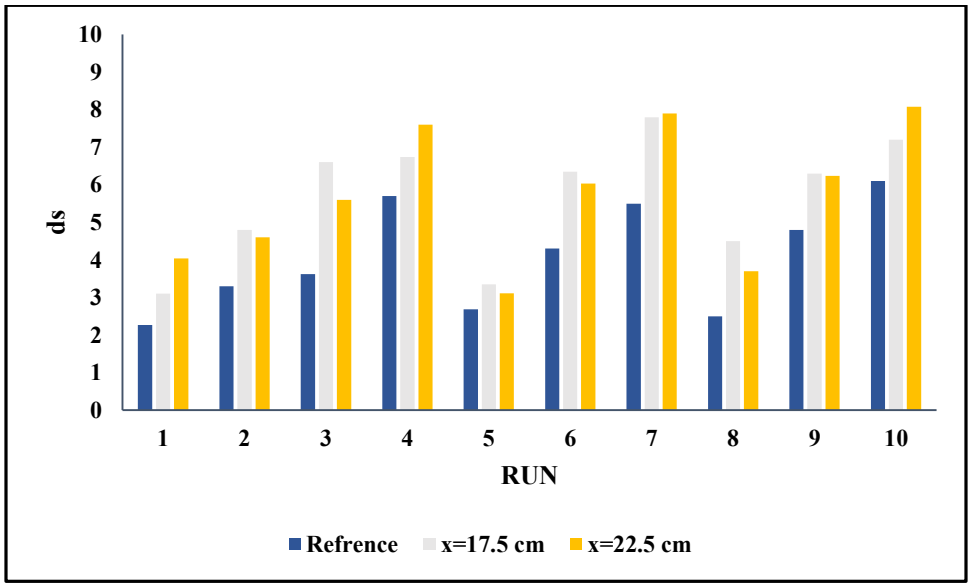

Figure 4-28: Variation of maximum scour depth around pier for wing wall Abutment at two spacing values (x = 17.5 cm and x = 22.5cm) compared to the reference case.

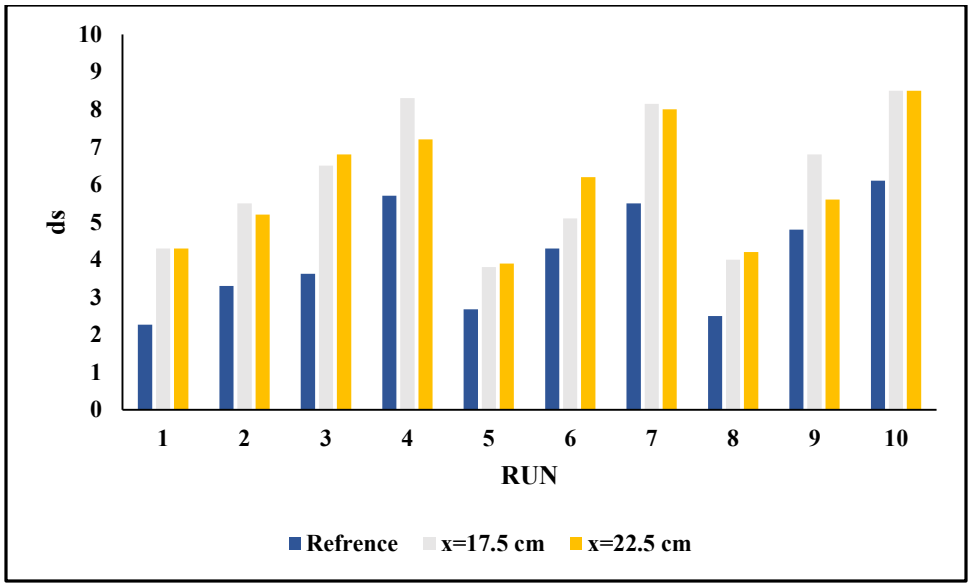

Figure 4-29: Variation of maximum scour depth around pier for trapezoidal Abutment at two spacing values (x = 17.5 cm and x = 22.5cm) compared to the reference case.

4.4 Dimensional Analysis

Dimensional analysis serves as a valuable tool for problem formulation and for revealing the relationships among different physical variables by expressing them in terms of their fundamental dimensions. By introducing appropriate dimensionless parameters, a more comprehensive understanding of the physical processes governing local scour around bridge piers can be obtained. The parameters affecting the maximum scour depth at piers and abutments encompass flow conditions, fluid properties, characteristics of the bed material, structural features of the pier and abutment, flume geometry, and time. These variables are typically expressed using the fundamental dimensions of mass (M), length (L), and time (T), as outlined in Table 4-3.

Table 4-3: Definition of dimensional analysis parameters.

Variable	Definition	Units	Dimensions
Fluid parameters			
ρ	Water density	kg/m^3	ML^{-3}
μ	Dynamic viscosity of water	kg/(m.s)	$ML^{-1}T^{-1}$
g	Gravitational acceleration	m/s^2	LT^{-2}
Flow parameters			
y	Flow depth	cm	L
v	Flow velocity	m/s	LT^{-1}
v_C	Critical velocity for sediment motion	m/s	LT^{-1}
Sediment parameters			
d_{50}	Median particle diameter	mm	L
σ_g	Geometric standard deviation	-	-
ρ_s	Sediment density	kg/m^3	ML^{-3}
Geometric parameters of the flume			
B	Flume width	cm	L
S	Flume bed slope	-	-
Geometric parameters of the pier and abutment			
D	Pier diameter	cm	L
L	Abutment length	cm	L
W	Abutment width	cm	L
X	Distance between the pier and abutment	cm	L
θ	Angle attack of the pier and abutment	-	-

In this study, each model will have a distinctive functional relationship to the prediction of scour depth since it looks at many abutment models and one pier model.The dimensional analysis method used in this study is the Buckingham π-theorem, which represents the maximum scour depth in clear water as a function of the variables listed below:

$$\boldsymbol{d_{smax} = f(\rho, v, \mu, y, g, d_{50}, \sigma_g, \rho_s, v_c, D, B, S, W, L, X, \theta)} \quad \textbf{(4.1)}$$

$$\boldsymbol{\therefore f1(d_{smax}, \rho, v, \mu, y, g, d_{50}, \sigma_g, \rho_s, v_c, D, B, S, W, L, X, \theta) = 0} \quad \textbf{(4.2)}$$

Given that there are seventeen variables (n = 17) and three dimension variables (m=3), the number of dimensionless groups according to

Buckingham's π-theorem is calculated as (n-m) = (17 - 3) = 14. Therefore, there are 14 dimensionless groups. As flowing;

$$\boldsymbol{f_2(\pi_1, \pi_2, \pi_3, \pi_4, \pi_5, \pi_6, \pi_7, \pi_8, \dots\dots\dots \pi_{14}) = 0} \quad \textbf{(4.3)}$$

For this study, the repeated variables were selected as (ρ, v, y)

Consequently, each π functional representation at maximum scour depth will be as follows:

$\pi_1=\rho^{a1}v^{b1}y^{c1}ds_{max}$, $\pi_2=\rho^{a2}v^{b2}y^{c2}\mu$, $\pi_3=\rho^{a3}v^{b3}y^{c3}d_{50}$, $\pi_4=\rho^{a4}v^{b4}y^{c4}D$

$\pi_5=\rho^{a5}v^{b5}y^{c5}v_C$, $\pi_6=\rho^{a6}v^{b6}y^{c6}g$, $\pi_7=\rho^{a7}v^{b7}y^{c7}B$, $\pi_8=\rho^{a8}v^{b8}y^{c8}L$

$\pi_9=\rho^{a9}v^{b9}y^{c9}\rho_s$, $\pi_{10}=\rho^{a10}v^{b10}y^{c10}X$, $\pi_{11}=\rho^{a11}v^{b11}y^{c11}W$, $\pi_{12}=\rho^{a12}v^{b12}y^{c12}\sigma_g$

$\pi_{13}=\rho^{a13}v^{b13}y^{c13}\theta$, $\pi_{14}=\rho^{a14}v^{b14}y^{c14}S$

Using the analysis for every phrase and figuring out for π_1

$M^0 L^0 T^0=(M L^{-3})^{a1} (L T^{-1})^{b1}(L)^{c1} L$

$M:0=a_1 \rightarrow a_1=0$

$L:0=-3a_1+b_1+c_1+1 \rightarrow b_1+c_1=-1$

$T:0=-b_1 \rightarrow b_1=0$ & $c_1=-1$

$\therefore \pi_1=\rho^0 v^0 y^{-1} ds \Rightarrow \pi_1=\frac{dsmax}{y}$, and by the same way $\pi_2=\frac{\mu}{\rho\, v\, y} \rightarrow \pi 2=\frac{\rho\, v\, y}{\mu}=Re$, $\pi_3=\frac{d_{50}}{y}$; $\pi_4=\frac{D}{Y}$; $\pi_5=\frac{V_C}{V}$; $\pi_6=\frac{gy}{v^2} \rightarrow \pi 6=\frac{v^2}{gy}=\frac{v}{\sqrt{gy}}=Fr$; $\pi_7=\frac{B}{Y}$; $\pi_8=\frac{L}{Y}$; $\pi_9=\frac{\rho s}{\rho}$; $\pi_{10}=\frac{X}{Y}$; $\pi_{11}=\frac{W}{Y}$; $\pi_{12}=\sigma_g$; $\pi_{13}=\theta$; $\pi_{14}=S$ so, the following functions obtained:

$$\boldsymbol{f_3\left(\frac{d_{smax}}{y}, \frac{d_{50}}{y}, \frac{D}{y}, \frac{vc}{v}, \frac{B}{y}, \frac{L}{y}, \frac{\rho_s}{\rho}, \frac{X}{y}, \frac{W}{y}, Re, Fr, \sigma_g, \theta, S\right) = 0} \quad \textbf{(4.4)}$$

To simplify the governing relationships, a set of assumptions was adopted to minimize the influence of secondary dimensionless parameters.

These assumptions ensured the necessary conditions for evaluating the maximum scour depth. Accordingly, the sediment was considered uniform (d_{50}, σ_g), the relative density (ρ and $\rho_{s)}$ was maintained constant, the fluid viscosity (μ) was assumed steady, the pier diameter (D) and flume width (B) were kept constant, the bed slope was fixed as horizontal (S=0), and both the pier and abutments were aligned with the flow direction (θ=0) Under these conditions, the functional relationship can be expressed as follows:

$$\boldsymbol{f_4\left(\frac{d_{smax}}{y}, \frac{vc}{v}, \frac{X}{y}, \frac{W}{y}, \frac{L}{y}, Fr\right) = 0} \quad \textbf{(4.5)}$$

By applying the properties of dimensional analysis, equation (4.5) can be represented in terms of maximum scour depth as:

$$\boldsymbol{\frac{d_{smax}}{y} = f_5\left(\frac{v}{vc}, \frac{X}{y}, \frac{W}{y}, \frac{L}{y}, Fr\right)} \quad \textbf{(4.6)}$$

4.5 Development of New Formulas

To develop new predictive equations based on the non-dimensional parameters that govern the maximum scour depth ratio (ds/y) about bridge piers influenced by abutment geometry, as introduced in Equation (4.6).

A statistical analysis was conducted using IBM SPSS Statistics 30. Non-linear regression techniques were applied to evaluate five separate models corresponding to five distinct abutment shapes. The resulting equations incorporate the effects of various hydraulic and geometric factors that influence local scour. The developed empirical expressions are presented below:

By vertical-wall abutment(V1):

$$\frac{ds_{max}}{y} = \exp\left(a+\frac{b}{\frac{V}{Vc}}\right).\exp\left(c+\frac{d}{\frac{x}{y}}\right).\exp\left(e+\frac{f}{\frac{W}{y}}\right).\exp\left(g+\frac{h}{\frac{L}{y}}\right).\exp\left(i+\frac{j}{Fr}\right) \quad (4.7)$$

Where:

a= -19.7 **b**=0.363 **c**=-0.182 **d**=0.9 **e**=14.56 **f**=4.8 **g**=-11.6 **h**=-20.63 **i**=17.83 **j**=- 0.4

The equation has a coefficient of determination of ($R^2 = 0.948$)

By vertical-wall abutment(V2):

$$\frac{ds_{max}}{y} = \exp\left(a+\frac{b}{\frac{V}{Vc}}\right) + (c + d\frac{x}{y} + e(\frac{x}{y})^2).(f(g^{Ly}).\exp\left(h+\frac{i}{Fr}\right) \quad (4.8)$$

Where:

a= 1.168 **b**=-0.396 **c**=0.56 **d**=1.125 **e**=-0.19 **f**=0.198 **g**=1.269 **h**=0.792**i**=-0.186

The equation has a coefficient of determination of ($R^2 = 0.931$)

By vertical-wall abutment(V3):

$$\frac{ds_{max}}{y} = \exp\left(a+\frac{b}{\frac{V}{Vc}}\right).(c + d\frac{x}{y} + e(\frac{x}{y})^2).(f + g\frac{w}{y} + h(\frac{w}{y})^2).(i + j\frac{L}{y} + k(\frac{L}{y})^2).\exp\left(l+\frac{m}{Fr}\right)$$

(4.3)

Where:

a= 1.38 **b**=1.82**c**=0.852 **d**=0.688 **e**=-0.117 **f**=0.427 **g**=-0.328**h**=0.117**i**=0.543**j**=-0.154 **k**=0.031 **l**=1.55 **m**=-0.91

The equation has a coefficient of determination of ($R^2 = 0.913$)

By wing-wall abutment:

$$\frac{ds_{max}}{y} = \exp\left(a+\frac{b}{\frac{V}{Vc}}\right).\exp\left(c+\frac{d}{Fr}\right).(e + f\frac{x}{y} + g(\frac{x}{y})^2 .(h.\exp\left(i\frac{l}{y}\right)) \quad (4.9)$$

Where:

a=0.933, **b**=-0.014, **c**=0.514, **d**=-0.294, **e**=3.308, **f**=0.322, **g**=-0.034, **h**=0.105, **i**=0.272

The equation has a coefficient of determination of (R^2 = 0.916)

By trapezoidal abutment:

$$\frac{ds_{max}}{y} = \exp\left(a+\frac{b}{\frac{V}{Vc}}\right).(c + d.Fr).\exp\left(e+\frac{f}{\frac{x}{y}}\right).\left(g.\exp\left(h\frac{l}{y}\right)\right) \quad \textbf{(4.10)}$$

Where:

a=0.787, **b**=0.392, **c**=-0.306, **d**=3.321, **e**=0.35, **f**=0.587, **g**=0.12, **h**=0.353

The equation has a coefficient of determination of R^2 = 0.936.

For each model, 70% of the data were used to fit the model, which included 14 runs from 20 runs, and the rest 6 runs, which represent 30% of the data, were used to evaluate. Predicted, observed, and residual with Scatterplots were illustrated in Appendix A, Tables A-13 to A-17.

4.6 Assessment of Abutment Geometry Effects on Scour Depth Using Artificial Neural Networks (ANN)

Using the collected datasets from experimental studies, IBM SPSS Statistics was used in applying Artificial Neural Networks (ANNs) to establish relationships between hydraulic parameters and local scour due to analytics properties. The purpose of the training process was to model the equilibrium scour depth (ds) based on the abutment, the Froude number, flow intensity, and the distance x between the abutment and the supporting bridge pier. To this end, a Single-Hidden-Layer Multi-Layer Perceptron (MLP) algorithm was chosen with 3-10 nodes. The data was split into 70 % training and 30 % testing. The performance of each model was determined through

relative error, Performance was evaluated using both the Root Mean Squar Error (RMSE) and Coefficient of Determination (R^2) statistics between the observed values and the predicted values. Individual ANN models were produced in the different abutment designs that varied in both shape and separation from the pier. The model according to the vertical-wall configuration abutment showed the largest R^2 of 0.983 among all the models tested, as shown in Table 4-4. The ANN models across the arrangements outdid the nonlinear regression models in the areas of prediction accuracy.

Table 4-4: Performance of ANN models.

Abutment model	Relative Error		RMSE	R^2	Number of hidden layers	Number of units in the hidden layer	Activation functions
	training	testing					
Vertical-wall 1	0.033	1.049	0.0393	0.966	1	3	Hyperbolic tangent
Vertical-wall 2	0.061	0.136	0.0571	0.936	1	4	Hyperbolic tangent
Vertical-wall 3	0.022	0.020	0.0324	0.983	1	6	Hyperbolic tangent
Wing-wall	0.013	0.107	0.0477	0.952	1	3	Hyperbolic tangent
Trapezoidal	0.065	0.162	0.0583	0.935	1	3	Hyperbolic tangent

4.7 Sensitivity Analysis

A sensitivity analysis was carried out to assess the impact of each input variable on the scour depth predictions obtained from both non-linear regression and ANN models. The goal was to identify the most influential parameter(s) that should be prioritized in future research. Although numerous factors influence scour depth around bridge piers as outlined in Chapter Two, this analysis specifically concentrates on the geometry of the abutment. This

focus was chosen because other influencing variables have already been extensively explored in previous studies, and their relative importance are well-established. The analysis examined various input combinations, as presented in Table 4-5, by systematically omitting one input parameter at a time. The resulting changes in model performance were evaluated using RMSE and R^2 as key performance metrics. Results in Table 4-3 by the ANN models propose that the abutment geometry influences the calculation of the local scour around the pier, in contrast to cases of removing the abutment dimensions. For vertical-wall abutments, both length and width affected the scour depth, while for trapezoidal abutments, only the length was affected, but the length of the wing-wall abutment didn't significantly influence it. On the contrary, in non-linear regression, it is affected for both models, the trapezoidal and wing-wall. In non-linear regression, vertical wall 1 and vertical wall 3, the removal of length or width, or both, didn't influence, though vertical wall 2 had a major influence.

The findings of this thesis align with those of Ali and Güna (2021), who demonstrated the effectiveness of ANNs in predicting scour depth more accurately than regression models. However, while their study focused on pier characteristics, the current research expands the application by incorporating abutment geometry and pier-abutment interaction, revealing through sensitivity analysis that abutment shape, particularly in vertical-wall configurations, plays a significant role in influencing scour depth.

Table 4-5: Sensitivity analysis.

Abutment model	Non-linear regression		ANN		Removed parameters	Input combination
	RMSE	R^2	RMSE	R^2		
Vertical-wall 1	0.0483	0.948	0.0393	0.966	-	x/y, L/y, Fr, w/y, v/vc
	0.118	0.947	0.0437	0.964	w/y	x/y, L/y ,Fr ,v/vc
	0.0399	0.947	0.0361	0.948	L/y	x/y, w/y, Fr, v/vc
	0.0389	0.943	0.0685	0.884	w/y,L/y	x/y, Fr, v/vc
Vertical-wall 2	0.1505	0.829	0.0571	0.936	-	x/y,L/y, Fr, w/y, v/vc
	0.0645	0.931	0.0542	0.943	w/y	x/y,L/y, Fr ,v/vc
	0.0549	0.926	0.0526	0.947	L/y	x/y, w/y, Fr ,v/vc
	0.1042	0.889	0.0848	0.869	w/y,L/y	x/y, Fr, v/vc
Vertical-wall 3	0.0596	0.913	0.0324	0.983	-	x/y,L/y, Fr ,w/y, v/vc
	0.0623	0.915	0.0694	0.926	w/y	,x/y,L/y, Fr, v/vc
	1.3593	0.92	0.0492	0.962	L/y	x/y, w/y, Fr, v/vc
	0.0865	0.901	0.0678	0.932	w/y,L/y	x/y, Fr, v/vc
Wing-wall	0.352	0.911	0.0477	0.952	-	,x/y,L/y, Fr, v/vc
	-	-	0.044	0.958	L/y	x/y , Fr, v/vc
Trapezoidal	0.0555	0.934	0.0583	0.935	-	x/y, L/y, Fr, v/vc
	-	-	0.0803	0.881	L/y	x/y, Fr, v/vc

4.8 Comparison with Previous Studies

The findings of the present study thesis align with earlier research investigating the interaction between bridge piers and abutments and its impact on local scour behavior. (Saeed et al., 2023) reported that the presence of an abutment in proximity to a pier can significantly increase the scour depth around the pier by up to 171%**,** while the influence on the abutment scour was minimal at larger distances ($X/D \geq 3$). Their results also demonstrated that placing a pier near an abutment caused an increase in scour hole volume by up to 87% due to the interaction between vortices, which supports the outcomes of the present study. Similarly, this study found that reducing the

spacing between pier and abutment significantly increased scour depth, particularly when abutments with more pronounced vortex generation (such as the trapezoidal shape) were used.

In the study conducted by Muhsen and Khassaf (2022), it was found that reducing the pier-abutment spacing from 23.5 cm to 9 cm led to an increase in pier scour depth by 6.4% to 11.7%**,** and a corresponding decrease in abutment scour depth by up to 19%**,** especially for the vertical-wall abutment. These findings are in good agreement with the current results, where vortex interference between the pier and abutment altered the flow field, leading to a redistribution of scouring. Specifically, the vertical-wall 3 abutment in this study showed increased scour at the abutment and decreased scour at the pier, highlighting the unique interaction patterns influenced by geometry and spacing.

Moreover, all three studies emphasized the importance of abutment geometry in determining scour initiation and location. The current study confirmed that sharp-edged abutments (e.g., vertical-wall) initiate scour near the corners, whereas inclined-face abutments (e.g., wing-wall and trapezoidal) tend to initiate scour near the upstream face. The present findings also supported the well-established conclusion that increased flow intensity and Froude number lead to higher scour depths. From a modeling perspective, both previous studies employed predictive formulations. (Muhsen and Khassaf, 2022) developed dimensionless empirical equations using IBM SPSS, achieving high coefficients of determination (R^2 = 0.958 and 0.977). In contrast, the current study utilized ANNs**,** with the MLP model reaching an even higher accuracy **(**R^2 = 0.983**),** demonstrating the effectiveness of ANN models in handling complex scour prediction problems.

Chapter Five : Conclusions and Recommendations

5.1 Conclutions

In this experimental study, several laboratory tests utilizing physical models in a flume channel were conducted to investigate the impact of abutment geometry arranged to the maximum local scour depth near a cylindrical bridge pier under controlled, identical hydraulic conditions. Five different abutment models were tested under clear-water conditions with a fixed testing duration of three hours per run. The study aimed to illustrate how scour holes form and determine the maximum scour depth caused by the interaction between the flow surrounding the abutment and the nearby pier, which is regarded as a crucial consideration in bridge foundation construction. This chapter presents the study's key results and offers suggestions for further research.

5.2 Main Research Conclusions

The main conclusions of this investigation can be summarized by the following points:

(1) Influence of Abutments on Pier Scour: The presence of an abutment near a bridge pier significantly increase the pier's scour depth. The magnitude varies based on the abutment's geometry (shape and width), the spacing between the pier and abutment, and hydraulic parameters.

(2) Scour Location and Initiation Patterns:Maximum scour depths were generally observed at the upstream faces of both the pier and abutment. However, the initiation point of scour differed depending on abutment geometry. For abutments with inclined ends (e.g., wing-wall and trapezoidal), scour initiated near the upstream face. In contrast, sharp-edged geometries

such as the vertical-wall abutment exhibited initial scour near the corners. In the case of the vertical-wall 3 abutments, maximum scour occurred at the side face directly facing the pier.

(3) Interaction Effects Between Pier and Abutment: When the spacing between pier and abutment decreased, scour depth at the pier increased while scour depth at the abutment decreased due to vortex interaction,especially horseshoe vortices. This trend was observed in all abutment models except vertical-wall 3, where the opposite occurred: abutment scour increased while pier scour decreased.

(4) Scour Depth Variation with Distance Reduction: Reducing the spacing from 22.5 cm to 17.5 cm led to increases in pier scour depth by 53.09%, 47.51%, and 42.67% for trapezoidal, vertical-wall 3, and wing-wall abutments, respectively. Similarly, for vertical-wall 1 and 2 abutments, decreasing the distance from 25 cm to 20 cm resulted in scour depth increases of 24.61% and 46.7%, respectively.

(5) Comparative Scour Intensity Between Abutment Models: Among all tested abutment geometries, the trapezoidal model produced the largest increase in scour depth at x = 17.5 cm, while the vertical-wall 1 model exhibited the least effect at x = 27 cm.

(6) Effect of Abutment Width and Spacing in Vertical-Wall Models: In vertical-wall abutments, the maximum pier scour depth decreased as abutment width decreased and spacing from the pier increased.

(7) Empirical Scour Prediction Model:A non-dimensional empirical formula developed using IBM SPSS Statistics 30 for different abutment shapes showed high determination coefficients, making it suitable for predicting maximum scour depth around piers under conditions similar to those studied.

(8) Artificial Neural Network (ANN) Performance: Equilibrium scour depth around piers influenced by adjacent abutments was effectively modeled using Artificial Neural Networks. The Multilayer Perceptron (MLP) model achieved high accuracy, especially for the vertical-wall 3 abutment (R^2 = 0.983). Overall, ANN models outperformed traditional nonlinear regression, demonstrating their reliability in complex scour prediction tasks.

(9) Key Parameters from Sensitivity Analysis: Sensitivity analysis revealed that abutment width and length are the most influential parameters in predicting pier scour depth.

5.3 Recommendations

The following suggestions are put up for more research:

1. Validation with field or large-scale flume Data: This involves comparing the proposed scour equations with empirical data or larger-scale physical models to evaluate their relevance in natural conditions.
2. Extension to live-bed and sediment transport conditions: Analyzing the relationship between sediment mobility and abutment geometry.
3. Impact of compound channels and floodplain geometry: Incorporating intricate geometrical and hydraulic boundaries to accurately represent the conditions at the bridge sites.
4. Investigation of composite pier and abutment arrangements in skewed flow: Investigation of the behavior of flow angles on the scour distribution as well as structural interaction.
5. Using complex models of pier and abutment, non-uniform sediment size, and supercritical flow.
6. Numerical simulation coupled with physical modeling: Employing a computational fluid dynamics (CFD) approach to enhance and broaden

experimental results, especially in the analysis of intricate flow patterns and vortex dynamics.

7. Using artificial intelligence tools to interpret and analyze the relationship between the abutment and the pier, in addition to developing extensive models that can predict the dimensions of the scour hole according to different shapes.

References

- Abdelaziz, A.A.E.F., Elawady, E.E.Z., Fathy, I., and Yehia, M.,(2019. Local scour around a complex pier group at varying orientations. River Research and Applications, 36(1), pp.84–97.
- Abed, B.S. and Majeed, H.Q., 2020, March. The behavior of scouring around multiple bridge piers having different shapes. In IOP Conference Series: Materials Science and Engineering (Vol. 745, No. 1, p. 012158). IOP Publishing.
- Ahmad, M., 1953. Experiments on design and behavior of spurdikes. In Proceedings of IAHR Conference (pp. 145-159).
- Alabi, P.D., 2006. Time development of local scour at a brıdge pıer fıtted wıth a collar (Doctoral dissertation, M. Sc Thesis, University of Saskatchewan, Canada).
- Al-Awadi, A.T. and Al-Khafaji, M.S., 2020. Scour Depth at Single Cylindrical Bridge Piers with Debris Jam: An Experimental Comparative Study. In IOP Conference Series: Materials Science and Engineering (Vol. 671, No. 1, p. 012101). IOP Publishing.
- Al-Awadi, A.T., 2020. Experimental and numerical investigation of the debris configuration effect on local scour around bridge piers. PhD thesis, University of Technology, Baghdad, Iraq.
- Ali, A.S.A. and Günal, M., 2021. Artificial neural network for estimation of local scour depth around bridge piers. Archives of Hydro-Engineering and Environmental Mechanics, 68(2), pp.87-101.

- Alkhouly, M., Shamaa, M., Sarhan, T. and Ezzeldin, R., 2019. Local scour around bridge abutment. International Journal of Scientific and Engineering Research, 8(1), pp.1–10.
- Al-Shukur, A.H.K. and Hussein, N.S., 2021. Effects of shape and skew-angle of bridge piers on local scour. J Eng Sci Technol, 16(3), pp.2748-2762.
- Ansari, S.A., Kothyari, U.C., and Ranga Raju, K.G., 2002. Influence of cohesion on scour around bridge piers. Journal of Hydraulic Research, 40(6), pp.717-729.
- Arneson, L.A., 2012. Evaluating scour at bridges (No. FHWA-HIF-12-003). United States. Federal Highway Administration.
- Ataie-Ashtiani, B. and Aslani-Kordkandi, A., 2013. Flow field around single and tandem piers. Flow, turbulence and combustion, 90(3), pp.471-490.
- Barbhuiya, A.K. and Dey, S., 2004. Local scour at abutments: A review. Sadhana, 29(5), pp.449-476.
- Ben Mohammad Khajeh, S. and Vaghefi, M., 2020. Investigation of abutment effect on scouring around inclined pier at a bend. Journal of Applied Water Engineering and Research, 8(2), pp.125-138.
- Breusers, H.N.C. and Raudkivi, A.J., 1991. Scouring, Hydraulic Structures Design Manual. Balkerna, Rotterdam, 2.
- Breusers, H.N.C., Nicollet, G. and Shen, H.W., 1977. Local scour around cylindrical piers. Journal of Hydraulic Research, 15(3), pp.211-252.
- Chabert, J. and Engeldinger, P. 1956. Etude des affouillements autour des piles de points (Study of scour at bridge piers). Bureau Central d

Etudes les Equipment d Outre-Mer, Laboratoire National d Hydraulique, France.

- Cheremisinoff, N.P. and Cheng, S.L., 1987. Hydraulic Mechanics 2, Civil Engineering Practice. Technomic Publ. Company, Lancaster, Pennsylvania, USA.
- Chiew, Y.M. and Melville, B.W., 1987. Local scour around bridge piers. Journal of Hydraulic Research, 25(1), pp.15-26.
- Chiew, Y.M., 1995. Mechanics of riprap failure at bridge piers. Journal of Hydraulic Engineering, 121(9), pp.635-643.
- Dey, S., 1999. Time-variation of scour in the vicinity of circular piers. Proceedings of the Institution of Civil Engineers-Water Maritime and Energy, 136(2), pp.67-75.
- Dongol, D.M.S. 1994 Local scour at bridge abutments. Report No. 544. School of Engineering, University of Auckland, Auckland, New Zealand.
- Ettema, R. 1980. Scour at bridge piers: phD Thesis, Auckland University, Auckland, New Zealand.
- Ettema, R., Constantinescu, G. and Melville, B., 2011. Evaluation of bridge scour research: Pier scour processes and predictions (No. NCHRP Project 24-27 (01)).
- Fakhimjoo, M.S., Ardeshir, A., Behzadian, K., and Karami, H., 2023. Experimental investigation and flow analysis of clear-water scour around pier and abutment in proximity. Water Science and Engineering, 16(1), pp.94–105.
- Fanzetti, S., Larcan, E. and M. 1982 "Influence of test duration on the evaluation of ultimate scour around circular piers ", International

Conference on the Hydraulic Modelling of Civil Engineering Structures, Organised and Sponsored by BHRA Fluid Engineering, University of Warwick, Coventry, England, September 22- 24, 16 p.

- Garde, R.J. and Ranga-Raju, K.G. 1985. Mechanics of sediment transportation and alluvial stream problems. John Wiley & Sons, 618 p.
- Gazi, A.H. and Afzal, M.S., 2020. A new mathematical model to calculate the equilibrium scour depth around a pier. Acta Geophysica, 68(1), pp.181-187.
- Gill, M.A. 1972 'Erosion of sand beds around spur dikes', *Journal of the Hydraulics Division*, 98(9), pp. 1587–1602.
- Heidarpour, M., Khodarahmi, Z. and Mousavi, S.F., 2003, August. Control and reduction of local scour at bridge pier groups using slot. In Proceedings, XXX IAHR Congress, Thessaloniki, Greece, August (pp. 24-29).
- Hirshfield, F., 2015. The impact of ice conditions on local scour around bridge piers (Doctoral dissertation, University of Northern British Columbia).
- Hoffmans, G.J.C.M. and Verheij, H.J. 1997. Scour manual. A.A. Balkema, Rotterdam, Netherlands, 205 p.
- ISO 2022 Measurement of fluid flow by means of pressure differential devices inserted in circular cross-section conduits running full, Part1: General principles and requirements (ISO 5167-1:2022).Geneva: International Organization for Standardization.
- Kandasamy, J.K., 1989. Abutment scour. University of Auckland, School of Engineering Report, (458).

- Kwan, R.T. and Melville, B.W., 1994. Local scour and flow measurements at bridge abutments. Journal of Hydraulic Research, 32(5), pp.661-673.
- Kwan, T.F. 1984. Study of abutment scour. Report No. 328. School of Engineering, University of Auckland, Auckland, New Zealand.
- Kwan, T.F., 1988. A study of abutment scour (Doctoral dissertation, ResearchSpace@ Auckland).
- Lagasse, P.F. and Richardson, E.V., 2001. ASCE compendium of stream stability and bridge scour papers. Journal of Hydraulic Engineering, 127(7), pp.531-533.
- Lauchlan, C. S. & Melville, B. W. 2001 'Riprap protection at bridge piers', Journal of Hydraulic Engineering, 127, pp. 412–418.
- Laursen, E. M. & Toch, A. (1956) Scour around bridge piers and abutments. Iowa Highway Research Board Ames, IA.
- Lee, S. O. 2006 "Physical modeling of local scour around complex bridge piers", PhD Thesis, School of Civil and Environmental Engineering.
- Lin, C., Han, J., Bennett, C. & Parsons, R. L. 2014 'Case history analysis of bridge failures due to scour', Climatic effects on pavement and geotechnical infrastructure.
- Maatooq, J.S. 2008 'Interference of scouring action between pier and abutment: primary approach', Engineering and Technology Journal, 26, pp. 565–569.
- Melville, B. 1975 Local scour at bridge sites. University of Auckland, School of Engineering, Auckland, New Zealand.

- Melville, B. 2008 ‘The physics of local scour at bridge piers’, Fourth international conference on scour and erosion, pp. 28–38.
- Melville, B. W. & Coleman, S. E. 2000 Bridge scour. Water Resources Publication.
- Melville, B. W. & Raudkivi, A. J. 1977 ‘Flow characteristics in local scour at bridge piers’, Journal of Hydraulic Research, 15, pp. 373–380.
- Melville, B. W. 1984 ‘Live-bed scour at bridge piers’, Journal of Hydraulic Engineering, 110, pp. 1234–1247.
- Melville, B. W. 1997 ‘Pier and abutment scour: integrated approach’, Journal of Hydraulic Engineering, 123, pp. 125–136.
- Melville, B.W. & Chiew, Y.M. 1999. Time scale for local scour at bridge piers. Journal of Hydraulic Engineering, ASCE, 125(1): 59-65.
- Melville, B.W. 1995 ‘Bridge abutment scour in compound channels’, Journal of Hydraulic Engineering, American Society of Civil Engineers, 121(12), pp. 863–868. Melville, B. 1992 ‘Local scour at bridge abutments’, Journal of Hydraulic Engineering, 118, pp. 615–631.
- Memar, S., Hosseinzadeh Dalir, A. & Arvnaghi, H. 2016 ‘An experimental study of impact of bridge pier on depth of scour hole in abutment’, Water and Soil Science, 26, pp. 59–67.
- Mia, M., Nago, H. 2003, "Design Method of Time-Dependent Local Scour at Circular Bridge Pier". Journal of Hydraulic Engineering, 129 (6), 420-427.
- Mohamed, T. A., Noor, M., Ghazali, A. H. & Huat, B. 2005 ‘Validation of some bridge pier scour formulae using field and

laboratory data', American Journal of Environmental Sciences, 1, pp. 119–125.

- Mohamed, Y. A., Abdel-Aal, G. M., Nasr-Allah, T. H. & Shawky, A. A. 2016 'Experimental and theoretical investigations of scour at bridge abutment', Journal of King Saud University-Engineering Sciences, 28, pp. 32–40.
- Mueller, D. S. & Wagner, C. R. 2005. Field observations and evaluations of streambed scour at bridges. United States. Federal Highway Administration. Office of Research.
- Muhsen, N. A. & Khassaf, S. I. 2022. The study of the local scour behaviour due to interference between abutment and two shapes of a bridge pier, Journal of Water and Land Development, pp. 240–250.
- Muzzammil, M., Gangadharaiah, T. & Gupta, A. 2004 'An experimental investigation of a horseshoe vortex induced by a bridge pier', Proceedings of the Institution of Civil Engineers-Water Management, Thomas Telford Ltd, pp. 109–119.
- Nama, A.H., Abdulameer, L., Al-Shammari, M.M.A., Mahdi, N., Al-Maimuri, L., Rashid, F.L., and Kezzar, M., 2025. Practical Evaluation of Scour at Bridge Piers Along River Banks: A Case Study of the Tigris River in Baghdad, Iraq. Journal of Advanced Research in Fluid Mechanics and Thermal Sciences, 127(1), pp.122-139.
- Oben-Nyarko, K. & Ettema, R. 2011 'Pier and abutment scour interaction', Journal of Hydraulic Engineering, 137, pp. 1598–1605.
- Raudkivi, A. J. & Ettema, R. 1977 'Effect of sediment gradation on clear water scour', Journal of the Hydraulics Division, 103, pp. 1209–1213.

- Raudkivi, A. J. & Ettema, R. 1983 ‘Clear-water scour at cylindrical piers’, Journal of Hydraulic Engineering, 109, pp. 338–350.
- Rezaie, A., Afzalimehr, H., Sohrabi, S., Nazari-Sharabian, M., Karakouzian, M. & Ahmadi, R. 2023 ‘Reducing scour around semi-elliptical bridge abutments: application of roughness elements’, Fluids, 8, 306.
- Richardson, E. V. & Davis, S. R. 2001. Evaluating scour at bridges. United States. Federal Highway Administration. Office of Bridge Technology.
- Shen, H. W., Schneider, V. R. & Karaki, S. 1969 ‘Local scour around bridge piers’, Journal of the Hydraulics Division, 95, pp. 1919–1940.
- Sheppard, D. M., Odeh, M. & Glasser, T. 2004 ‘Large-scale clear-water local pier scour experiments’, Journal of Hydraulic Engineering, 130, pp. 957–963.
- Tey, C. B., Raudkivi, A. & Melville, B. W. 1984 Local scour at bridge abutments: a report submitted to the road research unit of the national roads board, department of civil engineering. University of Auckland.
- Wardhana, K. & Hadipriono, F. C. 2003 ‘Analysis of recent bridge failures in the United States’, Journal of Performance of Constructed Facilities, 17, pp. 144–150.
- Wong, W. H. 1982 Scour at bridge abutments.
- Zarrati, A.M., Gholami, H. and Mashahir, M.B. 2004, "Application of collar to control scouring around rectangular bridge piers", Journal of Hydraulic Research, IAHR, Vol. 42, No.1, pp.97-103
- Zolghadr, M., Zomorodian, S. M. A., Fathi, A., Tripathi, R. P., Jafari, N., Mehta, D., Sihag, P., & Azamathulla, H. M. 2023 ‘Experimental

study on the optimum installation depth and dimensions of roughening elements on abutment as scour countermeasures', Fluids, 8, 175.

Appendices

Appendix A- Results of experimental tests

Table A-1: Results of references test of abutment (Model A), (w=10,l=15) cm.

RUN NO.	y (cm)	Q (l/sec.)	v (m/sec.)	vc (m/sec.)	v/vc	ds (cm)	Ws (cm)	Ls (cm)	T (min)
1	7	8.33	0.15	0.30	0.5	3.5	11	10	180
2	7	9.72	0.19	0.30	0.63	4.9	17.5	15	180
3	7	11.11	0.21	0.30	0.7	7.6	21.5	26.5	180
4	7	13.89	0.27	0.30	0.9	11.3	29.5	63	180
5	9	9.72	0.16	0.31	0.52	4.62	12	12.5	180
6	9	13.89	0.22	0.31	0.71	7.4	23.5	28	180
7	9	18.05	0.28	0.31	0.90	13.1	31	63	180
8	11	12.5	0.16	0.32	0.5	3.9	10.5	10.5	180
9	11	18.05	0.23	0.32	0.72	10	28	42	180
10	11	22.22	0.29	0.32	0.91	12.10	34.5	52.5	180

Table A-2: Results of references test of abutment (Model B), (w=10,l=20) cm.

RUN NO.	y (cm)	Q (l/sec.)	v (m/sec.)	vc (m/sec.)	v/vc	ds (cm)	Ws (cm)	Ls (cm)	T (min)
1	7	8.33	0.15	0.30	0.5	4.1	10	9	180
2	7	9.72	0.19	0.30	0.63	5.68	18.5	15	180
3	7	11.11	0.21	0.30	0.7	7.96	22.5	27.5	180
4	7	13.89	0.27	0.30	0.9	10.85	29	43	180
5	9	9.72	0.16	0.31	0.52	3	11	10.5	180
6	9	13.89	0.22	0.31	0.71	6.4	20	24	180
7	9	18.05	0.28	0.31	0.90	11.2	30	53	180
8	11	12.5	0.16	0.32	0.5	4.3	12.5	12.5	180
9	11	18.05	0.23	0.32	0.72	8.06	24.5	31	180
10	11	22.22	0.29	0.32	0.91	13.31	33.5	58.5	180

Appendix A Results of expeimental tests

Table A-3: Results of the pier scour affected by vertical-wall abutment w=5 cm.

RUN		Pier scour affected by vertical-wall abutment x=27cm							Pier scour affected by vertical-wall abutment x=22.5cm						
	w/y	x/y	ds (cm)	ds/y	Ws (cm)	Ls (cm)	xs (cm)	P.I%	x/y	ds (cm)	ds/y	Ws (cm)	Ls (cm)	xs (cm)	P.I%
1	0.714	3.86	3.6	0.514	15	14	20	58.6%	3.21	3.33	0.476	15	16	14	46.7%
2	0.714	3.86	4.25	0.607	19	19	17	28.8%	3.21	4.25	0.607	17.5	18	10	28.8%
3	0.714	3.86	5	0.714	22.5	24.5	11.5	38.12%	3.21	5.4	0.771	24	27.5	7.5	49.17%
4	0.714	3.86	6.06	0.866	27	32.5	5&Intersect	6.32%	3.21	6.6	0.943	24	29	Intersect	15.8%
5	0.556	3	2.9	0.322	13	13	20	8.21%	2.5	3.04	0.337	11	11.5	15	13.43%
6	0.556	3	4.6	0.511	22	24	14	6.98%	2.5	4.53	0.503	18	19.5	7	5.35%
7	0.556	3	6.7	0.744	29	33	8.5&Intersect	21.82%	2.5	7.4	0.822	26.5	30.5	Intersect	34.5%
8	0.455	2.45	2.96	0.269	12	12	20.5	18.4%	2.05	3.1	0.282	10	10	14.5	24%
9	0.455	2.45	5.37	0.488	24.5	26.5	11.5	11.88%	2.05	5.5	0.5	23	25	5.5	14.58%
10	0.455	2.45	6.37	0.579	31	35	7.5&Intersect	4.43%	2.05	6.94	0.631	25.5	30.5	Intersect	13.8%

Where P.I. Percentage increase in pier scour depth, xs= distance between pier and abutment before intersection.

Table A-4: Results of the pier scour affected by vertical-wall abutment w=7.5 cm.

RUN		Pier scour affected by vertical-wall abutment x=25cm							Pier scour affected by vertical-wall abutment x=20cm						
	w/y	x/y	ds (cm)	ds/y	Ws (cm)	Ls (cm)	xs (cm)	P.I%	x/y	ds (cm)	ds/y	Ws (cm)	Ls (cm)	xs (cm)	P.I%
1	1.071	3.6	2.84	0.406	8	7.5	16	25.11%	2.9	4.02	0.574	11	11.5	6	77.1%
2	1.071	3.6	4.7	0.671	15	13.5	9.5	42.42%	2.9	4.9	0.7	14.5	14	3	48.48%
3	1.071	3.6	5.9	0.843	18.5	18	4.5	62.98%	2.9	6.32	0.903	20	23.1	2.5&Intersect	74.58%
4	1.071	3.6	7.4	1.057	22.5	24	Intersect	29.82%	2.9	7.5	1.071	22	29	Intersect	31.58%
5	0.833	2.8	3.1	0.344	11	11	13.5	15.67%	2.2	3.53	0.392	9	9	8	31.72%
6	0.833	2.8	5.8	0.644	20	21.5	2.5	34.88%	2.2	6.8	0.756	20	24	2.5	58.14%
7	0.833	2.8	8.5	0.944	23	33	Intersect	54.55%	2.2	7.71	0.857	17.5	31	Intersect	40.2%
8	0.682	2.3	3.6	0.327	13.5	12	12	44%	1.8	3.93	0.357	13	13	6.5	57.2%
9	0.682	2.3	6.1	0.555	23	27	3&Intersect	27.1%	1.8	6.4	0.582	19.5	22	Intersect	33.3%
10	0.682	2.3	7.7	0.7	23.5	26	Intersect	26.23%	1.8	7.05	0.641	16	28.5	Intersect	15.57%

Appendix A Results of expeimental tests

Table A-5: Results of the pier scour affected by vertical-wall abutment w=10 cm

RUN		Pier scour affected by vertical-wall abutment x=22.5cm							Pier scour affected by vertical-wall abutment x=17.5 cm						
	w/y	x/y	ds (cm)	ds/y	Ws (cm)	Ls (cm)	xs (cm)	P.I%	x/y	ds (cm)	ds/y	Ws (cm)	Ls (cm)	xs (cm)	P.I%
1	1.43	3.21	4.1	0.586	14	14	10.5	80.62%	2.5	4.6	0.657	15	14.5	3	102.6%
2	1.43	3.21	5.6	0.8	20	25.5	3.5	69.7%	2.5	6.07	0.867	19.5	25	Intersect	83.85%
3	1.43	3.21	6.2	0.885	22.5	27.5	Intersect	71.3%	2.5	6.95	0.993	20.5	23.5	Intersect	92.1%
4	1.43	3.21	8.6	1.223	24	33	Intersect	50.8%	2.5	7.2	1.028	22	30	Intersect	26.31%
5	1.11	2.5	3.45	0.383	10.5	9.5	13.5	28.4%	1.94	3.9	0.433	12.5	12.5	4	45.14%
6	1.11	2.5	6.2	0.689	23	23	2	44.2%	1.94	6	0.667	20	24.5	Intersect	39.5%
7	1.11	2.5	8.37	0.93	24	40	Intersect	52.2%	1.94	6.88	0.765	32	72	Intersect	25.2%
8	0.091	2.05	2.9	0.264	10.5	9	12.5	16%	1.6	2.9	0.264	10	10	7	16%
9	0.091	2.05	7.02	0.638	22	29	Intersect	46.25%	1.6	6.3	0.573	18	21	Intersect	31.25%
10	0.091	2.05	8.3	0.755	22	30	Intersect	36.1%	1.6	6.9	0.627	36	58	Intersect	13.11%

Table A-6: Results of pier scour affected by the wing-wall abutment.

RUN		Pier scour affected by the wing wall abutment x=22.5cm							Pier scour affected by the wing wall abutment x=17.5cm						
	L/y	x/y	ds (cm)	ds/y	Ws (cm)	Ls (cm)	xs (cm)	P.I%	x/y	ds (cm)	ds/y	Ws (cm)	Ls (cm)	xs (cm)	P.I%
1	1.43	3.21	4.04	0.557	16.5	17.5	10.5	77.9%	2.5	3.1	0.443	9.5	9	7	36.6%
2	1.43	3.21	4.6	0.657	20	21	9	39.4%	2.5	4.8	0.686	13	14.5	7	45.5%
3	1.43	3.21	5.6	0.8	20	22	2	54.7%	2.5	6.6	0.943	21	27	Intersect	82.3%
4	1.43	3.21	7.6	1.086	24	30.5	Intersect	33.3%	2.5	6.74	0.963	20	28	Intersect	18.2%
5	1.11	2.5	3.11	0.346	10.5	11	13.5	16.04%	1.94	3.35	0.372	10	11	7	25%
6	1.11	2.5	6.03	0.67	26.5	26.5	Intersect	40.2%	1.94	6.35	0.706	22	23	Intersect	47.7%
7	1.11	2.5	7.9	0.878	25	34.5	Intersect	43.6%	1.94	7.8	0.867	16	23	Intersect	41.8%
8	0.91	2.05	3.7	0.336	12.5	12.5	7	48%	1.6	4.5	0.409	14.5	14	5.5	80%
9	0.91	2.05	6.24	0.567	26	30.5	3.5&Intersect	30%	1.6	6.3	0.573	22	26	Intersect	31.3%
10	0.91	2.05	8.08	0.735	24	30	Intersect	32.5%	1.6	7.2	0.654	20.5	53	Intersect	18.03%

Appendix A Results of expeimental tests

Table A-7: Results of pier scour affected by the trapezoidal abutment.

RUN		Pier scour affected by the trapezoidal abutment x=22.5cm							Pier scour affected by the trapezoidal abutment x=17.5cm						
	L/y	x/y	ds (cm)	ds/y	Ws (cm)	Ls (cm)	xs (cm)	P.I%	x/y	ds (cm)	ds/y	Ws (cm)	Ls (cm)	xs (cm)	P.I%
1	2	3.21	4.3	0.614	12.5	14.5	10	89.4%	2.5	4.3	0.614	10.5	10	4	89.4%
2	2	3.21	5.2	0.742	15.5	16.5	5	57.6%	2.5	5.5	0.786	17	16.5	2.5	66.7%
3	2	3.21	6.8	0.971	21	25	3.5	87.8%	2.5	6.5	0.929	20	20	Intersect	79.6%
4	2	3.21	7.2	1.028	22	31	Intersect	26.31%	2.5	8.3	1.186	18	29.5	Intersect	45.6%
5	1.56	2.5	3.9	0.433	11	11	8.5	45.5%	1.94	3.8	0.422	10	11	4	41.8%
6	1.56	2.5	6.2	0.689	18.5	20	7&Intersect	44.2%	1.94	5.1	0.567	13.5	20.5	Intersect	18.6%
7	1.56	2.5	8	0.889	23	27	Intersect	45.5%	1.94	8.15	0.906	21	21	Intersect	48.2%
8	1.27	2.05	4.2	0.381	13.5	12	11	68%	1.6	4	0.363	11	11	2.5	60%
9	1.27	2.05	5.6	0.509	20	21	5	16.7%	1.6	6.8	0.618	21	25	Intersect	41.7%
10	1.27	2.05	8.5	0.772	24.5	39	Intersect	39.34%	1.6	8.5	0.773	40	56	Intersect	39.3%

Table A-8: Results of vertical-wall abutment scour w=5 cm.

RUN	y (cm)	Q (l/sec)	Fr	w/y	v(m/sec)	v/vc	Abutment scour of vertical-wall x=27 cm			Abutment scour of vertical-wall x=22.5 cm		
							ds (cm)	Ws (cm)	Ls (cm)	ds (cm)	Ws (cm)	Ls (cm)
1	7	8.33	0.18	0.714	0.15	0.5	3.7	9	9	3.84	10	10
2	7	9.72	0.24	0.714	0.19	0.63	4.4	10.5	10	5.1	11	12.5
3	7	11.11	0.26	0.714	0.21	0.7	6.13	12.5	16	6.3	15.5	21.5
4	7	13.89	0.33	0.714	0.27	0.9	9.4	18	52.5	9.1	21	37
5	9	9.72	0.17	0.556	0.16	0.52	3.54	9	11	4.63	10.5	11
6	9	13.89	0.23	0.556	0.22	0.71	5.65	11	18	5.41	12	14.5
7	9	18.05	0.30	0.556	0.28	0.90	9.26	18	50	10.42	20.5	41.5
8	11	12.5	0.16	0.455	0.16	0.5	3.44	8.5	10	3.72	10	8.5
9	11	18.05	0.22	0.455	0.23	0.72	6.27	14	19	6.5	14	21
10	11	22.22	0.28	0.455	0.29	0.91	9.22	20	52	9.7	20.5	39.5

Table A-9: Results of vertical-wall abutment scour w=7.5 cm.

RUN	y (cm)	Q (l/sec)	Fr	w/y	v(m/sec)	v/vc	Abutment scour of vertical-wall x=25cm			Abutment scour of vertical-wall x=20cm		
							ds (cm)	Ws (cm)	Ls (cm)	ds (cm)	Ws (cm)	Ls (cm)
1	7	8.33	0.18	1.071	0.15	0.5	3.96	9.5	8	4.03	11	11.5
2	7	9.72	0.24	1.071	0.19	0.63	5.2	16	14	4.5	14.5	14
3	7	11.11	0.26	1.071	0.21	0.7	7.11	18.5	25.5	6	18	25.2
4	7	13.89	0.33	1.071	0.27	0.9	10.5	25	51.5	10.1	24.5	54
5	9	9.72	0.17	0.833	0.16	0.52	3.2	10	11	4.94	10.5	10
6	9	13.89	0.23	0.833	0.22	0.71	6.4	19	24	6.1	17.5	22.5
7	9	18.05	0.30	0.833	0.28	0.90	11.6	27	55	11.9	27.5	62.5
8	11	12.5	0.16	0.682	0.16	0.5	4.2	13.5	11	4.82	15.5	14
9	11	18.05	0.22	0.682	0.23	0.72	8.4	22	30.5	7.32	19.5	24
10	11	22.22	0.28	0.682	0.29	0.91	11	28	51.5	12.6	28.5	58.5

Table A-10:Results of vertical-wall abutment scour w=10 cm.

RUN	y (cm)	Q (l/sec)	Fr	w/y	V(m/sec)	V/VC	Abutment scour of vertical-wall x=22.5cm			Abutment scour of vertical-wall x=17.5cm		
							ds (cm)	Ws (cm)	Ls (cm)	ds (cm)	Ws (cm)	Ls (cm)
1	7	8.33	0.18	1.43	0.15	0.5	4	12	9	4	12.5	10.5
2	7	9.72	0.24	1.43	0.19	0.65	5.8	21	23.5	6.27	20	25
3	7	11.11	0.26	1.43	0.21	0.7	7.9	24	42.5	7.86	22	22.5
4	7	13.89	0.33	1.43	0.27	0.9	11.3	26	59	11.9	28	59
5	9	9.72	0.17	1.11	0.16	0.5	3.76	9.5	8.5	3	11.5	11.5
6	9	13.89	0.23	1.11	0.22	0.7	7.4	23	27	6.2	21	28
7	9	18.05	0.30	1.11	0.28	0.9	12.1	32	62	12.34	32	72
8	11	12.5	0.16	0.091	0.16	0.5	3.5	12.5	10.5	3.9	12	12
9	11	18.05	0.22	0.091	0.23	0.7	8.34	24.5	35	8.2	24.5	41
10	11	22.22	0.28	0.091	0.29	0.9	12.2	30	60	13.1	36	58

Table A-11: Results of wing-wall abutment scour.

RUN	y (cm)	Q (l/sec)	Fr	L/y	V(m/sec)	V/VC	Abutment scour of wing-wall x=22.5cm			Abutment scour of wing-wall x=17.5cm		
							ds (cm)	Ws (cm)	Ls (cm)	ds (cm)	Ws (cm)	Ls (cm)
1	7	8.33	0.18	1.43	0.15	0.5	4.52	13	12	4.1	9	10.5
2	7	9.72	0.24	1.43	0.19	0.63	5.71	14	14	5.44	13	10.5
3	7	11.11	0.26	1.43	0.21	0.7	7.6	23	37	8	21	27
4	7	13.89	0.33	1.43	0.27	0.9	10.9	28	63	11	31.5	54.5
5	9	9.72	0.17	1.11	0.16	0.52	3.6	11	8.5	4.17	9	8
6	9	13.89	0.23	1.11	0.22	0.71	8.9	20	26	6.9	19.5	33
7	9	18.05	0.30	1.11	0.28	0.90	11.84	23	51	14	30.5	71
8	11	12.5	0.16	0.091	0.16	0.5	4.1	11.5	9.5	4.5	14.5	13
9	11	18.05	0.22	0.091	0.23	0.72	8.56	21	40	7.6	22	36
10	11	22.22	0.28	0.091	0.29	0.91	10.86	27	58	10.5	20.5	53

Table A-12: Results of trapezoidal abutment scour.

RUN	y (cm)	Q (l/sec)	Fr	L/y	V(m/sec)	V/VC	Abutment scour of trapezoidal x=22.5cm			Abutment scour of trapezoidal x=17.5cm		
							ds (cm)	Ws (cm)	Ls (cm)	ds (cm)	Ws (cm)	Ls (cm)
1	7	8.33	0.18	2	0.15	0.5	3.8	11	10	3.8	7.5	9.5
2	7	9.72	0.24	2	0.19	0.65	5.4	16	17.5	5.3	11	11
3	7	11.11	0.26	2	0.21	0.7	7.3	21	22	7	17	17
4	7	13.89	0.33	2	0.27	0.9	9.4	27	50	9.5	23.5	43
5	9	9.72	0.17	1.56	0.16	0.5	3.8	8.5	9	4.3	9.5	9.5
6	9	13.89	0.23	1.56	0.22	0.7	5.2	18	18	6.1	16.5	16.5
7	9	18.05	0.30	1.56	0.28	0.9	11.4	26	60	10.6	26	53.5
8	11	12.5	0.16	1.27	0.16	0.5	4.5	12	14	4.27	11	10
9	11	18.05	0.22	1.27	0.23	0.7	6.4	18	25	7	20	35
10	11	22.22	0.28	1.27	0.29	0.9	10.5	26.5	54	10	40	56

Table A-13: Predicted, Observed scour depths, and residual of pier scour affected by vertical-wall abutment w=5 cm.

		Non-linear regression model			ANN
Run	ds/y (observed)	ds/y (predicted)	Residual	Scour predicted (by formula)	MLP_PredictedValue
1	0.514	0.46	0.06	0.48	0.464
2	0.607	0.64	-0.04	0.67	0.631
3	0.714	0.70	0.02	0.73	0.683
4	0.866	0.88	-0.02	0.92	0.861
5	0.322	0.34	-0.02	0.35	0.339
6	0.511	0.55	-0.03	0.57	0.540
7	0.744	0.71	0.03	0.75	0.728
8	0.269	0.27	0.00	0.28	0.273
9	0.488	0.45	0.04	0.48	0.457
10	0.579	0.61	-0.03	0.64	0.635
11	0.476	0.48	0.00	0.50	0.490
12	0.607	0.67	-0.07	0.71	0.670
13	0.771	0.73	0.04	0.77	0.723
14	0.943	0.92	0.02	0.97	0.896
15	0.337	-	-	0.38	0.349
16	0.503	-	-	0.61	0.567
17	0.822	-	-	0.79	0.761
18	0.282	-	-	0.30	0.275
19	0.5	-	-	0.51	0.474
20	0.631	-	-	0.69	0.662

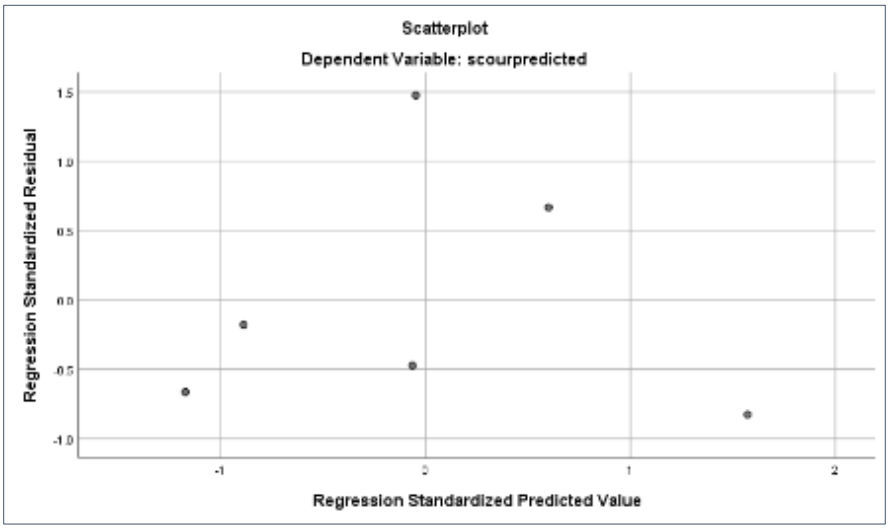

FigureA-1:Scatterplot of Non-linear regression model by vertical-wall abutment w=5 cm effect.

Table A-14:Predicted, Observed scour depths, and residual of pier scour affected by vertical-wall abutment w=7.5 cm.

		Non-linear regression model			ANN
Run	ds/y (observed)	ds/y (predicted)	Residual	Scour predicted (by formula)	MLP_PredictedValue
1	0.406	0.47	-0.06	0.47	0.516
2	0.671	0.71	-0.04	0.71	0.698
3	0.843	0.78	0.06	0.79	0.811
4	1.057	1.05	0.01	1.05	0.994
5	0.344	0.39	-0.04	0.39	0.344
6	0.644	0.67	-0.03	0.67	0.660
7	0.944	0.91	0.04	0.91	0.870
8	0.327	0.30	0.03	0.30	0.305
9	0.555	0.53	0.02	0.53	0.602
10	0.7	0.73	-0.03	0.73	0.728
11	0.574	0.50	0.08	0.50	0.500
12	0.7	0.76	-0.06	0.76	0.804
13	0.903	0.84	0.07	0.84	0.901
14	1.071	1.12	-0.04	1.12	0.989
15	0.392	-	-	0.35	0.355
16	0.756	-	-	0.61	0.702
17	0.857	-	-	0.83	0.849
18	0.357	-	-	0.25	0.325
19	0.582	-	-	0.45	0.642
20	0.641	-	-	0.62	0.719

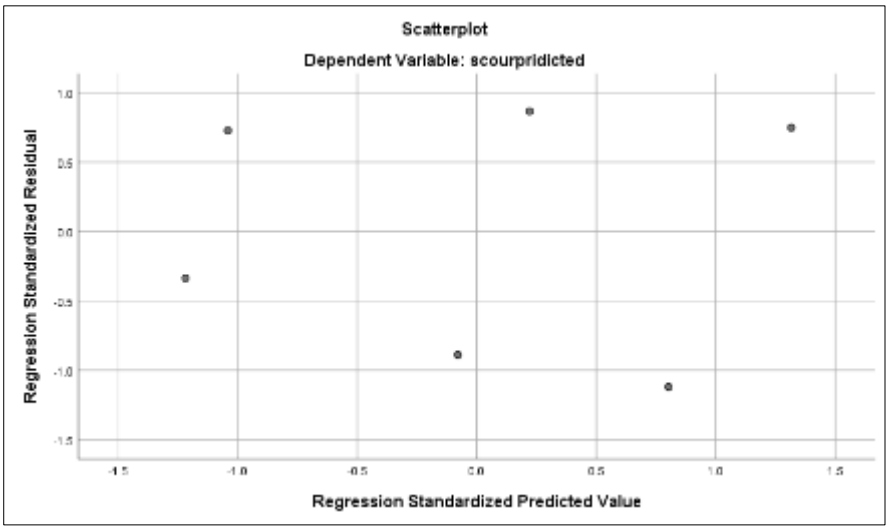

Figure A-2:Scatterplot of Non-linear regression model by vertical-wall abutment w=7.5 cm effect.

Table A-15:Predicted, Observed scour depths, and residual of pier scour affected by vertical-wall abutment w=10 cm.

		Non-linear regression model			ANN
Run	ds/y (observed)	ds/y (predicted)	Residual	Scour predicted (by formula)	MLP_PredictedValue
1	0.586	0.62	-0.04	0.62	0.570
2	0.8	0.85	-0.05	0.85	0.802
3	0.885	0.92	-0.03	0.92	0.908
4	1.223	1.14	0.09	1.14	1.176
5	0.383	0.41	-0.03	0.41	0.367
6	0.689	0.69	0.00	0.69	0.744
7	0.93	0.92	0.01	0.92	0.940
8	0.264	0.30	-0.03	0.30	0.231
9	0.638	0.56	0.08	0.56	0.595
10	0.755	0.80	-0.04	0.80	0.748
11	0.657	0.62	0.04	0.62	0.621
12	0.867	0.85	0.02	0.85	0.892
13	0.993	0.91	0.08	0.91	0.947
14	1.028	1.13	-0.10	1.13	1.065
15	0.433	-	-	0.39	0.382
16	0.667	-	-	0.65	0.673
17	0.765	-	-	0.87	0.777
18	0.264	-	-	0.28	0.305
19	0.573	-	-	0.52	0.569
20	0.627	-	-	0.74	0.662

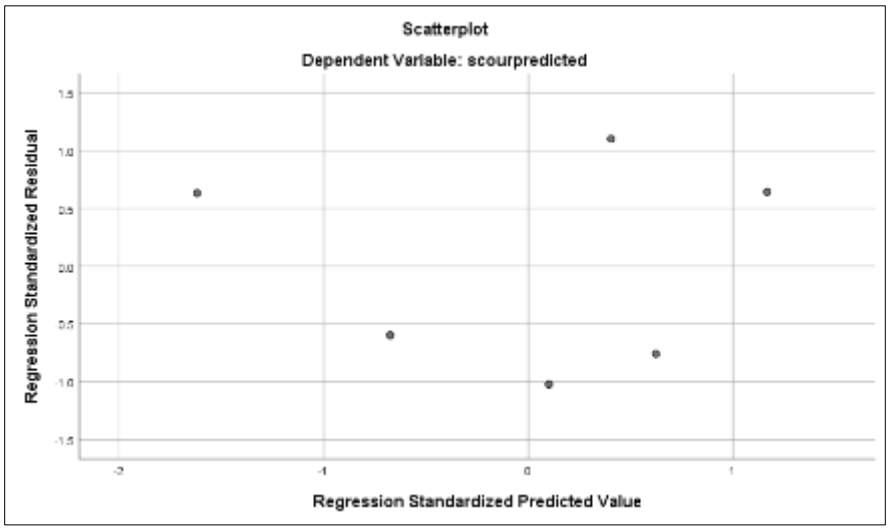

Figure A-3:Scatterplot of Non-linear regression model by vertical-wall abutment w=10 cm effect.

Table A-16:Predicted, Observed scour depths, and residual of pier scour affected by wing-wall abutment.

		Non-linear regression model			ANN
Run	ds/y (observed)	ds/y (predicted)	Residual	Scour predicted (by formula)	MLP_PredictedValue
1	0.577	0.51	0.07	0.51	0.524
2	0.657	0.74	-0.08	0.74	0.676
3	0.800	0.81	-0.01	0.81	0.786
4	1.086	1.05	0.03	1.05	1.072
5	0.346	0.39	-0.05	0.39	0.380
6	0.670	0.65	0.02	0.65	0.628
7	0.878	0.87	0.01	0.87	0.867
8	0.336	0.32	0.02	0.32	0.339
9	0.567	0.55	0.01	0.55	0.574
10	0.735	0.75	-0.02	0.75	0.758
11	0.443	0.49	-0.05	0.50	0.446
12	0.686	0.72	-0.04	0.72	0.700
13	0.943	0.79	0.15	0.79	0.807
14	0.963	1.03	-0.07	1.03	0.981
15	0.372	-	-	0.38	0.360
16	0.706	-	-	0.64	0.669
17	0.867	-	-	0.85	0.794
18	0.409	-	-	0.31	0.336
19	0.573	-	-	0.54	0.623
20	0.654	-	-	0.73	0.722

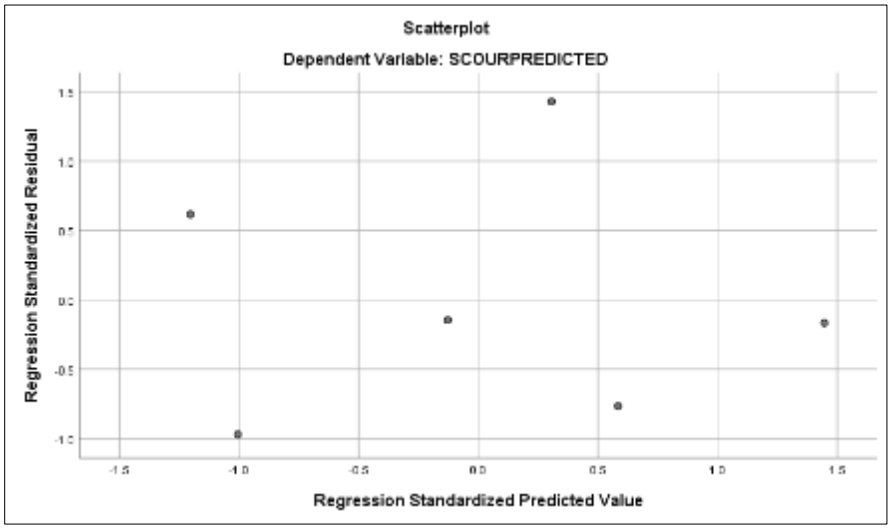

Figure A-4:Scatterplot of Non-linear regression model by wing-wall abutment effect.

Table A-17:Predicted, Observed scour depths, and residual of pier scour affected by trapezoidal abutment.

		Non-linear regression model			ANN
Run	ds/y (observed)	ds/y (predicted)	Residual	Scour predicted (by formula)	MLP_PredictedValue
1	0.614	0.59	0.02	0.59	0.667
2	0.743	0.80	-0.05	0.80	0.812
3	0.971	0.86	0.11	0.86	0.873
4	1.029	1.10	-0.07	1.10	1.044
5	0.433	0.45	-0.01	0.44	0.410
6	0.689	0.67	0.02	0.67	0.674
7	0.889	0.88	0.01	0.88	0.947
8	0.382	0.36	0.02	0.36	0.325
9	0.509	0.57	-0.06	0.57	0.506
10	0.773	0.75	0.02	0.75	0.760
11	0.614	0.63	-0.01	0.62	0.618
12	0.786	0.84	-0.05	0.84	0.830
13	0.929	0.90	0.02	0.90	0.902
14	1.186	1.16	0.03	1.16	1.052
15	0.422	-	-	0.48	0.389
16	0.567	-	-	0.72	0.657
17	0.906	-	-	0.94	0.911
18	0.364	-	-	0.39	0.331
19	0.618	-	-	0.62	0.519
20	0.773	-	-	0.82	0.724

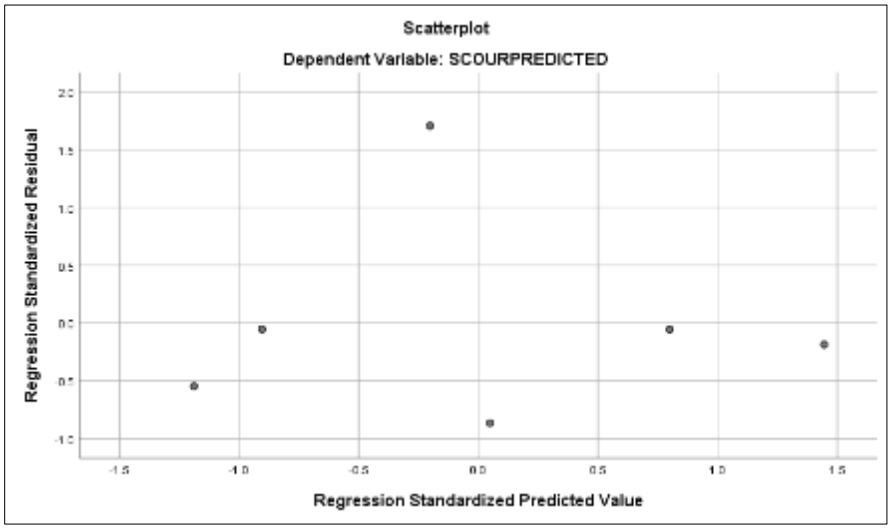

Figure A-5:Scatterplot of Non-linear regression model by trapezoidal abutment effect.

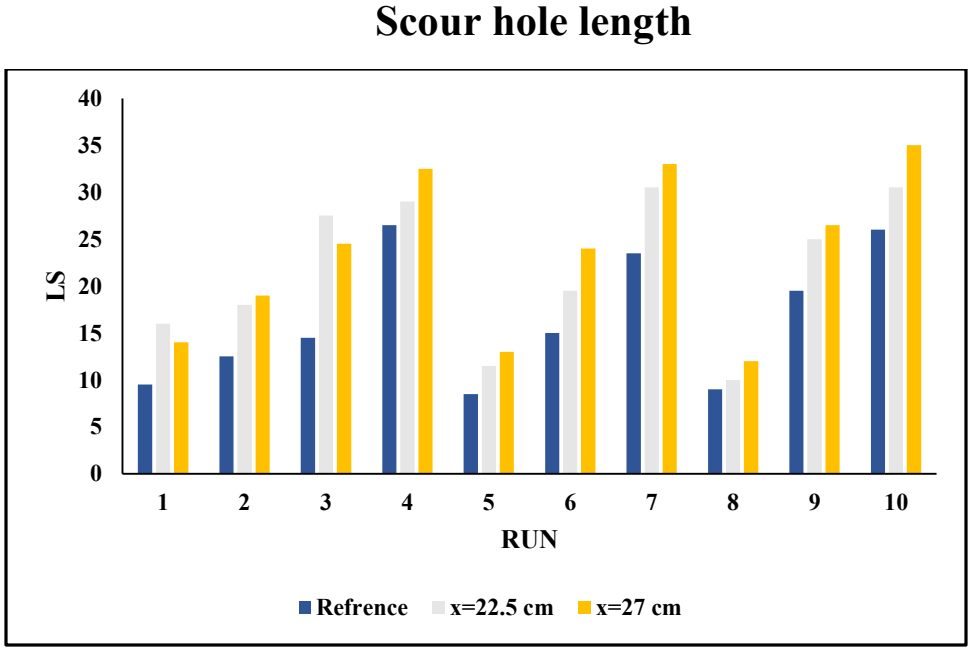

Figure A-6:Variation of scour length of pier hole for vertical-wall abutment (w = 5 cm) at two spacing values (x = 22.5 cm and x = 27 cm) compared to the reference case.

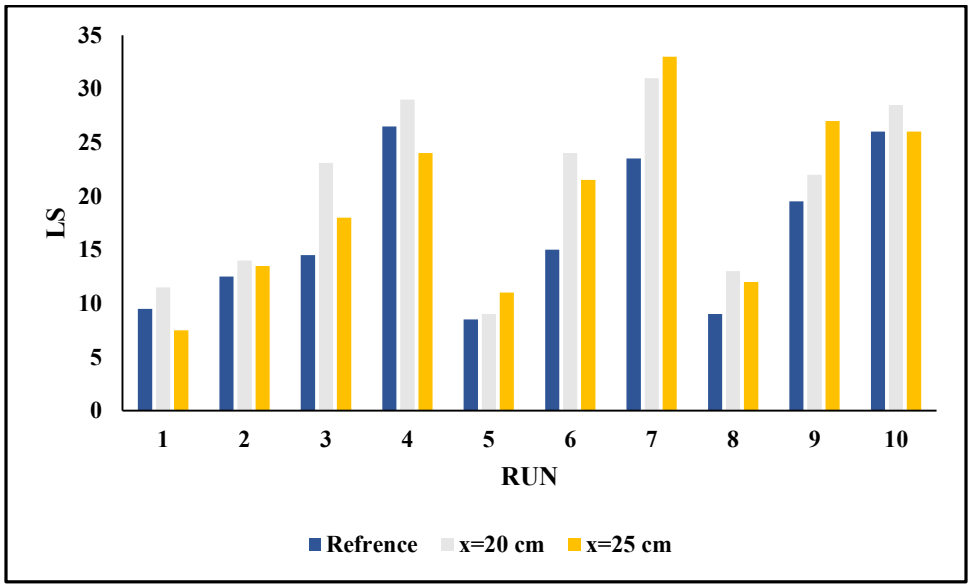

Figure A-7:Variation of scour length of pier hole for vertical-wall abutment (w =7.5 cm) at two spacing values (x = 20 cm and x = 25 cm) compared to the reference case.

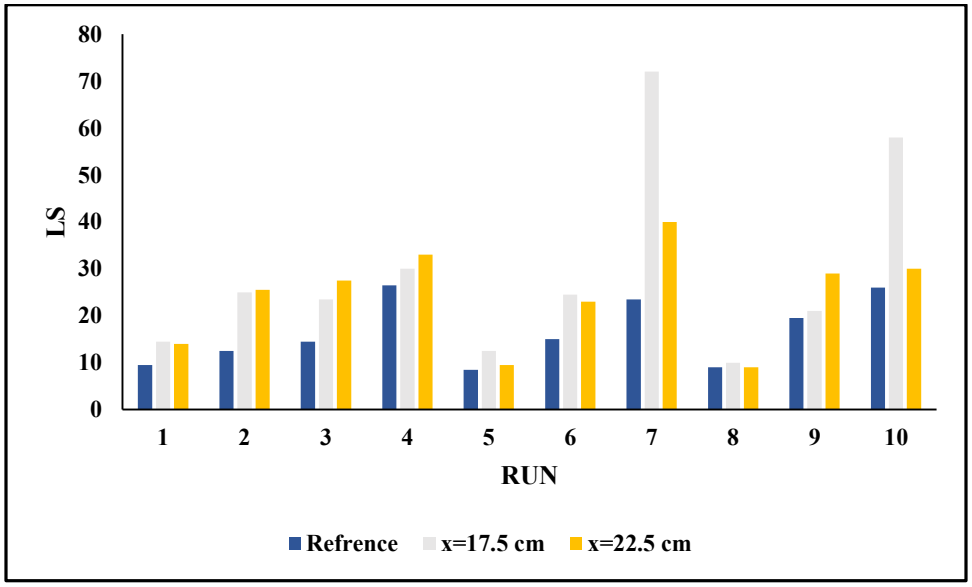

Figure A-8:Variation of scour length of pier hole for vertical-wall abutment (w =10 cm) at two spacing values (x = 17.5 cm and x = 22.5 cm) compared to the reference case.

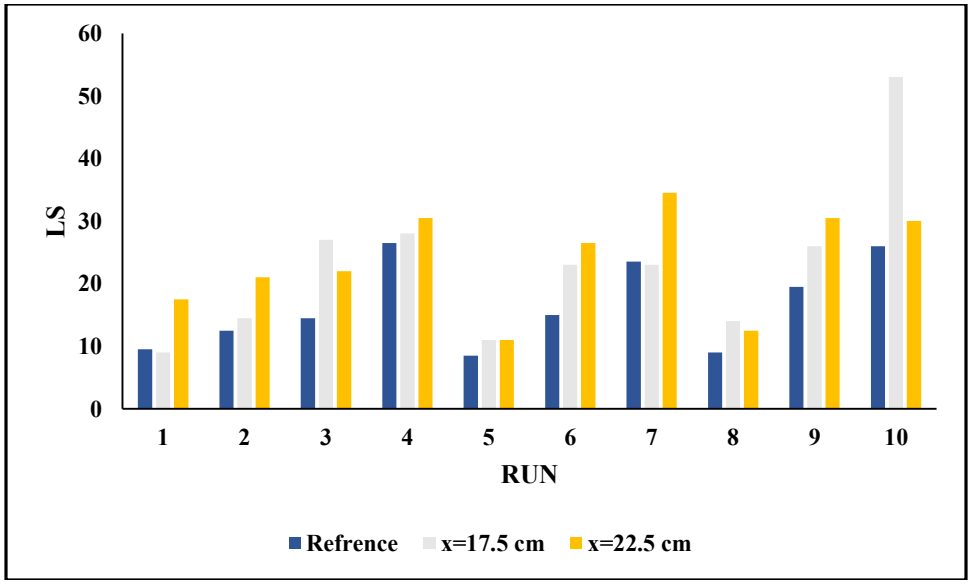

Figure A-9:Variation of scour length of pier hole for wing-wall abutment at two spacing values (x = 17.5 cm and x = 22.5 cm) compared to the reference case.

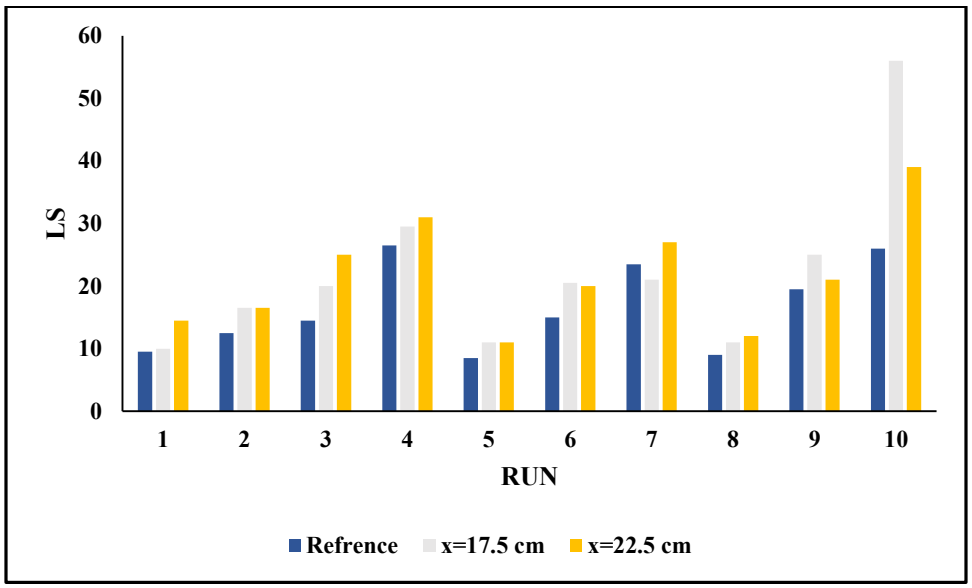

Figure A-10:Variation of scour length of pier hole for trapezoidal abutment at two spacing values (x = 17.5 cm and x = 22.5 cm) compared to the reference case.

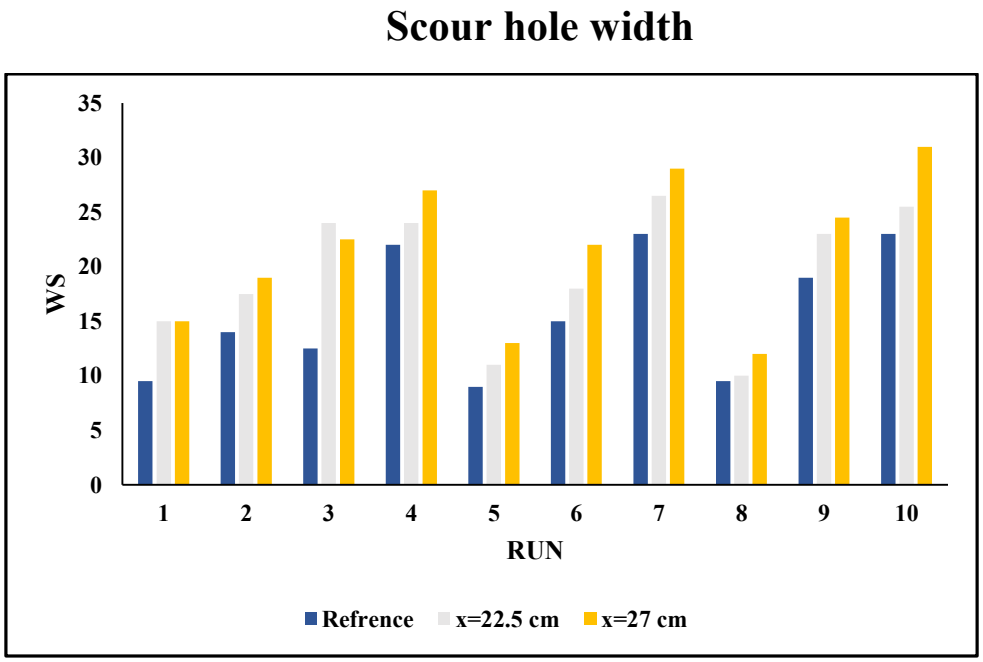

Figure A-11:Variation of scour width of pier hole for vertical-wall abutment (w = 5 cm) at two spacing values (x = 22.5 cm and x = 27 cm) compared to the reference case.

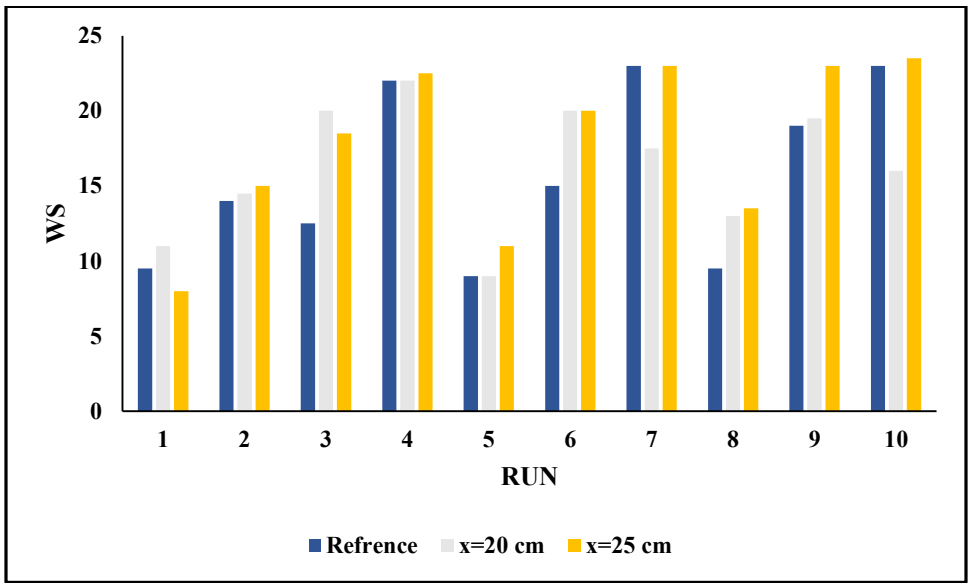

Figure A-12:Variation of scour width of pier hole for vertical-wall abutment (w =7.5 cm) at two spacing values (x = 20 cm and x = 25 cm) compared to the reference case.

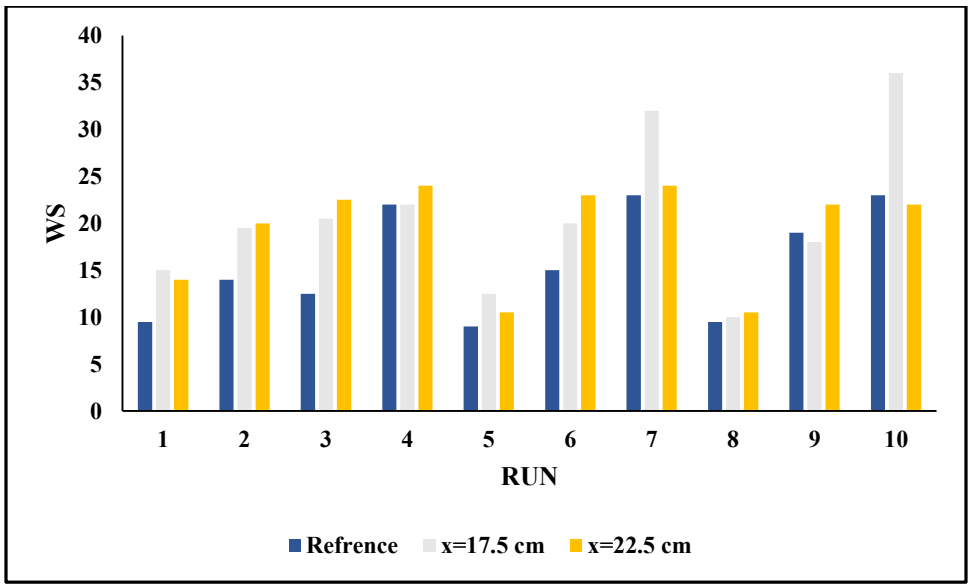

Figure A-13:Variation of scour length of pier hole for vertical-wall abutment (w =10 cm) at two spacing values (x = 17.5 cm and x = 22.5 cm) compared to the reference case.

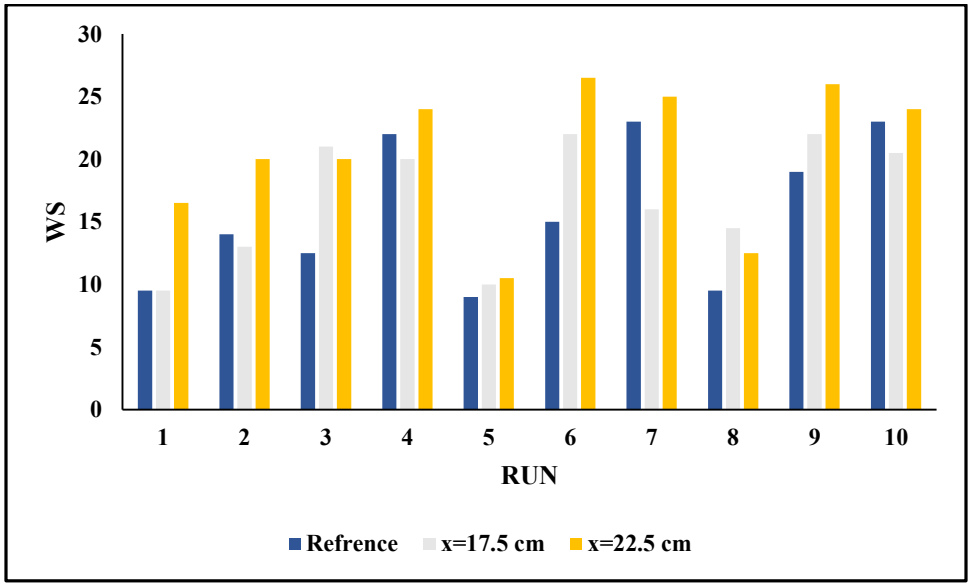

Figure A-14:Variation of scour length of pier hole for wing-wall abutment at two spacing values (x = 17.5 cm and x = 22.5 cm) compared to the reference case.

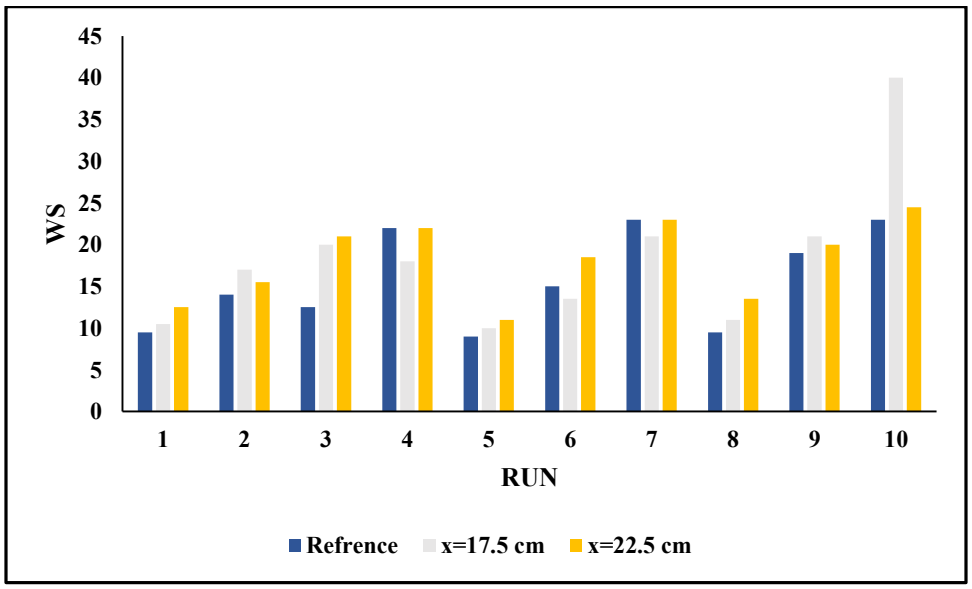

Figure A-15:Variation of scour length of pier hole for trapezoidal abutment at two spacing values (x = 17.5 cm and x = 22.5 cm) compared to the reference case.

Appendix B-Selected Photos of Experimental Tests

B-1: Reference tests of the pier

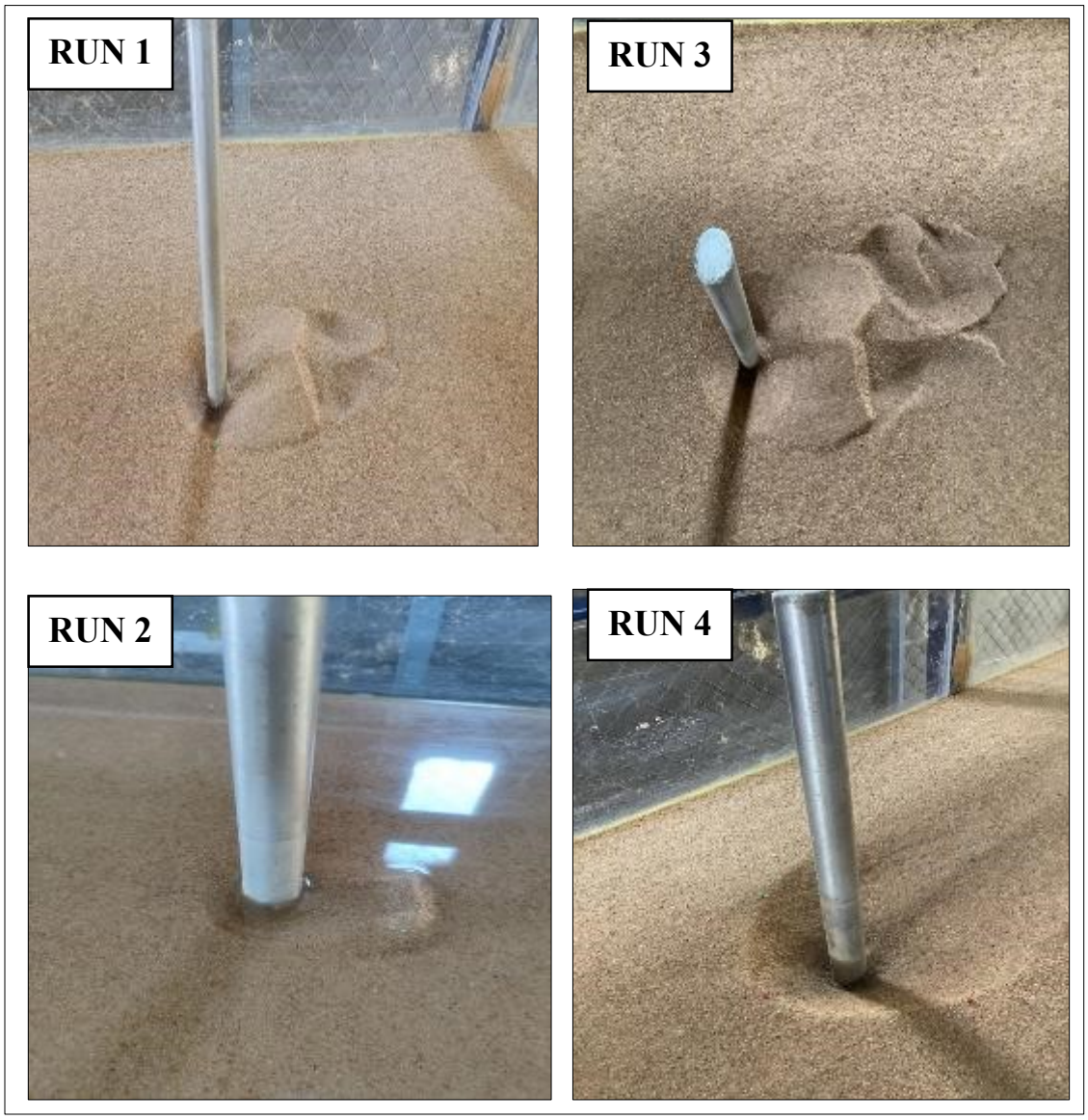

Figure B-1: Reference tests of the pier RUNS(1-4).

Appendix B Selected Photos of Experimental Tests

Figure B-2: Reference tests of the pier RUNS(5-10).

B-2: Reference tests of the Abutment-A

Figure B-3: Reference tests of the Abutment-A RUNS (1,3,5,6).

Appendix B Selected Photos of Experimental Tests

Figure B-4: RUN 2 of Reference tests of the Abutment-A.

Figure B-5: RUN 4 of Reference tests of the Abutment-A.

Appendix B Selected Photos of Experimental Tests

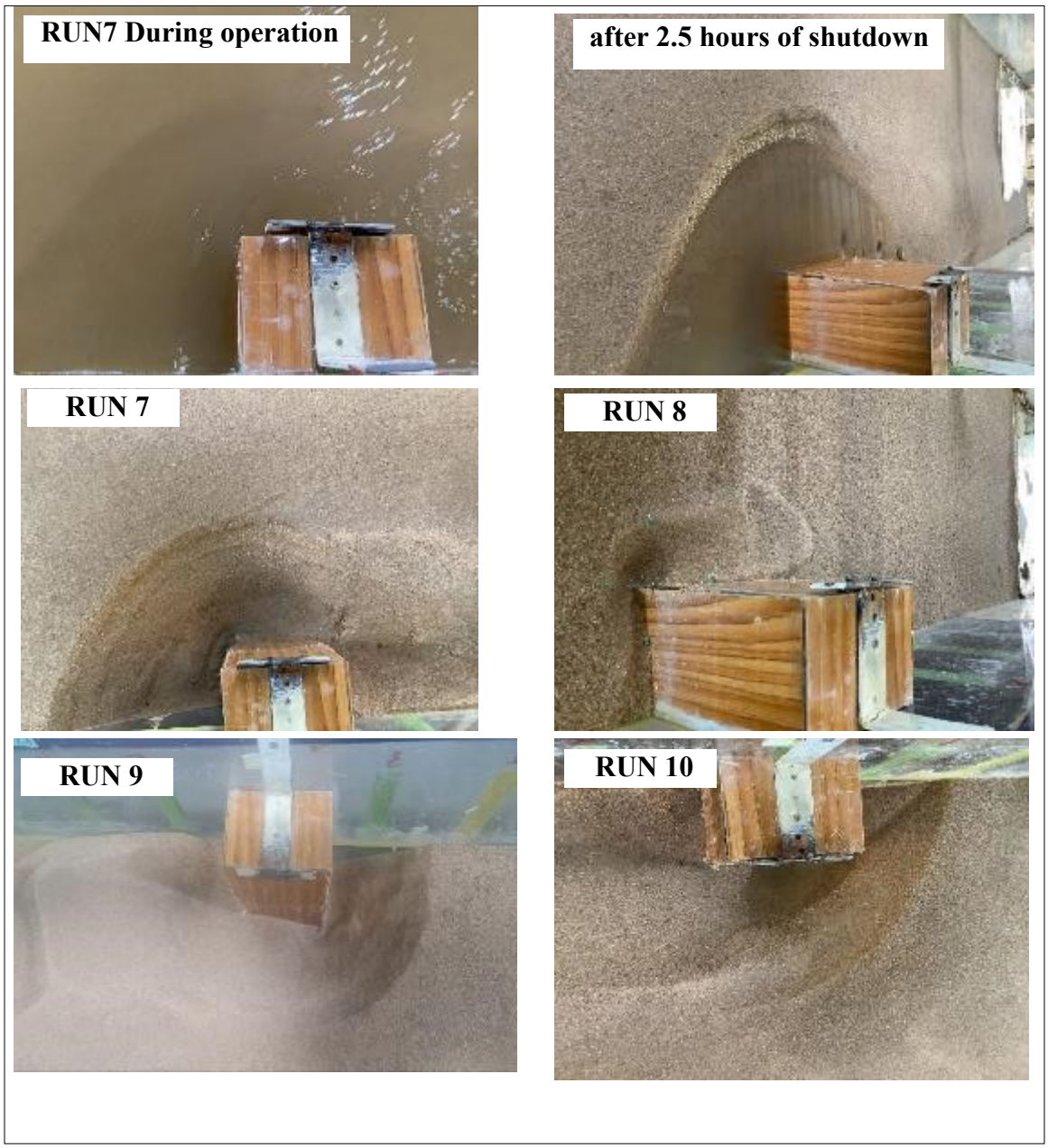

Figure B-6: Reference tests of the Abutment-A RUNS (7,8,9,10).

B-3: Reference tests of the Abutment-B

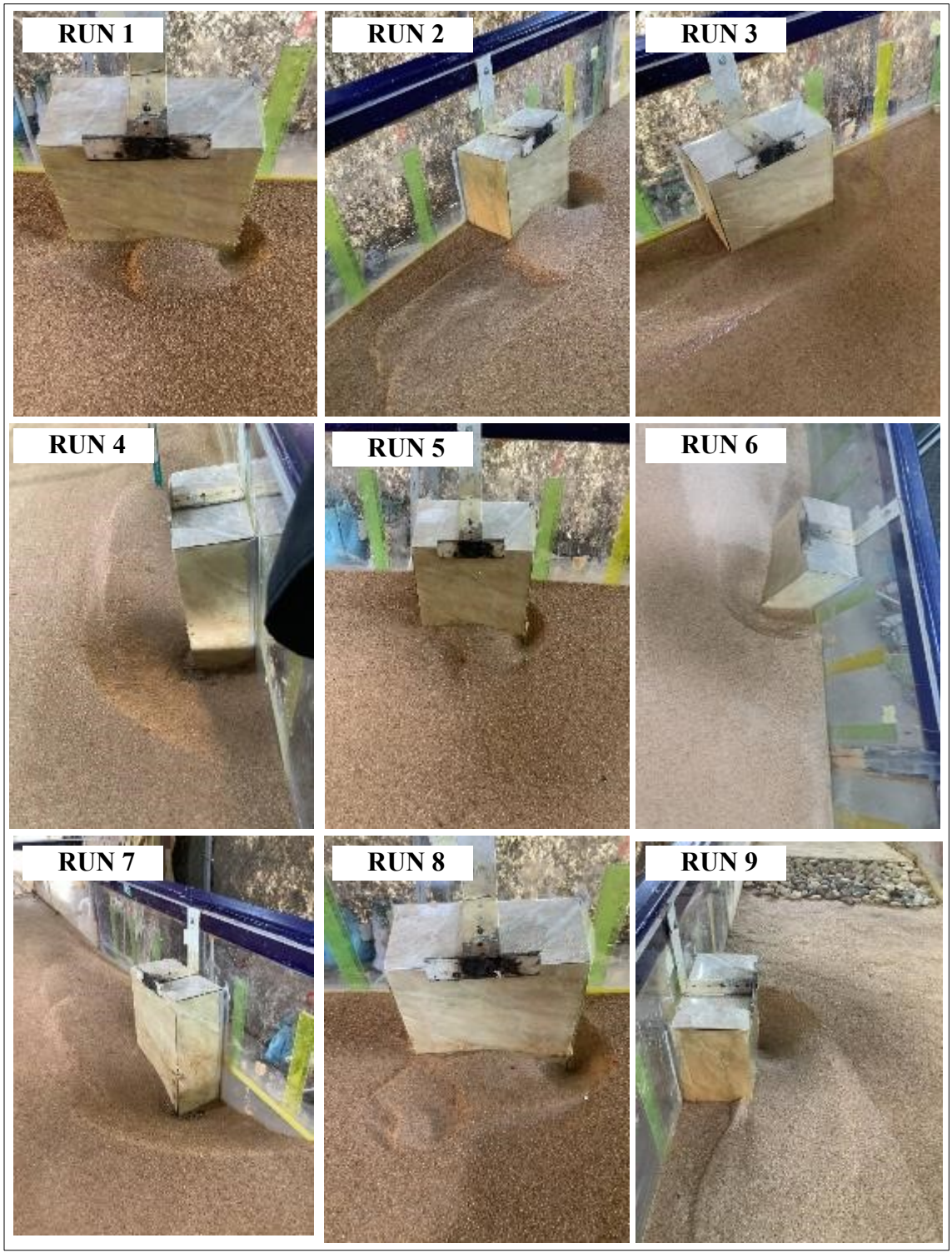

Figure B-7: Reference tests of the Abutment-B RUNS (1-9).

الخلاصة

يُعد النحر الموضعي قرب الأكتاف والدعامات من العوامل الرئيسة التي تسهم في فشل الجسور الهيدروليكية. وعلى الرغم من وجود عدد كبير من الدراسات التي تناولت هذا الموضوع، إلا أن هناك نقصًا في الأبحاث التي تتناول تأثير التفاعل بين الكتف والدعامة من حيث الأثر المشترك على عمق النحر، خصوصًا عند أخذ شكل الكتف والمسافة الفاصلة بين الكتف والدعامة بعين الاعتبار. تهدف هذه الدراسة إلى تحليل تأثير أشكال مختلفة من الأكتاف على حجم وشكل حفرة النحر المحلي المتشكلة حول دعامة دائرية مفردة لجسر. تم إجراء التجارب مختبريًا في ظروف الجريان النقي (clear-water) وتحت تدفق ثابت تحت الحرج (subcritical)، باستخدام نماذج لخمسة أنواع مختلفة من الأكتاف. شملت النماذج ثلاثة أشكال من الأكتاف العمودية بابعاد جانبية مختلفة (5 سم، 7.5 سم، و10 سم)، بالإضافة إلى نموذجين لأكتاف ذات جدار مائل (wing-wall) وشكل شبه منحرف (trapezoidal).

أظهرت النتائج أن وجود الكتف بالقرب من الدعامة يؤثر بشكل واضح على عمق النحر حول الدعامة، وأن هذا التأثير يختلف باختلاف شكل الكتف، وعرضه، والمسافة الفاصلة بين الكتف والدعامة، وكذلك وفقًا للخصائص الهيدروليكية. حيث لوحظ انخفاض في عمق النحر حول الكتف وزيادة حول الدعامة نتيجة لتداخل حفر النحر عند تقليل المسافة بينهما. فعلى سبيل المثال، عند تقليص المسافة من (27 سم إلى 22.5 سم)، (25 سم إلى 20 سم)، و(22.5 سم إلى 17.5 سم) في ظل نفس الظروف، زاد عمق النحر حول الدعامة بنسب تقريبية بلغت (20.88%)، (28.79%)، (2.60%)، و(2.02%) لكل من نماذج الأكتاف العمودية 1 و2، والجدار المائل، وشبه المنحرف، على التوالي. بينما أظهرت نتائج الكتف العمودي 3 انخفاضًا في عمق النحر بنسبة 4.14% عند تقليل المسافة من (22.5 سم إلى 17.5 سم).

كما أظهرت النتائج أن زيادة شدة الجريان وعدد فرويد تؤدي إلى زيادة واضحة في عمق النحر، في حين أن زيادة عمق الجريان كانت لها تأثير عكسي، حيث انخفض عمق النحر مع زيادة عمق الماء عند ثبات المسافة والتصريف. وبينت النتائج أن وجود الكتف في مجال تأثير الدعامة يغير من خصائص النحر المحلي، إذ أن تقليل المسافة بينهما يؤدي إلى تداخل حفر النحر وتشكّل حفرة

واحدة بدلاً من اثنتين.وبمقارنة نتائج النماذج المختلفة من الأكتاف من حيث نسبة الزيادة في عمق النحر، تبين أن أعلى نسبة زيادة سُجلت لنموذج الكتف شبه المنحرف عند المسافة x = 17.5 سم، في حين أن أقل نسبة سُجلت لنموذج الكتف العمودي 1 عند x = 27 سم.

تم اشتقاق معادلات تجريبية جديدة باستخدام تقنية التحليل البُعدي (dimensional analysis) وبرنامج IBM SPSS الإصدار 30 للتنبؤ بأقصى عمق نحر حول الدعامة تحت تأثير شكل الكتف. أظهرت النتائج أن معاملات تحديد المعادلات (R^2) كانت على النحو التالي: 0.948، 0.931، 0.913، 0.916، و0.936 لكل من نماذج الأكتاف العمودية (V1، V2، V3)، الجدار المائل، وشبه المنحرف على التوالي، مما يشير إلى وجود علاقة قوية بين القيم المرصودة والقيم المتنبأ بها.

وأخيرًا، أثبتت الشبكات العصبية الاصطناعية (ANNs) كفاءتها العالية في محاكاة عمق النحر المتزن حول دعامات الجسور المتأثرة بوجود الأكتاف. حيث أظهر أنموذج الشبكة متعددة الطبقات (MLP) دقة تنبؤية مرتفعة، خصوصًا في حالة الكتف العمودي 3، إذ بلغ معامل التحديد R^2 = 0.983. وبشكل عام، تفوقت نماذج ANN على التحليل غير الخطي في القدرة على التنبؤ، مما يؤكد موثوقيتها في المهام المعقدة الخاصة بتنبؤ النحر الموضعي. كما بين تحليل الحساسية أن عرض وطول الكتف لهما التأثير الأكبر في عمق النحر المتوقع حول الدعامة. وتوفر هذه النتائج إسهامًا مهمًا في فهم تفاعل الكتف مع الدعامة في عمليات النحر الموضعي، بما يوجه نحو تصميم أكثر أمانًا للجسور، ويساعد في التنبؤ الدقيق بعمق النحر. كما أن المخرجات ذات فائدة خاصة في تحسين معايير التصميم الهيدروليكي، وتحقيق أفضلية في اختيار شكل الكتف بالنسبة لموقع الدعامة، وتعزيز النماذج التنبؤية الخاصة باستقرار أساسات الجسور تحت ظروف جريان مختلفة.

جمهورية العراق

وزارة التعليم العالي و البحث العلمي

جامعة كربلاء

كلية الهندسة

قسم الهندسة المدنية

دراسة تجريبية لتاثير شكل المسند الطرفي على النحر الموضعي بالقرب من دعامات الجسور

رسالة مقدمة الى مجلس كلية الهندسة / جامعة كربلاء وهي جزء من متطلبات نيل درجة الماجستير في علوم الهندسة المدنية

المؤلف:

عذراء عبد الواحد خلف

باشراف :

أ.م.د.أيسر طعمة جودة

أ.م.د.رياض جاسم محمد

محرم الحرام - 1447 حزيران - 2025